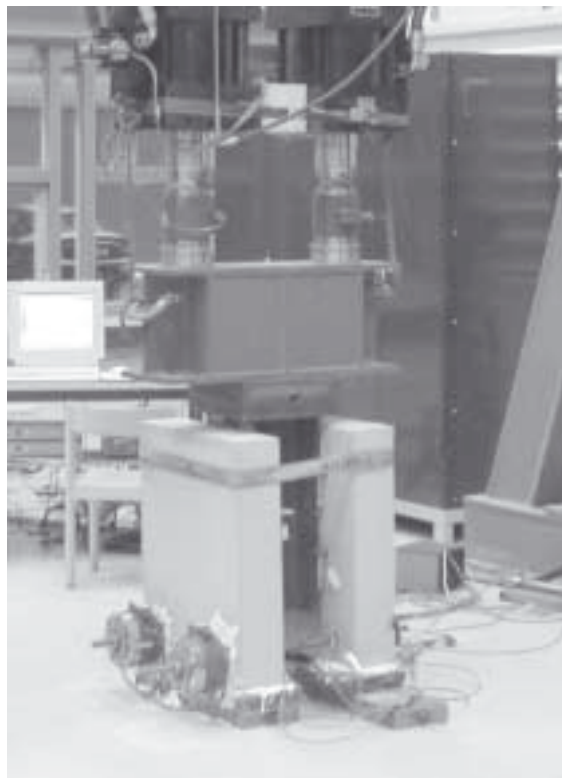


MASTER'S THESIS

Influence of Fatigue on Headed Stud Connectors in Composite Bridges



MARKUS BRO • MARIE WESTBERG

MASTER OF SCIENCE PROGRAMME

Department of Civil and Environmental Engineering
Division of Steel Structures

2004:147 CIV • ISSN: 1402 - 1617 • ISRN: LTU - EX - - 04/147 - - SE

Preface

The work in this thesis was carried out at the Division of Structural Engineering - Steel Structures, Department of Civil and Environmental Engineering at Luleå University of Technology between August 2003 and May 2004. It is part of a project called “Increased Load Bearing Capacity of Railway Bridges by Utilisation of Steel-Concrete Composite Action in Ultimate Limit States” and is financed by the Swedish National Road Administration (Vägverket) and the Swedish National Railway Administration (Banverket).

We would like to thank BRISAB Industri AB, Öjebyn, and Tibnor AB, Luleå, for welding and material.

The experimental study had been impossible to perform without all help from the staff of TESTLAB; thank you all for your support and for valuable discussions.

We would like to express our deep gratitude to our supervisor Associate Professor Milan Veljovic for his help, ideas, guidance and encouragement.

Luleå, May 2004

Markus Bro

Marie Westberg

Abstract

Composite bridges are used for road and railroad bridges in Sweden and worldwide. The advantage of composite bridges is that concrete and steel is used optimally, steel in tension and concrete in compression. In order to get the interaction between steel and concrete headed stud shear connectors are used.

Fatigue loading makes cracks, initiated by welding, propagate and in this way the strength of shear connectors are decreased during the fatigue life.

The aim in this thesis is to investigate the residual strength of 22 mm headed stud connectors and if possible derive an equation for residual strength. In BV BRO the residual strength is neglected in design of ultimate limit state, but in e.g. Eurocode and BRO 2002 it is taken into account. One objective is to evaluate the assumption made in BV BRO.

A state of art on the subject has been performed. Most previous research is focused on the endurance rather than residual strength, but some relevant research was found. From previous research and literature the fatigue life was found to be mainly affected by the range and the peak load.

A literature survey on fatigue, fracture mechanics and the behaviour of shear studs have been performed to improve the understanding of the subject.

The experimental work carried out within this master's thesis is 10 push-out tests, five static and five fatigue. The push-out specimens were made according to Eurocode 4 and the headed shear studs used were 125 x 22mm.

Differences and similarities in Swedish design standards and Eurocode have been investigated. These design standards have also been compared to experimental results and to previous research.

The results of tests and literary survey show that the residual strength under fatigue loading constantly reduces and this reduction seems to linearly depend on the number of cycles applied. An equation was derived for residual strength. The design models Eurocode and BRO 2002 gives a bit lower residual strength than that derived from experiments performed. Arguments to support the assumption in BV BRO were not found.

Sammanfattning

Samverkansbroar används i Sverige och resten av världen till både vägbroar och järnvägsbroar. Fördelen med samverkans broar är att stål och betong används optimalt, stål i drag och betong i tryck. Svetsbultar används för att överföra krafter mellan stål och betong och på så sätt uppnå samverkan.

Under utmattningslast kommer svetsbulten att börja spricka beroende på mikrosprickor som initierats i svetsprocessen. När sprickan ökar i storlek minskar bultens statiska hållfasthet vilket sker under hela tiden bulten utsätts för utmattningslast.

I den svenska beräkningsnormen för järnvägsbroar (BV BRO) försummas kvarstående bärförmågan i brottgränstillstånd men i tex. Eurocode och BRO 2002 antas den vara konstant. Målet med examensarbetet är att undersöka antagande i BV BRO samt att ta fram en ekvation för beräkning av kvarstående bärförmåga

En sammanställning av forskning på området är genomförd. Till stor del är denna forskning fokuserad på att ta reda på uthålligheten och inte kvarstående bärförmåga, men viss forskning har hittats inom ämnet. Forskning och litteratur visar att lastvidd och maxlast har störst effekt på utmattning.

En kort genomgång av litteratur inom utmattning, brottmekanik och beteende hos svetsbultar, är genomförd för att få en bättre förståelse av ämnet.

Det experimentella arbete som utförts inom ramen för detta examensarbete är 10 push-out tests, 5 statiska och 5 utmattning. Dessa tillverkades i enlighet med Eurocode 4. Svetsbultarna i provkropparna var 125 x 22 mm.

Skillnader och likheter mellan svenska normer och Eurocode har undersökts och jämförts med resultaten från den experimentella delen av examensarbetet och tidigare forskning.

Resultaten visar att den kvarstående bärförmåga är linjärt avtagande under utmattningslast. En ekvation för beräkning av kvarstående bärförmåga presenteras i rapporten. Dimensioneringsnormerna Eurocode och BRO 2002 ger en lägre kvarstående bärförmåga än den som framkommit genom försök. Inga argument som stöder antagandet i BV BRO har hittats.

Notations and symbols

a = crack length

A_{sh} = area of shank

da/dN = crack growth

D_{corr} = static resistance reduced for horizontal force

D_{max} = static resistance

$D_{residual}$ = static resistance after fatigue loading

E = endurance = number of cycles to failure

E_a = asymptotic endurance

E_c = Young's modulus of concrete

E_s = Young's modulus of steel

f_{ck} = cubic compressive strength of concrete

f_u = yield strength of steel

K = stress intensity factor

K_{Ic} , K_{Id} = critical stress intensity factor

m = slope of S-N curve

N = number of cycles

P_{max} = peak load

P_{min} = trough load

R = load range, $P_{max} - P_{min}$

ν = Poisson's value

δf = slip growth

ULS = ultimate limit state

SLS = serviceability limit state

Table of Contents

PREFACE.....	I
ABSTRACT.....	III
SAMMANFATTNING	V
NOTATIONS AND SYMBOLS	VII
TABLE OF CONTENTS	IX
1. INTRODUCTION.....	1
1.1. BACKGROUND.....	1
1.2. AIM AND OBJECTIVES	1
1.3. SCOPE AND METHODS	2
1.4. LIMITATIONS.....	2
2. STATE OF THE ART	3
2.1. ENDURANCE TESTS	3
2.1.1. Mainstone & Menzies.....	3
2.1.2. Hallam.....	4
2.1.3. Taplin & Grundy.....	4
2.1.4. Oehlers, Seracino and Yeo.....	5
2.2. RESIDUAL STRENGTH TESTS	5
2.2.1. Oehlers	5
2.2.2. Hanswille, Porsch & Üstündag.....	6
2.3. EVALUATION OF PREVIOUS RESEARCH.....	7
2.3.1. Oehlers	7
2.3.2. G. Taplin & P. Grundy.....	8
2.3.3. Johnson & Oehlers.....	8
2.3.4. Johnson	9
2.3.5. D. J Oehlers, C & G Coughlan	9
3. SHEAR STUDS	11
3.1. COMPOSITE STRUCTURES	11
3.2. COMPOSITE ACTION	12
3.2.1. Slip	14
3.2.2. No composite action.....	15
3.2.3. Partial composite action	16
3.2.4. Full composite action.....	17
3.3. FORCES AND FAILURE MODES OF STUD SHEAR CONNECTORS	18
3.3.1. Static failure	21
3.3.2. Fatigue failure.....	22
3.4. PUSH TESTS.....	25

4. FATIGUE.....	29
4.1. INTRODUCTION TO FATIGUE	29
4.2. SHORT OVERVIEW OF ELASTIC FRACTURE MECHANICS.....	30
4.2.1. <i>General cases of cracking and stress intensity factor</i>	31
4.2.2. <i>Fatigue-crack-propagation threshold</i>	34
4.2.3. <i>Fatigue crack propagation</i>	35
4.3. FACTORS GOVERNING THE FATIGUE LIFE	38
4.3.1. <i>Material properties</i>	38
4.3.2. <i>Load properties</i>	41
4.3.3. <i>Peak load</i>	43
4.4. FATIGUE TESTING	44
4.4.1. <i>Endurance testing</i>	44
4.4.2. <i>Accumulated damage</i>	46
4.4.3. <i>Residual strength based procedures</i>	47
5. DESIGN CODES.....	49
5.1. SHORT INTRODUCTION TO DESIGN.....	49
5.1.1. <i>Static resistance of stud shear connectors</i>	51
5.1.2. <i>Fatigue design</i>	51
5.2. EUROCODE	51
5.2.1. <i>Road bridges</i>	52
5.2.2. <i>Railway bridges</i>	52
5.2.3. <i>Static strength of stud shear connectors</i>	53
5.2.4. <i>Fatigue strength of stud shear connectors</i>	53
5.3. SWEDISH CODE.....	57
5.3.1. <i>BSK 99</i>	57
5.3.2. <i>BRO 2002 (Swedish code for road bridges)</i>	59
5.3.3. <i>BV BRO (Swedish code for railroad bridges)</i>	60
5.4. DESIGN IN BRITISH BRIDGE CODE AND PEAK LOAD MODEL	60
5.5. COMPARISON BETWEEN DESIGN IN DIFFERENT CODES	61
6. EXPERIMENTAL STUDIES	63
6.1. GENERAL ABOUT TEST SET-UP.....	63
6.1.1. <i>Preliminary support set-up</i>	65
6.1.2. <i>Standardized support set-up</i>	66
6.2. MANUFACTURING OF SPECIMENS	67
6.2.1. <i>Concrete properties</i>	68
6.2.2. <i>Characteristics of headed shear studs</i>	68
6.2.3. <i>Reinforcement</i>	69
6.3. TESTING PROCEDURE	69
6.3.1. <i>Static tests</i>	70
6.3.2. <i>Fatigue testing and residual test</i>	70
6.4. MEASUREMENT.....	71
6.5. RESULTS OF STATIC TESTS	73

6.5.1. <i>Summary of the static tests</i>	73
6.6. RESULTS OF ENDURANCE AND RESIDUAL STRENGTH TESTS	76
6.6.1. <i>Observed Failure modes for cyclic loading</i>	76
6.6.2. <i>Endurance test</i>	77
6.6.3. <i>Summary of residual strength tests</i>	78
7. DISCUSSION	81
7.1. STATIC TESTS.....	81
7.1.1. <i>Slip for static tests</i>	81
7.1.2. <i>Horizontal force for static tests</i>	81
7.1.3. <i>Comparison between test results and theoretical prediction</i>	81
7.2. RESIDUAL STRENGTH TESTS	82
7.2.1. <i>Residual strength test and asymptotic endurance</i>	82
7.2.2. <i>Slip</i>	88
7.2.3. <i>Failure modes</i>	90
8. CONCLUSIONS	91
9. REFERENCES.....	93
APPENDIX A.....	95
APPENDIX B	105
APPENDIX C	111
APPENDIX D.....	113
APPENDIX E	121
APPENDIX F	130

1. Introduction

This master's thesis is part of a research project carried on at Luleå University of Technology, called "Increased Load Bearing Capacity of Railway Bridges by Utilisation of Steel-Concrete Composite Action in Ultimate Limit States". This project is financed by the Swedish National Road Administration (Vägverket) and the Swedish National Railway Administration (Banverket).

1.1. Background

Composite bridges where steel girders and a concrete deck are connected by headed stud shear connectors are the most common in Sweden as well as worldwide. Shear studs welded to a steel girder resist the slip between steel and concrete and transfer longitudinal shear forces between the two. This interaction makes efficient use of steel and concrete, with the assumption that the concrete is only subjected to compression and that part of the steel girder is constrained by the concrete slab. This also render possible to build slender bridges.

Traffic load and movement due to change of temperature and shrinkage of the concrete cause a fluctuating load. This fatigue load must be considered in the design of a bridge. Fatigue loading of shear studs makes cracks, initiated by e.g. the welding procedure, propagate. Due to this the static strength after fatigue, called residual strength, is decreased compared to the initial strength.

The extremely high but rare loads are accounted for in the ultimate limit state.

The fatigue and ultimate limit state design of bridges is governed by national codes, which at present are BRO 2002 and BV BRO in Sweden. The work on a standard that will be governing in EU, Eurocode, is forth going. One of the major discrepancies in the design codes is the fatigue design of railway bridges. In the Swedish Railway code, BV BRO, no interaction between the concrete slab and steel girder is accounted for in the ultimate limit state. This is because the residual strength decrease with time and it is thus assumed that the safety of the bridge may become under required level during the late part of the design life.

The purpose of this project is to examine the effects of fatigue loading on 22 mm headed shear studs and to investigate the relevance in the afore mentioned assumption.

1.2. Aim and objectives

The aim is to investigate the residual strength of 22 mm headed shear studs through experimental studies. The results are to be compared with previous research.

The objectives of the thesis are:

- To derive an equation for residual strength based on experimental studies of 22 mm headed shear studs.

- To evaluate the assumption in BV BRO that composite action may not be used in the calculation of ULS.

1.3. Scope and methods

A short literature survey of fatigue and fracture mechanics, design codes and the behaviour of headed shear studs were made to improve understanding of the subject. A number of research reports were studied and some of them are presented in state of the art.

Experiments were performed on push out specimens in order to find the static strength, residual strength and endurance of 22 mm headed shear studs. The tests performed were five static and five fatigue tests, of which one was an endurance test.

1.4. Limitations

The experimental studies are limited to one range and one peak load. The range and peak loads are relatively high to reduce the endurance. Residual strength tests are only performed once on each chosen number of cycles.

There are differences in the behaviour of shear studs in beams and push-out tests, e.g. the number of connectors is much larger in a bridge beam and the shear studs in a push-out test are loaded directly. The result from push-out tests has to be interpreted for use in bridge beams, but this relation is not included in the scope of this thesis. Push-out tests are standard procedure and have been used to investigate behaviour of shear studs for many years.

2. State of the art

This chapter includes summaries of the research on slip, static strength, endurance and residual strength of headed stud shear connectors.

In the endurance and residual strength tests also static tests have been performed.

Expressions used in this chapter are explained later in the report.

2.1. Endurance tests

A number of endurance tests have been performed on different push out specimens since the mid 60's.

2.1.1. Mainstone & Menzies

Shear connectors in steel-concrete composite beams for bridges (1967).

Mainstone & Menzies performed static and fatigue tests on push-out specimens, using stud shear connectors, channel connectors and bar connectors. Only the results from stud shear connectors are presented here.

Stud properties: $d = 19 \text{ mm}$, $L = 100 \text{ mm}$.

11 static and 23 fatigue tests. Both unidirectional and reverse loading with varying ranges were performed. Push-out specimen with two connectors on one level, not constrained from horizontal movement at the base.

Results:

The failure modes in the fatigue loading were due to fracture in weld or shank or due to yielding of the stud shear connector. The latter was also the failure mode observed in the static tests. It was found that

$$f_{\max} = k_0 N^{-\alpha}$$

where

f_{\max} = is the maximum nominal shear stress, k_0 = constant, α = constant

Only in a few cases the number of observations was sufficient to give the slope of the line, α , and in those cases it agreed closely to that of earlier tests, but the value is not presented in the article.

Some variation in the fatigue strength of a connector for a given life and load ratio is to be expected when the concrete strength varies. This is because the connector is influenced to some extent by the deformation of the concrete and hence by its strength. The influence was thought to be greater for a more flexible connector, that is a stud connector is more influenced than e.g. a bar connector.

2.1.2. Hallam

The behaviour of stud shear connectors under repeated loading (1976).

Stud properties: $d = 19 \text{ mm}$, $L = 76 \text{ mm}$.

1 static test, 13 fatigue with constant amplitude but varying range between tests, 4 fatigue with programmed spectrum of amplitude. Push-out specimen with two studs on each side, concrete slabs prevented from separation by a steel rod. Varying concrete strengths.

When the first side failed during fatigue loading, this side was removed, holes were drilled in the steel flange and a pre-cast concrete slab was bolted. The fatigue loading was then continued until the studs on the second side failed.

Results:

Some correlation between the failure mode and the applied stud loading was found. Hallam describes three different failure modes.

A general fatigue curve for predicting behavior under spectrum loading was established as

$$\log N = 7,303 - 5,993q$$

$$\text{where } q = \frac{Q_{\max} - Q_{\min}}{Q_{\text{ult}} - Q_{\min}}$$

Q_{\max} = maximum cyclic load, Q_{\min} = minimum cyclic load, Q_{ult} = static strength

The effect of concrete strength both on fatigue life and on slip characteristics was found to be a significant factor.

Miner's linear cumulative damage law was concluded to be adequate for predicting the fatigue life of stud connectors under variable amplitude repeated loading.

2.1.3. Taplin & Grundy

The incremental slip behaviour of stud shear connectors (1995).

Stud properties: $d = 12,7 \text{ mm}$, $L = 50 \text{ mm}$.

Push-out specimen with four studs in two rows. 4 static, 3 fatigue with reverse loading and 1 unidirectional loading tests were performed. The loading in the unidirectional case is shown in Figure 2-1, the load ranging from 10 to 100 % of P_{\max} .

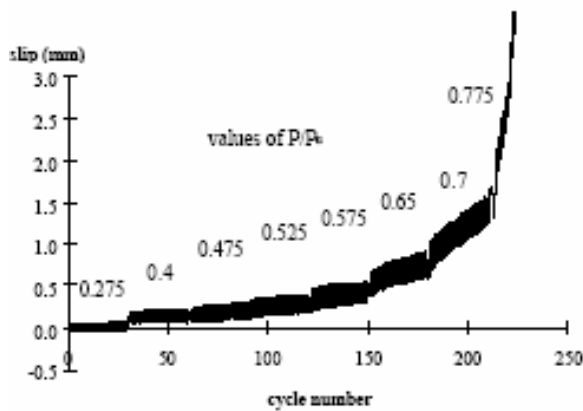


Figure 2-1. Unidirectional loading by Taplin & Grundy.

Results:

The following equation for slip growth of unidirectional load was derived:

$$\delta_f = 3,36 \cdot 10^{-6} e^{12,7 \left(\frac{P}{P_u} \right)} \text{ mm/cycle}$$

2.1.4. Oehlers, Seracino and Yeo

Reverse-Cycle Fatigue tests on stud shear connectors (1999)

Stud properties: $d = 12,7 \text{ mm}$, $L = 75 \text{ mm}$

The aim for these tests was made in order to investigate how stud shear connectors behaved under cyclic loading. In the tests 4 fatigue and 2 static tests were performed. Test specimen had two studs in two rows.

Results:

It was concluded from the research that the residual strength is constantly reducing during fatigue loading. It is also concluded that rate of slip increase is constant until approximately 50 % of the asymptotic endurance.

2.2. Residual strength tests

Only a few test series of residual strength has been carried out.

2.2.1. Oehlers

Deterioration in strength of stud connectors in composite bridge beams (1990)

Stud properties: $d = 12,7 \text{ mm}$, $L = 75 \text{ mm}$.

3 static, 6 endurance tests with constant $R = 0,25 D_{\max}$ but different peak load, 5 residual strength tests with $R = 0,25 D_{\max}$ and $P_{\max} = 0,29 D_{\max}$ but different number of cycles. Push-out specimen with four studs in two rows.

Results:

It was concluded that the fatigue crack propagation starts at the commencement of cyclic loading and that fatigue loads reduce the static strength at all stages of the design life.

The maximum shear load applied does not affect the fatigue damage, i.e. the peak load does not affect the reduction rate of the residual strength. Increasing the maximum shear load reduces the fatigue life, as it reduces the area of the stud over which fatigue cracking can occur but this is not an issue taken to account in present design code.

Regression analysis using all experimental results gave the following equation:

$$N = E_a \cdot \left(1 - \frac{D_{\text{residual}}}{D_{\text{max}}} \right) \quad \text{Eqn. 2-1}$$

From Eqn 2.1 and the accumulated damage law the following equation was derived:

$$\frac{R_1}{D_{\text{max}}} = \left[\frac{10^K \left(1 - \frac{D_{\text{residual}}}{D_{\text{max}}} \right)}{C n_t + C n_t \left(\frac{R_2}{R_1} \right)^m + \dots + C n_t \left(\frac{R_r}{R_1} \right)^m} \right]^{1/m} \quad \text{Eqn. 2-2}$$

where

R = range of shear load induced by standard fatigue vehicle, r = number of ranges of cyclic load, C = spectral constant, a function of the frequency and weight of vehicles, n_t = number of loading events, m = exponent of fatigue endurance equation

This equation can be used in either a design or analysis mode. In the design mode, the monotonic strength D_{residual} to resist the maximum design load is first calculated and then the static strength D_{max} , which is required when the bridge is first constructed, can be determined from an iterative solution. In the analysis of an existing structure, the static strength D_{max} when it was first constructed is known, and hence the eqn. can be used to determine the residual strength D_{residual} that remains after fatigue loading.

2.2.2. Hanswille, Porsch & Üstündag

Modelling of damage mechanisms to describe the fatigue life of composite steel-concrete structures. (2004)

The aim was to investigate the predamage by systematic experiments with push-out specimens and to find the reduced static strength after high-cycle preloading. The project is in progress

Stud properties: d = 22 mm, L = 125 mm.

Push-out specimen according to EC 4. 4 series of tests, each consisting of 3 static tests and 9 unidirectional cyclic tests (3 endurance tests and 6 residual strength tests) were performed. The peak load was $0,44D_{\max}$ and $0,71D_{\max}$ and the range was $0,2D_{\max}$ and $0,25D_{\max}$.

Results:

The static tests were found in good agreement of the calculation model given in Eurocode 4. The fatigue tests gave $m = 8,658$ and $K = 24$, which should be compared to $m = 8$ and $21,93$.

The effect of high cycle preloading was evident, as the residual strength was decreased compared to the static strengths. After the residual strength tests the fracture surfaces was examined and found to consist of a typical fatigue fracture area and a forced fracture zone.

Two types of failure modes were found; for high peak loads the fracture was initiated at the weld collar/stud interface and propagated through the shank. For low peak loads the fracture was as above or initiated at the weld collar/shank interface or flange/weld interface and propagated through the flange. For the first failure mode it was possible to determine the crack development and a linear correlation between the reduced static strength and the size of the fatigue cracking zone was found. The results indicated an early crack initiation in approximately 10~20 % of the fatigue life which is causing reduction in residual strength.

2.3. Evaluation of previous research

2.3.1. Oehlers

Methods of estimating the fatigue endurance of stud shear connections (1990)

Oehlers used results from two hundred and eighty push tests (Mainstone & Menzies and Hallam among others) to derive estimates to the fatigue endurance of stud shear connectors. Of the two hundred and eighty, one hundred and fifty six were used in the analyses, the rest were omitted for different reasons. The endurance was assumed to be dependant of the following parameters:

$$N_e = f(A, R, f_c, P)$$

where N_e = endurance.

The significance of each variable was determined by multivariable linear regression analysis. The results from the regression analysis were also improved using parallel regression.

Results

The results from Oehlers analysis is shown in Table 2-1.

Table 2-1. Values of exponent m .

Reference results	(No of	$N_e = f(R/F_p)^{-m}$ (1)	$N_f = f(R/F_p)^{-m}$ (2)	$N_e = f(R/A)^{-m}$ (3)
156 (regression)		4,63	4,41	3,51
156 (parallel regression)		5,42	5,1	5,09

N_f in the above table is $N_f = N_e / (1 - P / F_p)$

The equations above is recognized as the one used in the British Code (1), The Peak Load model (2) and the one used in Eurocode (3).

2.3.2. G. Taplin & P. Grundy.

Steel-concrete composite beams under repeated load (1999)

Seventeen of the author's own tests presented in other reports were evaluated and a FEM model for evaluating slip for shear studs was produced. The main part of this report is the FE-modelling with contact elements and different stiffness matrix evaluations. In this summary the modelling is not presented due to the complexity.

Results

The result of the FEM analysis showed good agreement with results from tests in some cases (deflection) and in some cases the agreement is less good (slip).

A formula for calculation of slip growth was formulated for 12,7 mm studs to be

$$\delta_f = 10^{\left(3,91 \cdot \frac{P_{\max}}{D_{\max}} - 4,71\right)} \left[\text{mm/cycle} \right] \quad \text{Eqn. 2-3}$$

2.3.3. Johnson & Oehlers

Integrated static and fatigue design or assessment of stud shear connections in composite bridges (1996).

Results

Johnson & Oehlers used the results from Oehlers (1990) and presented a method for checking ultimate strength, taking account of fatigue damage. It can be used for design or to evaluate the reduction in safety that occurs in the latter part of the design life. This design method directly gives the number of connectors required, with no need for a separate fatigue check.

The remaining life can also be estimated by this equation. Johnson & Oehlers also conclude that the value of $m = 8$ used in British Standard BS 5400 is too high.

2.3.4. Johnson

Resistance of stud shear connectors to fatigue (2000).

Johnson investigated the wide range of the exponent m in design codes with reference to all relevant test data.

If m is low, most fatigue damage is said to be done by the high-frequency low-stress-range part of the loading spectrum, if it is high the rare but exceptionally heavy loads matter. The limited data from fatigue tests on beams generally show that the fatigue performance of the studs is better than in push tests.

The results from Oehlers (1990) was used and applied to the design model according to EC 4, BS and the Peak load model by Oehlers (1990).

Results

The peak-load model had the lowest scatter. The analysis showed that for $P_{\max}/D_{\max} \leq 0,6$ the peak load has a fairly small influence and thus EC 4 and BS are reasonable simplifications.

The reason for discrepancy in the value of m is believed to be that in e.g. BS the linear regression was made of $\log \Delta\tau$ on N (which gave $m = 8$), while Oehlers used treated N as the dependent variable and did regressions of $\log N$ on $\log \Delta\tau$ (which gave $m = 5$).

The Peak Load model appeared to fit the test data best and was clearly the best for load ranges with high peak values. Johnson also mention that in drafting ENV 1994-2 it was assumed that other verifications would ensure that P_{\max} would be less than $0,6D_{\max}$, but this was not specified as a limit and Johnson advocate such a limit.

2.3.5. D. J Oehlers, C & G Coughlan

The shear stiffness of stud shear connections in composite beams (1996).

116 push tests of 12,7, 19 and 22 mm shear studs were evaluated to see the stiffness and slip increase for fatigue tests. The concrete strengths used were between 20 and 70 N/mm². All test results are used to perform different regression analyses.

Result

An equation describing the slip growth/cycle in fatigue testing was derived:

$$\delta_f = 1,70 \cdot 10^{-5} \cdot \frac{R^{4,55}}{D_{\max}}$$

3. Shear studs

The following parts are included in this chapter:

Composite structures where composite structures are defined.

Composite action in which composite action and slip in a composite bridge is described.

Forces and failure modes of stud shear connectors in which the forces acting on headed shear studs and failure modes during static and fatigue loading is described.

Push tests in which the test specimen and set-up for the testing of shear connectors are described.

3.1. Composite structures

Composite structures consist of two or more parts of different materials, attached to each other to act as one. The advantage is that desirable properties of the different materials can be used more efficiently. The most common composite structures are those of steel and concrete, but composite structures of e.g. wood and carbon fibre, steel and carbon fibre and concrete and carbon fibre are also in use. In this report composite structures from here on refer to steel concrete composite structures.

Steel and concrete are materials widely used in the construction of various structures. Both have properties very useful and properties that may cause problems. Concrete is very effective in compression, but the tensile strength is poor. The tensile and compressive strengths for steel are almost the same, but steel parts are often made by thin plates and compressive forces therefore cause local and global buckling, strongly reducing the resistance of the component.

In composite steel and concrete structures, a steel element and a concrete element are bonded together to act like one. The steel part in a composite structure is placed so that it will be subjected mainly to tension and the concrete to compression. There are various types of composite structures used in e.g. buildings and bridges. In buildings profiled steel sheet covered with concrete are often used as joists and composite columns are also common, examples of this can be seen in Figure 3-10. In composite beams steel beams attached to a concrete plate are common, see Figure 3-3. In order for a composite structure to work properly the forces must be transmitted between the different parts, either by interface forces as in the composite structures showed in Figure 3-10 or by means of mechanical shear connectors. This translation of force is called composite action.

3.2. Composite action

Figure 3-1 shows a composite beam loaded with a force F in midspan.

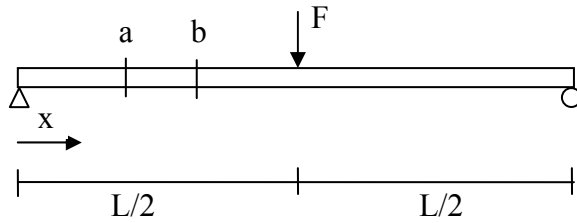


Figure 3-1. Transversal loaded beam

The moment distribution for the beam is

$$M = \frac{F}{2} \cdot x \quad \text{for } 0 \leq x \leq L/2 \quad \text{Eqn. 3-1}$$

$$M = \frac{F}{2} \cdot (L - x) \quad \text{for } L/2 \leq x \leq L \quad \text{Eqn.3-2}$$

The stress distribution from moment in a beam is shown in figure 3-2, and described as

$$\sigma = -\frac{M \cdot y}{I} \quad \text{Navier's formula}$$

I is moment of inertia.

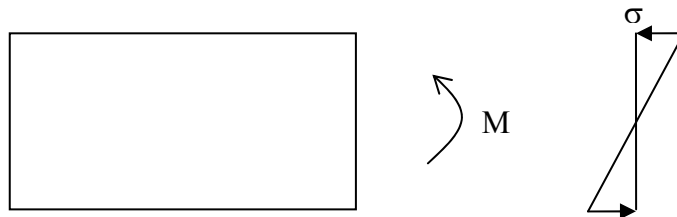


Figure 3-2 . Stress distribution in a beam

The points a and b in figure 3-1 are arbitrary in order to calculate the forces (F) in the interface between steel and concrete.

Multiplying the tension given by Navier's formula with area gives a force.

$$F_b = \int_{A_{\text{Concrete}}} -\frac{M_b \cdot y}{I} dA$$

Eqn. 3-3

F_b is the force in the steel concrete interface.

For a beam with constant M and I Eqn. 3.3 gives:

$$F_b = -\frac{M_b}{I} \int_{A_{\text{Concrete}}} y dA = -\frac{M_b \cdot \bar{y} \cdot A_{\text{Concrete}}}{I}$$

$$Q = A \cdot \bar{y} \Rightarrow F_b = -\frac{M_b \cdot Q}{I}$$

\bar{y} is defined as in figure 3-2.

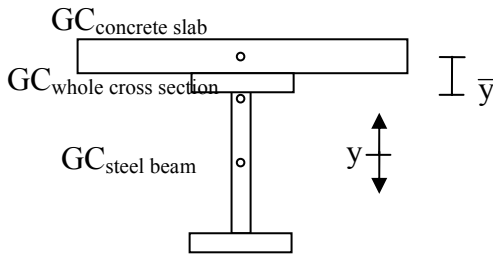


Figure 3-3. Definitions of parameters for a beam

If the moment varies along the beam $M_a \neq M_b$ (as the load in Figure 3-1) and $F_a \neq F_b$

$$dF = |F_b| - |F_a| = (M_a + dM) \frac{Q}{I} - (M_a) \frac{Q}{I} = \frac{dM \cdot Q}{I}$$

In order to get force per unit length dF is divided by $dx = x_a - x_b$.

$$\frac{dF}{dx} = q$$

q is denoted as the shear flow

$$q = \frac{dF}{dx} = \frac{dM \cdot Q}{I \cdot dx} = \frac{dM}{dx} \cdot \frac{Q}{I} = \frac{V \cdot Q}{I}$$

Shrinkage of the concrete and change of length due to different temperatures also give rise to longitudinal shear forces that must be added to the shear flow.

The shear flow has to be taken by the interaction between steel and concrete in order to get composite action (see Figure 3-4a). In the case where the steel and concrete does not work together at all the result is seen in Figure 3-4b). The different levels of composite action is to be described in chapter 3.2.2 to 3.2.4.

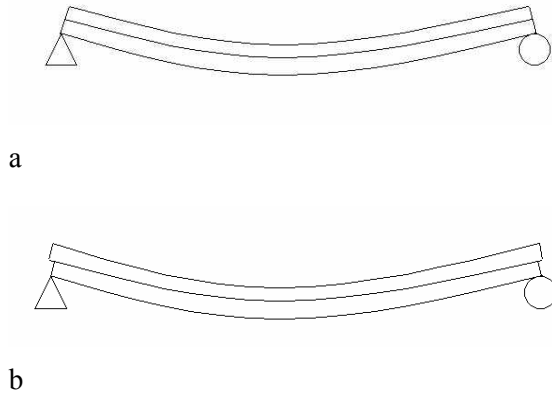


Figure 3-4. a) beam with composite action b) beam with no composite action.

3.2.1. Slip

When a composite beam, where the parts are not attached to each other, is loaded the concrete slab slide in relation to the steel element. In figure 3-5 a, before loading point B is in the concrete slab and point C is adjacent to point B in the flange of the steel beam. When the force P is applied point B moves $L + u_c$ and point C moves $L + u_s$. The difference in movement is called the slip, s. In the figure the slip is $s = u_c - u_s$.

When a beam is loaded as in Figure 3-1 the whole cross-section but the neutral axis is strained. The strain in the lower edge of the concrete is denoted ϵ_c . The slip u_c in the concrete is

$u_c = \int_L \epsilon_c dx$. In the same way the slip of the upper part of the steel beam is given by $u_s = \int_L \epsilon_s dx$. The slip strain is the rate of change of slip along the beam

and defined as $\frac{ds}{dx} = \Delta\epsilon = \epsilon_c - \epsilon_s$.

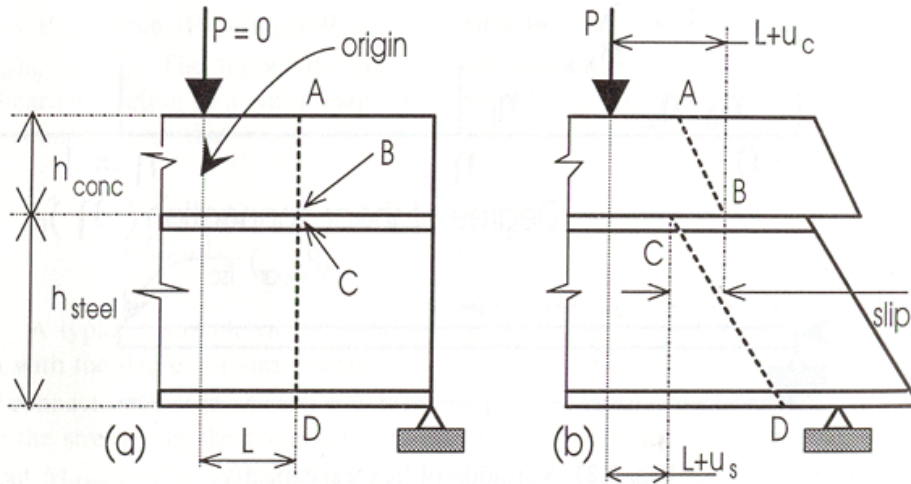


Figure 3-5. Slip, Taken from Oehlers & Bradford (1995)

The slip in a composite beam has to be resisted by longitudinal shear forces. These shear forces consist of frictional forces and adhesion between steel and concrete elements, and of forces introduced by mechanical shear connectors such as e.g. stud shear connectors, bolts, channels and ribs (see figure 3-8).

For steel beam and concrete slab to interact like one member there has to be interaction forces. When there is no adhesion, frictional forces or mechanical shear connectors between steel and concrete to prevent the slip in the composite member, this is called no-interaction.

When slip is totally prevented, it is called full composite action. In practise full composite action is very difficult to achieve and in most composite members the type of interaction can be denoted partial composite action, which means that a certain slip is unavoidable. In this project the only connectors considered is shear studs (see figure 3-8 a).

These three types of interaction are described in the next three parts.

3.2.2. No composite action

No composite (see Figure 3-4b) action in a beam arises where there are no connections between the components in a composite beam. This state is not considered in design, except for BV BRO, since the aim is to achieve composite action. The strains (ϵ) and stresses (σ) in a beam with no composite action are as shown in Figure 3-6. In no composite action the parts behave like two separate beams and have the neutral axis in the gravity centre of each part.

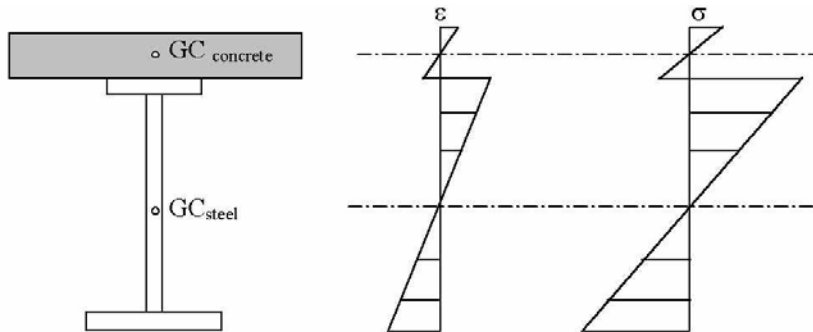


Figure 3-6. Strain and stress in a beam without composite action.

3.2.3. Partial composite action

Partial composite actions are the cases where the parts are partially connected to each other. In e.g. composite bridges a certain slip is necessary in order to transfer the shear, more about this in chapter 3.2, therefore this case is the most common. Stress and strain in these types of beams have the form shown in figure 3-7. The slip between steel and concrete gives a leap in the strain distribution for the cross section but not as big as in the case with no composite action.

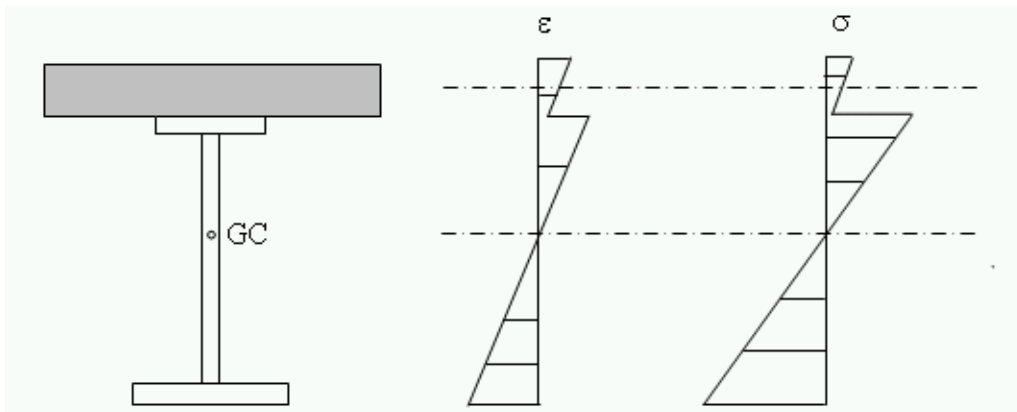


Figure 3-7. Stress and strain for partial composite action

For the mechanical shear connectors shown in Figure 3-8 to transmit shear force a certain slip has to be introduced. (due to Oehlers and Bradford 1995) The stud shear connector in Figure 3-8a is the most common in Swedish road and railroad bridges.

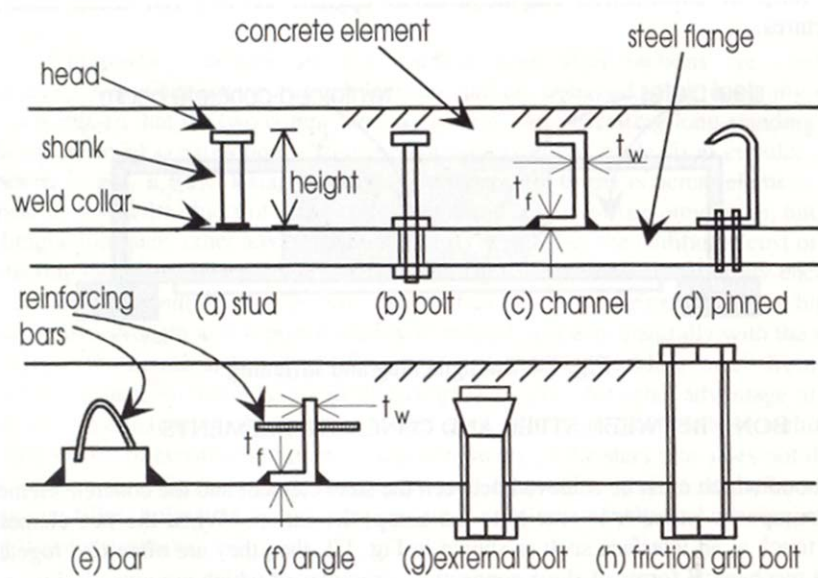


Figure 3-8. Shear connectors for composite action

3.2.4. Full composite action

Full composite action is, like it sounds, full interaction between steel and concrete. This means that no slip between the two parts is allowed. These connections are not common in Swedish road and railroad bridges, they are more common in joists for e.g. multi-story car park or industrial buildings and columns see figure 3-10. The stress and strain distribution can be seen in Figure 3-9. Composite structures where full composite action can be achieved are shown in Figure 3-10. These structures are mostly used in buildings.

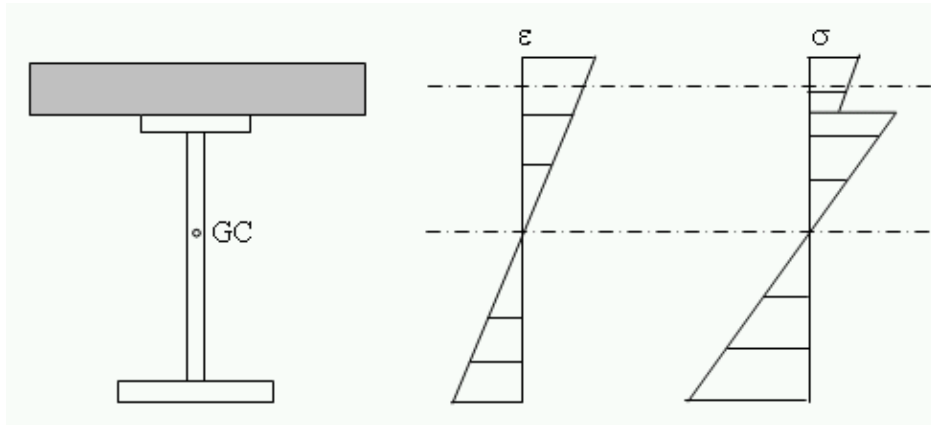


Figure 3-9. Stress and strain for full composite action

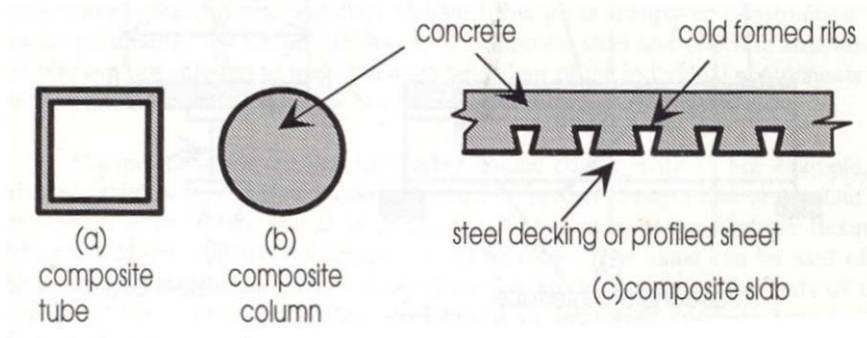


Figure 3-10. Full composite action members

3.3. Forces and failure modes of stud shear connectors

In the above descriptions all types of composite steel and concrete structures were considered, but in the following part the focus is on composite bridges. As shown in Figure 3-8 there are various types of mechanical shear connectors. Headed stud shear connectors are very common and also the only connector with strength specified in Eurocode and BRO 2002. In the scope of this project only headed shear studs are considered, therefore shear studs and stud shear connectors from here on refers to headed stud shear connectors.

In a composite beam where the interaction is achieved by means of stud shear connectors, the forces acting on the stud are sketched in Figure 3-11. This is a simplified model taken from Oehlers & Bradford (1995). The shank and weld collar of a shear stud is designed to resist longitudinal shear force, and the head is designed to

resist tensile forces normal to the steel/concrete interface due to separation of the concrete and steel.

In order for the stud shear connectors to start transmitting shear forces, a certain slip has to be introduced. This slip forces the shank of the stud to bear on to the concrete. According to Oehlers & Bradford (1995) the forces in the bearing zone can become as high as seven times the cylinder strength of the concrete. This is possible due to the tri-axial restraint imposed by the steel element, the shank and the surrounding concrete. The force F in the bearing zone of the concrete is horizontally resisted by the shear force in the weld-collar/steel flange interface. Since the bearing zone of the concrete has a certain height, the force on the shank of the stud acts with an eccentricity, and moment is introduced in the stud shear connector (F multiplied by e). The bending moment due to this eccentricity is balanced by a moment in the flange stud interface (F_e).

The resistance of the stud shear connector is called dowel action.

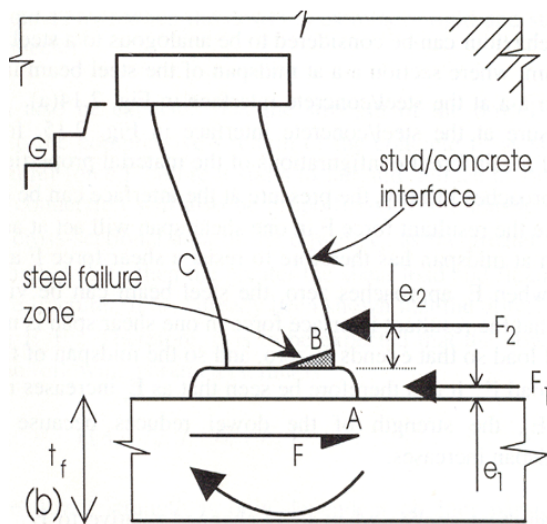


Figure 3-11. Failure zones for a stud shear connector. From Oehlers & Bradford (1995).

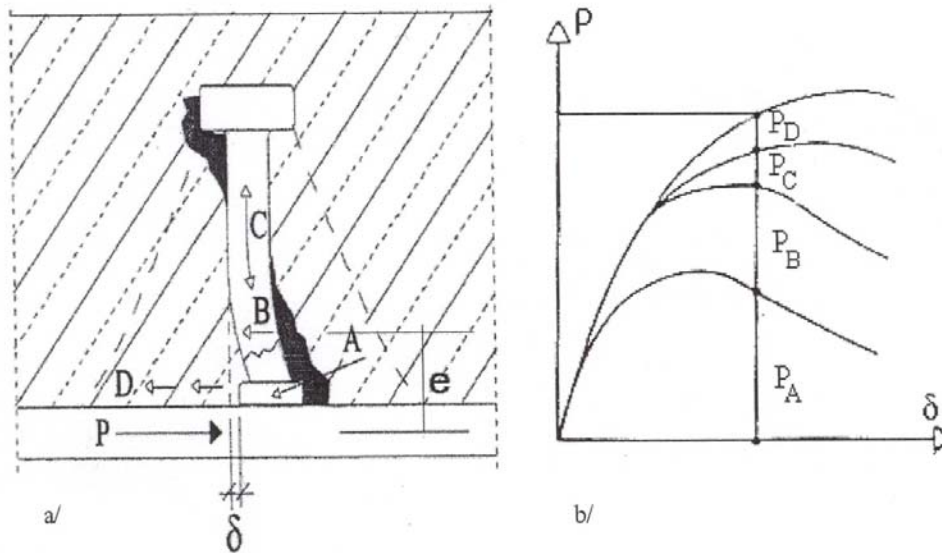


Figure 3-12a) Transfer of the longitudinal shear by dowel action. b) Schematic visualisation of contributions to the shear resistance.

Figure 3-12a shows a stud moving to the right. Figure 3-12b schematically show the active forces. P_A is the force acting on the weld collar; it is biggest in the beginning of the dowel action. When the concrete in front of the weld collar crushes the force resultant moves up and the value of P_A decreases. The force resultant acting on the stud shank, P_B give rise to an increasing bending moment, $P_B \cdot e$. P_C is the tensile force acting in the stud, as the bending moment increases so does the tensile forces. Compressive forces in the concrete lead to additional frictional forces in the interface between the concrete slab and steel flange, denoted as P_D .

The size of the bearing zone of the concrete is dependent of the ratio E_c/E_s . Keeping E_c constant and decreasing E_s (as is the case when the stud is cracking) means that the stud is more prone to bending, and so the height of the bearing zone is decreased as E_s decrease. If E_c is decreased (the case when the concrete cracks), the stud is less prone to bending, and so the height of the bearing zone is increased.

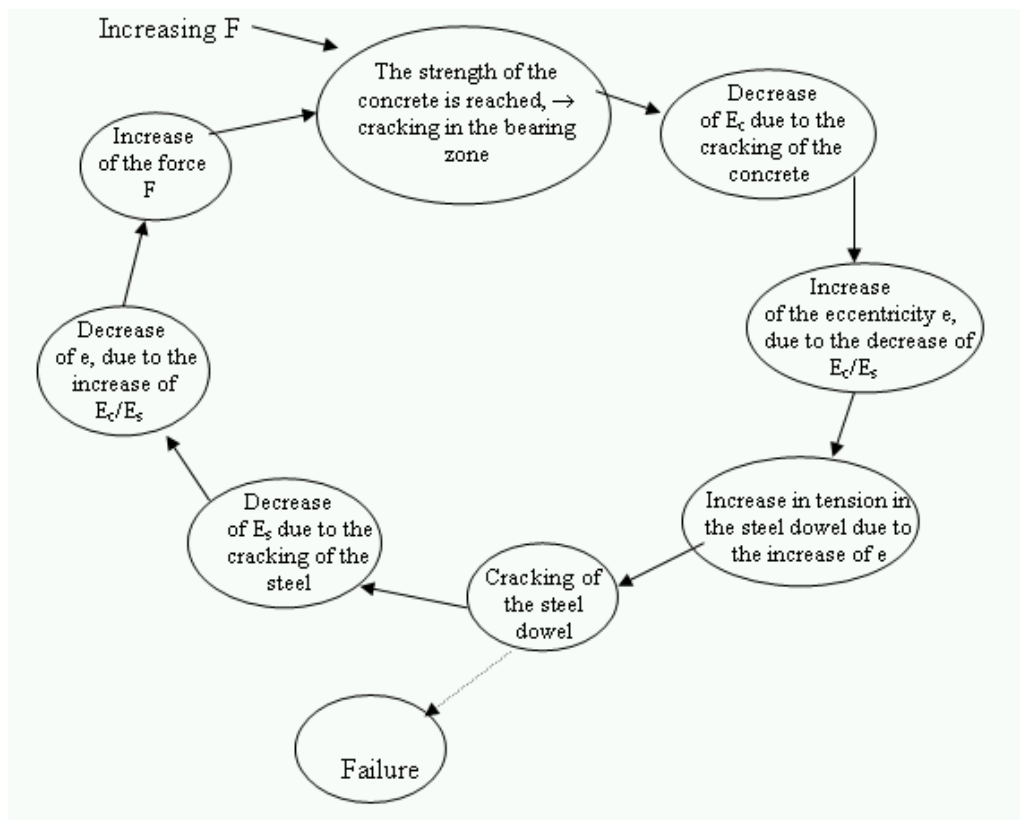
High compressive forces in the concrete bearing zone cause the concrete to crush.

The horizontal forces introduce shear forces, and the bending moment give rise to high tensile stresses in the weld-collar/shank interface where the steel failure zone is. Increasing the eccentricity e means introducing higher tensile stresses in the steel failure zone, and thus, decreasing the ration E_c/E_s decreases the strength of the dowel.

3.3.1. Static failure

During static loading three different modes of failure occur in a stud shear connector. All three types illustrate the strong interaction between the steel and concrete elements on the dowel action.

1. Concrete failure \rightarrow steel failure
Assume that E_s and E_c are constants. A force F is applied to the composite member.



2. Concrete failure \rightarrow no steel failure \rightarrow bending
In this case, a large volume of concrete crushes, but the steel is strong enough to withstand the increase in tension by $F \cdot e$ and is bent over.
3. Steel failure \rightarrow concrete failure
The same mechanism as in 1) but the steel starts to fail before the concrete, decreasing E_s and increasing e , which lead to increased bearing pressure in the concrete and eventually cracking of the concrete and so on.

When a shear load is applied to a stud shear connector, according to figure 3-12, the shank is bent and cause the head of the stud to rotate in an anti-clockwise direction. This rotation give rise to tensile cracks in the concrete in G, which in turn allow an increase in the bending of the shank and rotation of the head, and hence the tensile stress of the shank in B.

3.3.2. Fatigue failure

During fatigue loading there are four different modes of failure in a stud shear connector.

1. The first failure mode and also the most common is when a crack starts in the weld collar/shank interface (point B in Figure 3-11) and propagates in one of three different ways according to Figure 3-14. This failure mode is introduced because of discontinuities in the connection between weld and shear stud.
2. The second failure mode is when a crack starts in the weld collar/flange interface (point A in Figure 3-11) and propagates across the flange of the beam during fatigue loading. This failure mode has the same background as failure mode one.
3. The third failure mode is a crack starting in the middle of the shank (point C) due to tension in the shear stud. This tension comes from the fact that the stud is bending but the head of the stud is constraint from bending in all directions because of the embedment in concrete.
4. The fourth failure mode is a combination of failure mode one or two and failure mode three. This failure mode allows the shank between A and C (in Figure 3-11) to rotate to a more horizontal position.

Figure 3-15 show the failure of one shear stud in the endurance test performed by Bro & Westberg. This failure is clearly of mode 1, and when comparing it to Figure 3-14 it is clear that it has taken path 1.

3.3.2.1. Mechanisms of fatigue failure

Consider the forces on a shear connector subjected to cyclic loading with a constant load range. Using the assumption that fatigue cracks are the main cause of failure for the connector and using Paris' equation gives that the stress intensity factor (defined in chapter 4) is the main parameter affecting the crack growth per cycle. This stress intensity factor is also a function of the energy release rate referred to as G in Figure 3-13. There are two simplified ways to see the forces on the shear stud.

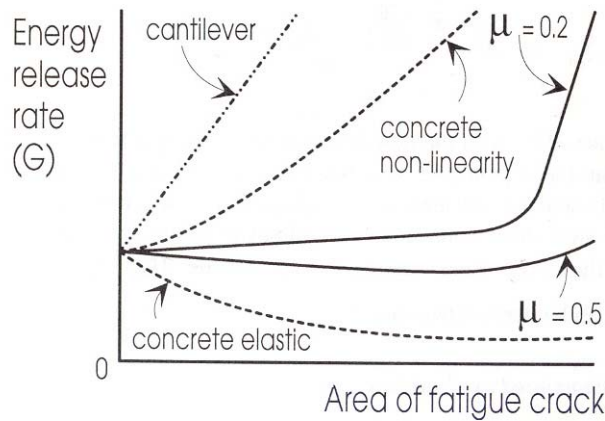


Figure 3-13. Energy release rate for different approaches on shear studs.

The first way is to assume the shear stud as a cantilever not encased in concrete. The force will act on the stud as in Figure 3-11 and the eccentricity e remains the same during loading. Cyclic loading will cause a crack to start at the interface between shank and weld or between weld and flange and propagate into the shank or flange. The crack propagation will reduce the area of the shank which means that the stress range will increase and that means increasing the crack propagation (or G) seen in Figure 3-13. An increasing crack propagation rate means a rapid loss of strength of the shear connector.

The second way is to see the stud as a steel beam supported by elastic concrete. The forces acting on the shear stud are as shown in Figure 3-11. If the concrete is assumed to be elastic it can resist any stress and does not crack. When the shank of the stud cracks the eccentricity, e , is reduced and the energy release rate and crack propagation will be reduced. This is an ideal mechanism, in reality the area of concrete resisting F reduces and the compressive stresses in the concrete increase and the concrete crushes. The crushing of concrete means that the energy release rate increases which means increasing crack propagation rate and loss in fatigue life. In reality friction between the shank of the stud and concrete resist opening of the crack which leads lower crack propagation rate and a higher fatigue life.

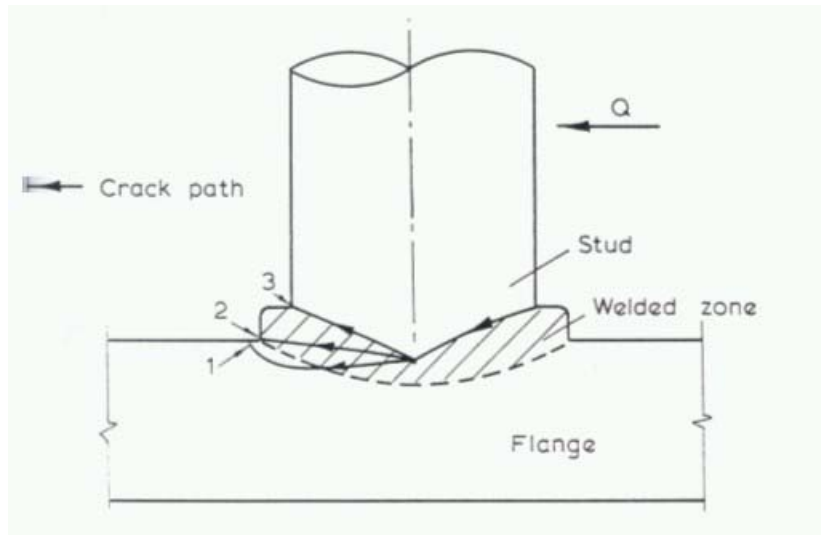


Figure 3-14. Different propagation for failure mode 1 (from Hallam(1976)).

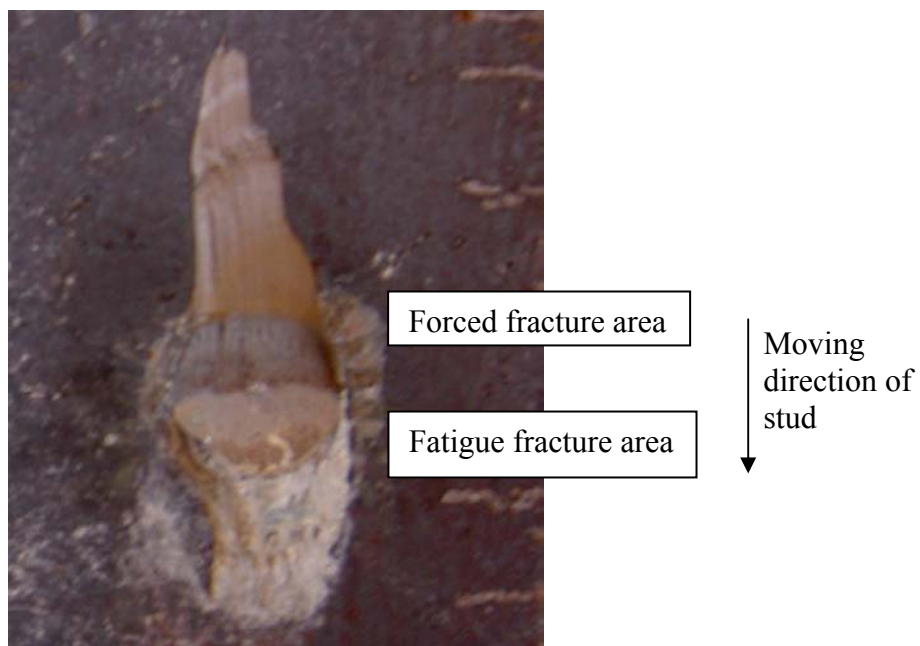


Figure 3-15. Failure of shear stud in endurance test by Bro & Westberg.

3.3.2.2. Shear resistance of studs according to Oehlers & Johnson

According to Oehlers & Johnson (1987), Ollgaard, Slutter and Fisher (1971) used statistical analysis to derive an equation for the static strength of a stud shear connection. Their result was

$$P_{Rd} = 0,5 \cdot A_{sh} \sqrt{f_c \cdot E_c}$$

but this equation is made for the steel tensile strength of 486 MPa.

Oehlers and Johnson (1987) modified the work done by Ollgaard, Slutter and Fisher (1971) in accordance with results from Hawkins (1973), which resulted in the following prediction equation for the dowel strength of stud shear connectors in push tests:

$$(D_{max})_{push} = \left(5,3 - \frac{1,3}{\sqrt{n}} \right) A_{sh} f_u^{0,65} f_c^{0,35} \left(\frac{E_c}{E_s} \right)^{0,40} \quad \text{Eqn. 3-4}$$

3.4. Push tests

Push test are a type of testing for shear connectors used in order to evaluate the static strength, residual strength (static strength after fatigue loading) and fatigue endurance. Testing is essential in order to design composite structures, because empirical results are the only way to get design values.

In a composite beam the studs are loaded indirect due to the flexural forces from bending of the beam. The force on a connector is not directly proportional to the load applied to the beam, but depends on the stiffness of various components in the composite beam. It is therefore difficult to know the exact force on each connector from composite beam tests. Instead push-out specimens, where the shear studs are loaded directly and the load applied to the specimen is resisted by shear in the studs. The forces introduced in a push-out specimen are not exactly the same as those in a composite beam, and so the strengths and failure modes can be somewhat different.

Push tests can have different forms as shown in Figure 3-16.

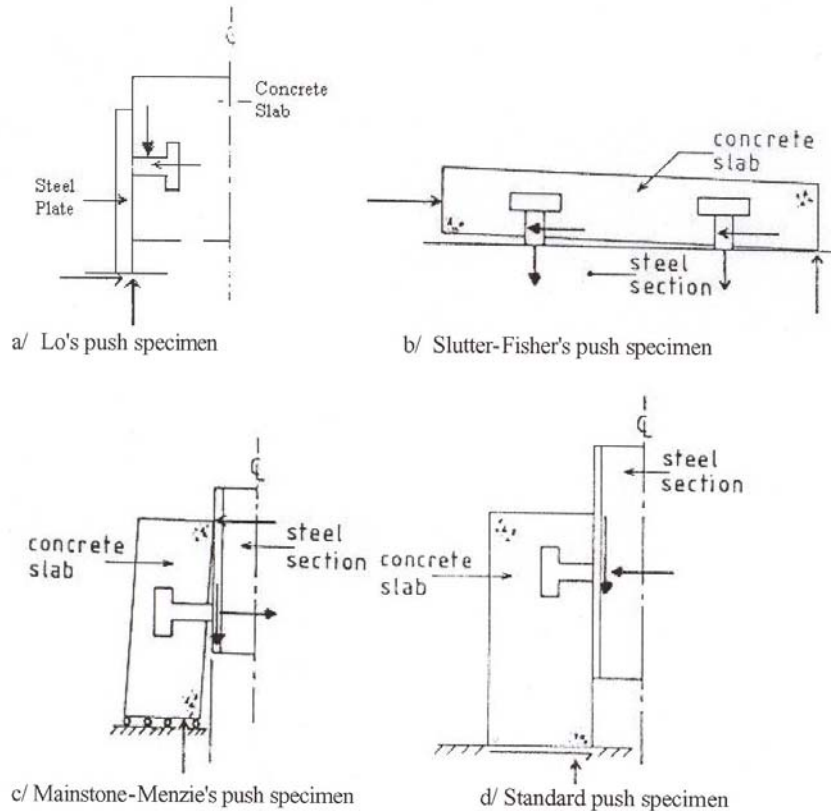


Figure 3-16. Different push test set up

As seen in Figure 3-16 there are forces that tend to pull the concrete and steel apart. In a real structure the vertical load is applied on top of the concrete and the steel and concrete will be pushed together. Analysis in Oehlers & Johnson (1987) show strong interaction between axial force and shear force on a stud; in tests with axial tensile forces on the shear studs the static strength was 81 % of that where no axial tensile forces were present. In a test set up, that will simulate forces acting on the shear connector, the separation between the slabs and steel part, and thus the axial tensile forces, should be prevented. The test set up used in this project is based on the test set up recommended in EC4 (see figure 6-1), more detailed test set up for this project is in chapter 6.

Oehlers & Johnson (1987) showed that push-specimens with a single row of studs have virtually no capacity to redistribute the force, and will thus fail at the strength of the weaker connection. A push-specimen with more than one row of studs can redistribute the force and will fail at the mean strength of the studs. Figure 3-17 show a schematic presentation of the behaviour of three brittle connectors, A, B and C. When a slip s_1 is applied, connector A will fail at a force P_A . The whole force applied

will then be taken by connector B and C, and they will immediately fail as their limit is reached. If the connectors are instead ductile, connector A will reach its maximum capacity and start to deform plastically. As connector A still keep the maximum force, the others will reach their maximum capacity one after one and continue to deform plastically. When all connectors have reached their maximum capacity the structure will fail and the maximum load will thus be the mean strength of the connectors. Connectors are seldom perfectly ductile, and so the truth is somewhere between ductile and brittle.

The necessity of ductile connectors that can redistribute the force among themselves in a bridge is obvious.

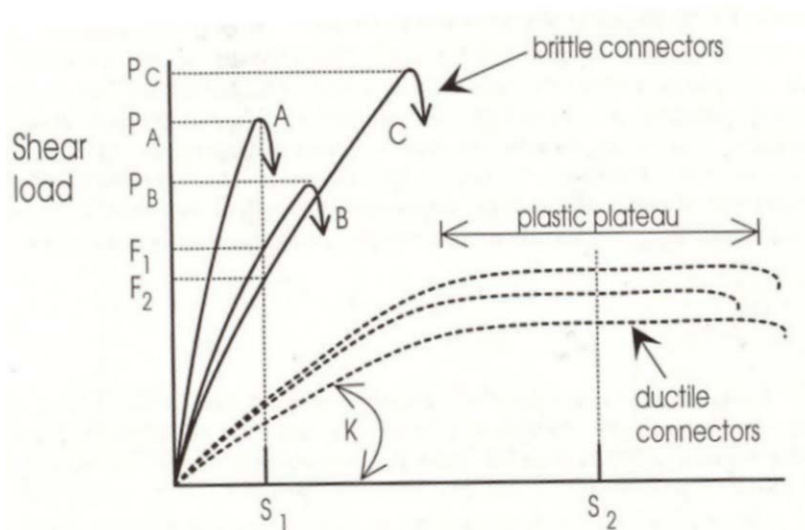


Figure 3-17. Load/slip characteristics of shear connectors. (from Oehlers & Bradford)

4. Fatigue

In this chapter the following parts are included:

Introduction to fatigue, in which a basic introduction to the fatigue problems are described.

Short overview of elastic fracture mechanics, in which the general cases of cracking, stress intensity factors and fatigue crack propagation for structural steel elements are described.

Factors governing the fatigue life, in which the effect of material and loading properties for structural steel elements applicable to steel as well as other materials are described.

Fatigue testing, in which endurance testing, accumulated damage and residual strength based testing procedures are described. This part is general for all fatigue testing procedures.

4.1. Introduction to fatigue

Fatigue is a process in which a material is subjected to a cyclic load, eventually resulting in failure even if the maximum load is well below the elastic limit of the material. The phenomenological details of the fatigue process differ from one material to another, and this chapter focuses mainly on the fatigue degradation of steel. In a structural component undergoing cyclic load, cracks will be initiated and start to propagate. The propagation of cracks reduces the stress-bearing area of the structure, and when the tensile strength in the remaining stress-bearing area is exceeded failure occur. Fatigue failure is caused by tensile stresses alone, since only tensile stresses cause a crack to open and propagate. Despite this, caution need be taken to compressive forces as well, since they may introduce tensile stresses.

In short the fatigue life of a steel member can be divided into three steps; initiation, propagation and failure. These steps are to be described more in detail.

1. Initiation

For smooth and mildly notched parts subjected to small load cycles this part of the fatigue life can be 90 % of the total life. In most cases the initiation process is concentrated to a small area of high local stress.

In smooth-surfaced parts subjected to cyclic loading, dislocation and deformations of crystallographic planes result in a roughening of the surface. Due to this process, numerous micro-cracks grow along slip planes. Continued cyclic loading cause some of these micro-cracks to merge together and form a few dominating cracks. The magnitude of stress at the toe of these larger cracks is very high and causes them to propagate more rapidly.

In welded structures, such as shear studs, the cracks will almost certainly start to grow from welds. Due to minute metallurgical discontinuities left from the welding process, the initiation part of the fatigue life is almost non-existent.

2. Propagation

When cracks have been initiated, they will start to propagate. To get some insight into this phase, a short introduction to fracture mechanics is given in chapter 4.1.

3. Failure

When the cyclic load has caused the cracks to propagate to a length such that the resistance is smaller than the applied load, failure is inevitable. This length is called the critical crack length.

4.2. *Short overview of elastic fracture mechanics*

The basis of the elastic fracture mechanics was developed during the 19th and 20th century, when problems with brittle fracture and fatigue cracking in several structures, such as ships, pipelines and storage tanks.

The very base of the fracture mechanics was laid in 1921 by Griffith. His theory is true for wholly brittle materials.

The Griffith criterion states that crack growth result in an elastic energy release, and that crack propagation will occur only if the energy released upon crack growth is enough to provide the energy required for crack growth. From this discussion it can be

$$\text{shown that the condition for crack growth is } \frac{dU}{da} = \frac{2\pi\sigma^2 a}{E} \quad \text{Eqn. 4-1}$$

where U = elastic energy

For crack growth to occur, the stress must reach a certain critical value, σ_c .

$$\sigma_c = \sqrt{\frac{E \cdot G_{lc}}{\pi \cdot a}} \quad \text{Eqn. 4-2}$$

where G_{lc} is the elastic energy release rate per crack tip defined as

$$G_{lc} = (1 - \nu^2) \frac{K_{lc}^2}{E} \quad \text{Eqn. 4-3}$$

The following part is focused on fracture mechanics of materials which could develop some plastic deformation and is general for most metals, but focuses on steel structural members.

4.2.1. General cases of cracking and stress intensity factor

The important region from the crack propagation point of view is the crack tip. In a non-cracked element subjected to a tensile force the stress field is uniformly distributed, but in a cracked element the stress flow that would normally pass through the cracked part will “go around” the crack. The stress-field will not be uniformly distributed, but will be much higher in the vicinity of the crack tip and more or less the magnitude of stress in an un-cracked element at a large distance from the crack.

In linear-elastic fracture mechanics the magnitude and distribution of the stress field around a crack tip is described in terms of the stress intensity factor, K .

The stress intensity factor is related to the nominal stress level in the member and the size and orientation of the crack. Three types of cracks are usually used to establish equations for stress intensity. The superposition of these modes describes the general case of cracking. Figure 4-1a shows an infinitesimal element containing a crack front, where normal stresses give rise to mode I or “opening mode” cracks, in plane shear to mode II or “sliding mode” and out-of-plane shear to mode III or “tearing mode”.

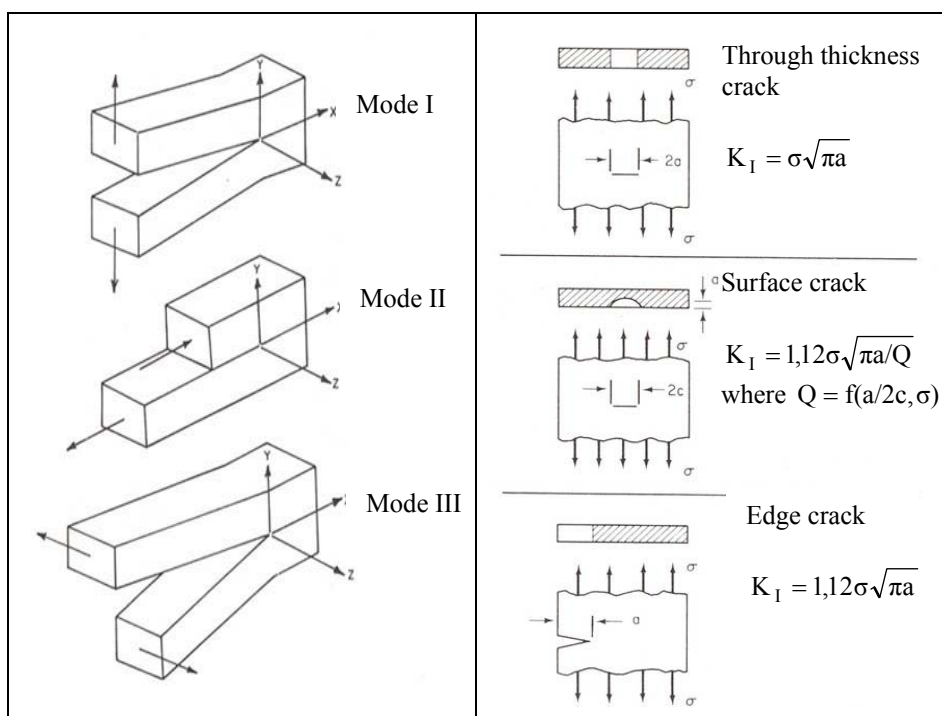


Figure 4-1.a) The basic modes of cracking. b) Examples of stress intensity factors for various crack geometries. (From Rolfe & Barsom)

The stresses for the different crack modes are established as

$$\sigma_{ij} = \frac{K_n \cdot f(\Theta)}{\sqrt{2 \cdot \pi \cdot r}} \quad \text{Eqn. 4-4}$$

where K_n is the stress intensity factors K_I , K_{II} and K_{III} that corresponds to mode I, II and III, respectively, and r and Θ are defined as in Figure 4-2.

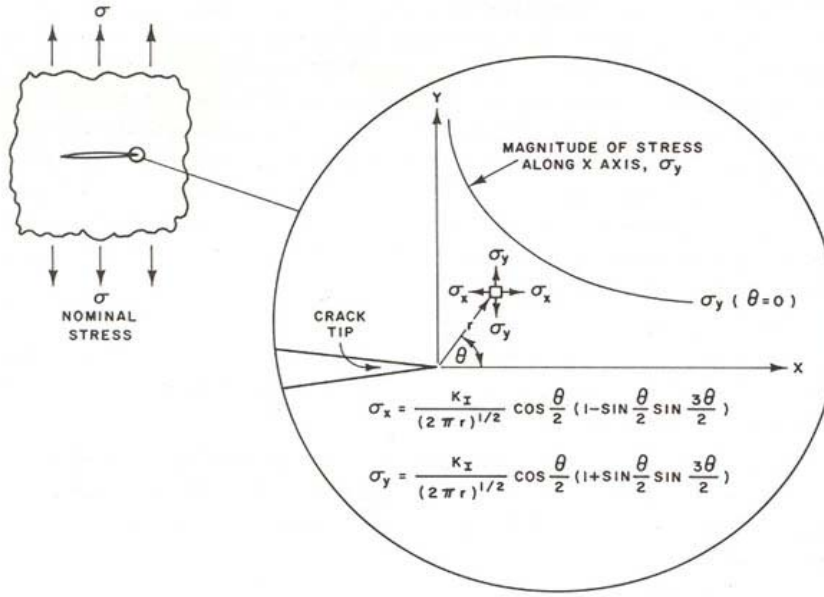


Figure 4-2. Elastic-stress-field distribution ahead of crack (From Rolfe & Barsom).

The stress intensity factor depends on for example effects of free surface, width and shape of the crack and the stresses acting on the crack. Figure 4-1b shows some examples of different stress intensity factors.

Putting $r = 0$ and $\theta = 0$ in eqn. (4.4) gives $\sigma = \infty$, which for real materials is obviously absurd. What in fact happens is that the material at the crack-tip yields as soon as the load is applied, and as the load increases the plastic zone enlarges. This does not invalidate the methods of linear elastic fracture mechanics provided that the plastic zone is small compared with the crack length and with the distance to a free surface.

Crack extension will occur when the stress intensity factor reach a critical value. The limit in static loading cases is K_{Ic} and in dynamic loading is K_{Id} . The values of K_{Ic} and K_{Id} are called the toughness of the material. The material toughness is dependant of material, temperature and loading rate and has to be determined from experiments. At a specified temperature and loading rate of a specified material the critical stress intensity factor or material toughness is

$$K_{Ic} \text{ or } K_{Id} = C \sigma \sqrt{a} \quad \text{Eqn. 4-5}$$

where

C = constant, function of crack geometry (see e.g. Figure 4-1b)

σ = nominal applied stress

a = crack length as a critical dimension for a particular crack geometry

The maximum flaw size in a structural member is thus

$$a = \left[\frac{K_{Ic} \text{ or } K_{Id}}{C \cdot \sigma} \right]^{1/2} \quad \text{Eqn. 4-6}$$

An example taken from Rolfe & Barsom (1977) show the meaning and use of the stress intensity factor:

Example 4.1

Assume that the material being analyzed has a K_{Ic} value at the service temperature of $1740 \text{ MPa}\sqrt{\text{mm}}$ and yield strength of 700 MPa. A through thickness crack then gives

$$K_{Ic} = \sigma \sqrt{\pi \cdot a} \quad \text{Eqn. 4-7}$$

and in Figure 4-3 the critical crack size at different levels of the nominal stress are plotted for this value of K_{Ic} .

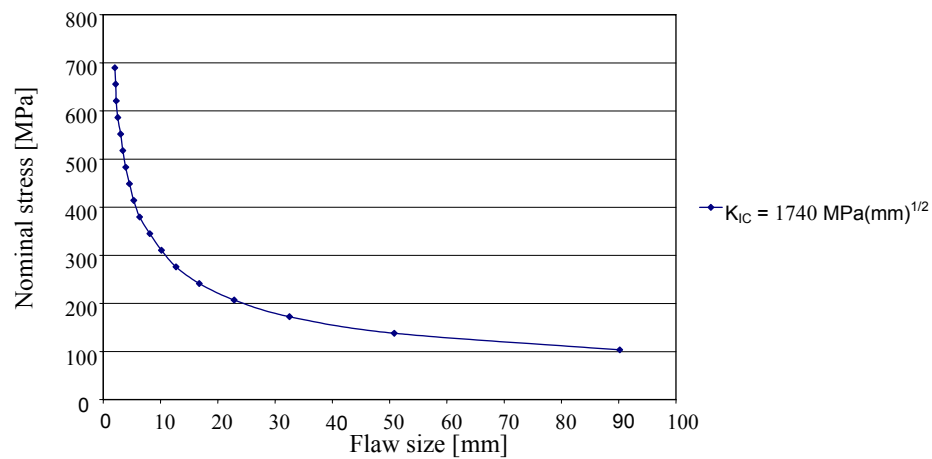


Figure 4-3. Stress-flaw-size relation for through-thickness crack in material having $K_{Ic}=1740 \text{ MPa}\sqrt{\text{mm}}$. (from Rolfe & Barsom).

Figure 4-4 shows the relationship between material toughness, K_{Ic} , nominal stress, σ , and crack size, a . If the value of K_I , which is a combination of a particular crack size and stress level reaches the level of K_{Ic} , fracture can occur.

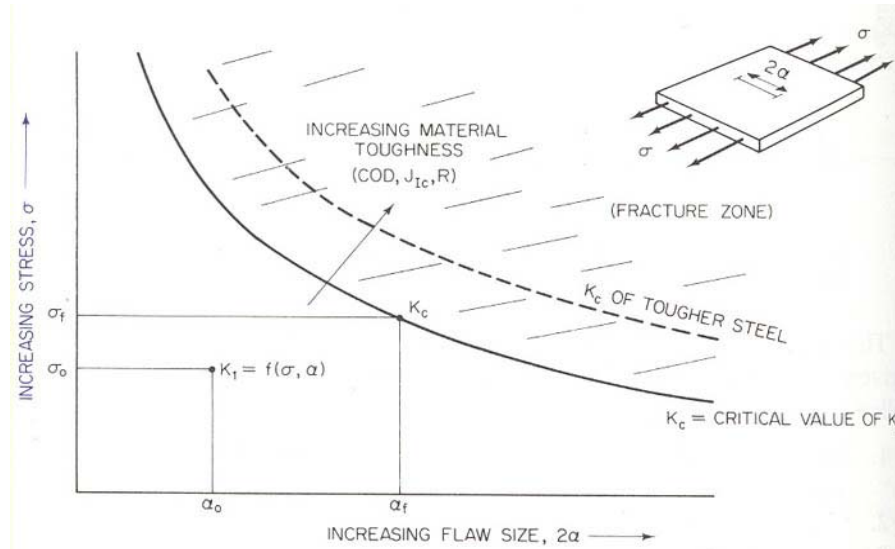


Figure 4-4. Schematic relation among stress, flaw size and material toughness (from Rolfe & Barsom).

4.2.2. Fatigue-crack-propagation threshold

For a fatigue load varying between a maximum value, σ_{max} , and minimum value, σ_{min} , the stress intensity factor varies between K_{max} and K_{min} and thus over a range $\Delta K = K_{max} - K_{min}$.

For members containing cracks from the start of a fatigue loading, and for members where cracks are initiated during the fatigue loading, there exists a fatigue-crack-propagation threshold. Below this threshold-value existing fatigue cracks will not propagate. The threshold is dependant on the ratio of the stress-intensity-factor fluctuation, ΔK_I , and the square root of the tip radius of the crack, $\Delta \rho$, as is shown in Figure 4-5.

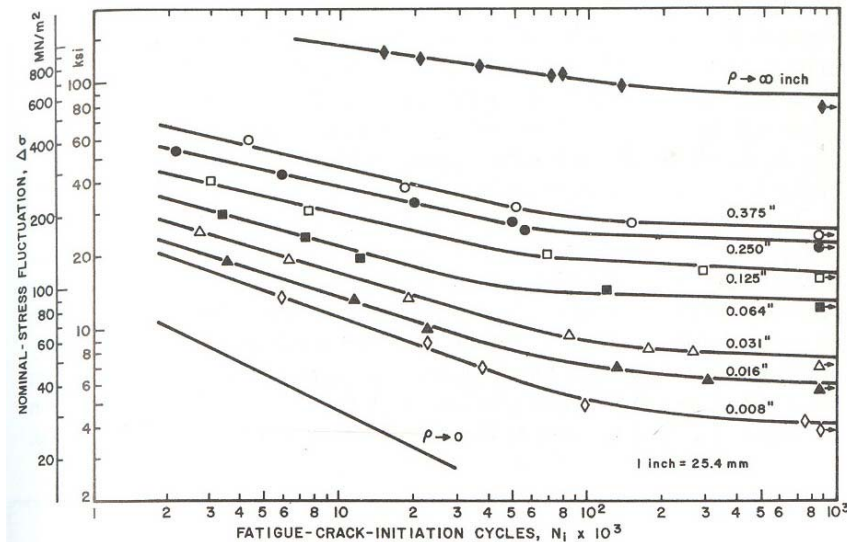


Figure 4-5. Dependence of fatigue-crack initiation of HY-130 steel on nominal-stress fluctuations for various notch geometries (from Rolfe & Barsom).

4.2.3. Fatigue crack propagation

When ΔK is above the threshold value, cracks will propagate due to the fatigue loading, and eventually cause the fracture of the structure.

In non-destructive testing and inspections, the size of cracks is important. There is a limit to the size of cracks that can be detected. To decide the period between the inspections of a structure, the cracks must be assumed to be the biggest non-detectable. Based on this assumption the shortest time for a crack to grow to a size that affects the strength of the structure is known, and thus the maximum period to the next inspection.

Figure 4-6 show a plot of the crack length of a member versus the number of load cycles. It clearly shows that the rate of growth of the crack length is increased as the crack length is increased. This means that the crack spends most of its life as very small, and grows to a considerable length only in the last, short, stage of its life.

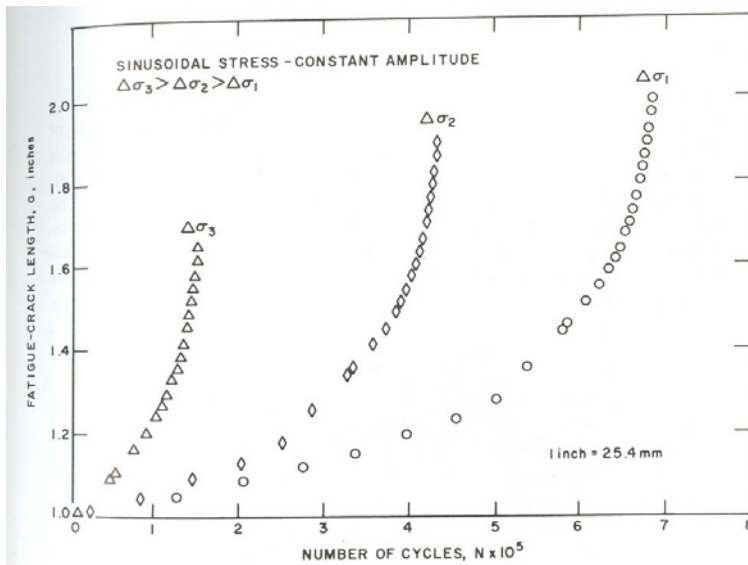


Figure 4-6. Schematic figure showing the effect of cyclic-stress range (see chapter 4.3.2) on crack growth (from Rolfe & Barsom).

These curves reduce to one single curve if represented in terms of crack-growth rate per cycle of loading, da/dN . The most common way of presenting the fatigue-crack-growth data is a $\log \Delta K - \log da/dN$ -curve, as shown in Figure 4-7.

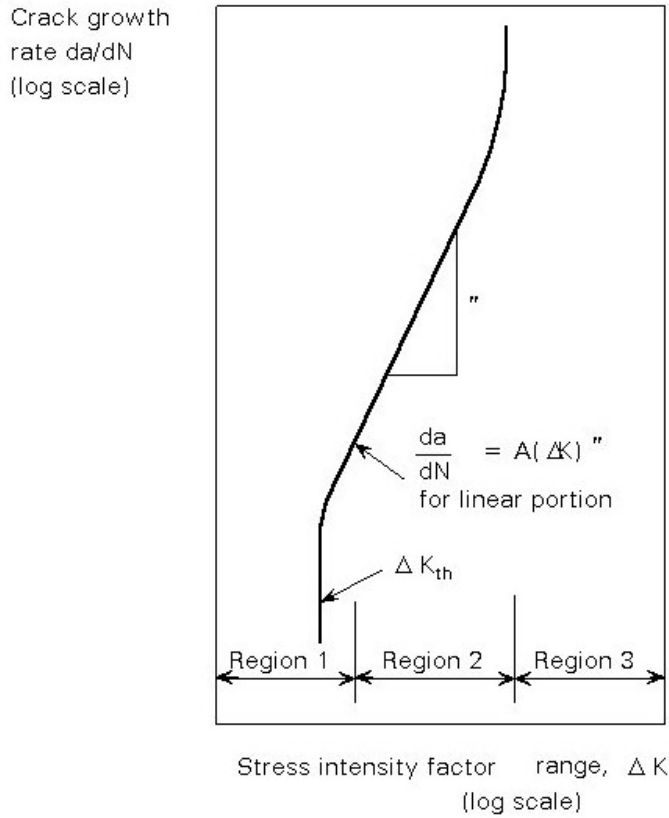


Figure 4-7. Crack growth curve (from *Advanced introduction to fatigue*)

The crack-growth curve consists of three regions. In the first region crack propagation does not occur since ΔK is below the fatigue-crack-propagation threshold.

Paris proposed an empirical equation to express the fatigue crack growth rate $\left(\frac{da}{dN}\right)$ as a function of the stress intensity factor range (ΔK). In the second region he described the curve as

$$\frac{da}{dN} = f(\Delta K) = A \cdot (\Delta K)^n \quad \text{Eqn. 4-8}$$

where A and n are constants,

known as the Paris power law. This description has proved to be a good estimate when applied to simple as well as more complex structures.

The behaviour in region 3 is somewhat more complicated and the fatigue-rate transition from region 2 to region 3 depends on K_{max} and on the stress ratio, R .

The slow propagation of a crack gives a smooth crack surface containing so called striations that can be seen in an electron microscope. The striations in an aluminium alloy is shown in Figure 4-8a, the striations in a steel alloy are similar. Figure 4-8b shows the failure zone of a shear stud from experiment d2 performed in this project. The smooth region on the right is the fatigue fracture zone. The failure zone is the bright irregular region to the left. The size of the failure zone gives information of the force at failure. If the failure zone is e.g. 60 % of the area of the shank, the force at fracture was approximately 60 % of the static strength of the stud.

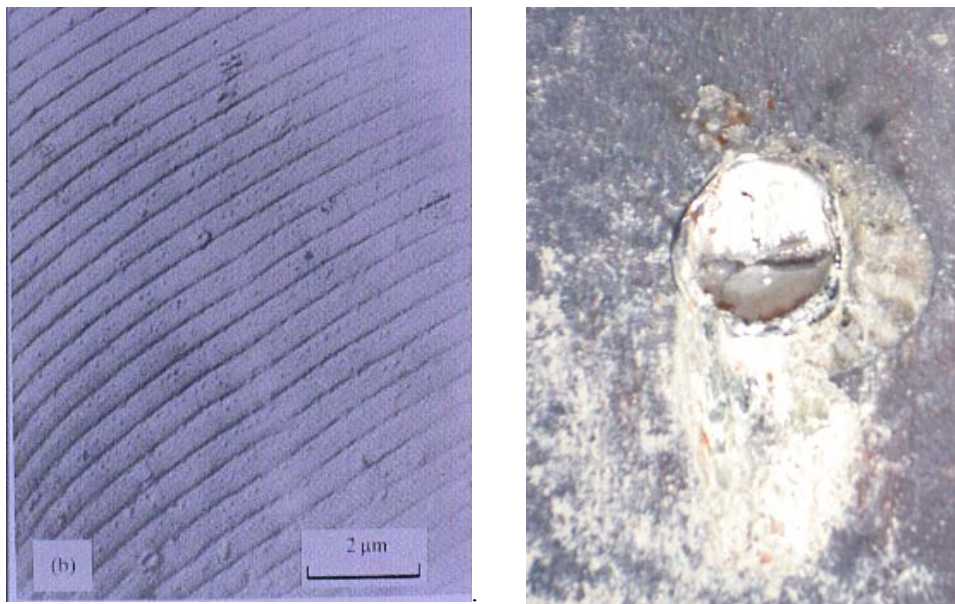


Figure 4-8a) Striations in an aluminium alloy. b) Failure zone of stud in test 2d.

4.3. Factors governing the fatigue life

Full scale models of structural elements often appear to have poorer fatigue strength than small test specimens tested in laboratory. The possible difference in fatigue life in laboratory test and in full scale structural elements can be explained by the various factors that influence the fatigue life.

4.3.1. Material properties

Material properties affect the fatigue resistance in various ways and the most important properties are described here.

4.3.1.1. Effect of static strength

The fatigue limit for high-cycle fatigue (10^6 to 10^7 cycles) is for unnotched, polished specimens about 50% of the ultimate tensile strength for the material.

For notched parts the ultimate strength of the material has less influence on the fatigue (see Notch effect), for high strength materials this effect is stronger than for ordinary materials. For fatigue life on notched parts the crack growth is the main parameter and the static strength does not influence the fatigue life that much.

4.3.1.2. Crack growth data

The crack growth is less dependent on static strength than crack initiation. A comparison, made by Barsom (according to Advanced Introduction to Fatigue), of crack growth for steel with yield strength ranging from 250 to 2000 MPa found that grouping the steel according to micro structure would minimize scatter in experimental analysis.

4.3.1.3. Notch effect

Notch is a discontinuity in the material that comes from e.g. welds or holes for bolts or rivets. Notches can also come from mechanical influence which have the same effect as notches from e.g. welding.

Fatigue life is affected if the part is notched, the notch is acting like an initiation of a crack. The effect of a notched part is that the initiation phase does not exist which means that the fatigue life is reduced. For sharply notched parts the ultimate tensile strength does not influence the crack propagation at all, example on sharply notch parts are welded joints which contains small crack like defects where the crack starts growing almost instantly.

4.3.1.4. Size effect

One important fact when performing fatigue tests is so called size effects; increasing the size of a structure generally gives a lower resistance to fatigue. This means that the specimens tested in laboratory will generally have a higher resistance than the structure in use, since the test specimens are as small as possible. The size effect comes from the stress concentrations appearing when e.g. welding.

4.3.1.5. Residual Stress effect

Residual stresses may affect the fatigue life in both increase or decrease fatigue of the life. Increase of fatigue life appears when the residual stresses have the opposite direction than the stress that is causing the crack propagation. If the residual stress has the same direction as the stress that cause the crack propagation the fatigue life is reduced. In the case of shear studs welded to a flange the effect of residual stresses in the flange is less important, since the cracks will most certainly be initiated in the weld or the area affected by the welding.

4.3.1.6. Effect of Corrosion

The effect of corrosion on fatigue life is seen in Figure 4-9. Corrosion can take place if the structure is subjected to e.g. water. The corrosion can have large effect on fatigue life for a structure. Effects of corrosion appear in structures where the time between cycles is so big that the crack surface can be affected by the water. When water and oxygen get in contact with the crack surface a part of the un-cracked part gets affected and the crack grows bigger and the fatigue life gets shorter (see Figure 4-9). According to Advanced Introduction to Fatigue (2004-02-19) the effect of corrosion is biggest on un-notched specimens, which is shown in Figure 4-10.

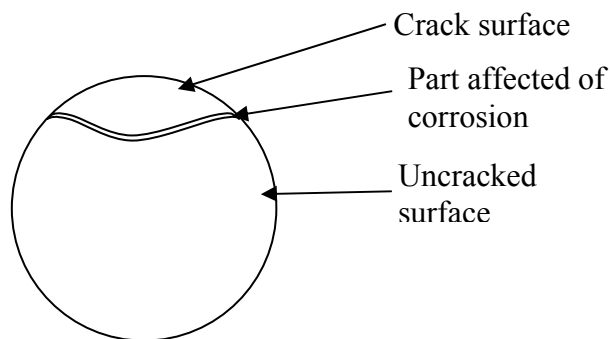


Figure 4-9. Principal figure for corrosion effects for fatigue

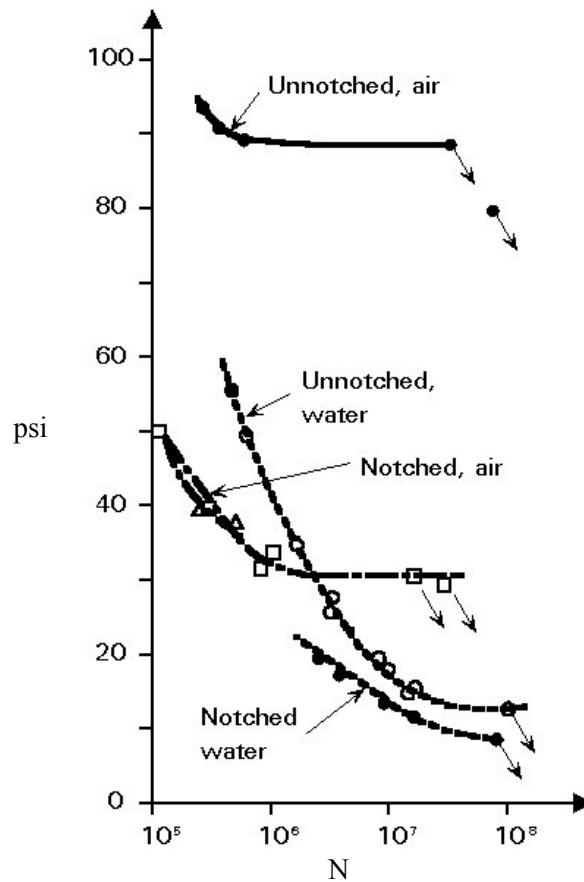


Figure 4-10. Effects of corrosion for fatigue life (from *Advanced introduction to fatigue*).

4.3.2. Load properties

Effects of loading for fatigue life are described in this chapter.

4.3.2.1. Load Range

Load range (referred to as R) is the difference between peak load (P_{\max}) and trough load (P_{\min}) se figure Figure 4-11.

Load range in a real structure is important to control because in laboratory tests the load range is defined as input data.

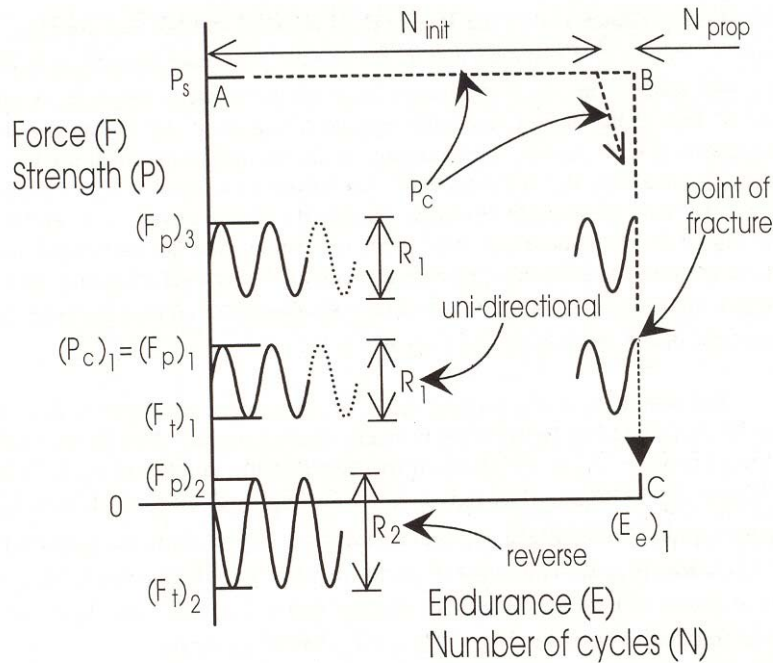


Figure 4-11. Schematic figure of fatigue strength during fatigue testing (from Oehlers and Bradford)

In a real structure the load often varies and the assumption that the load have a constant range and a constant peak load is not accurate. The best way to get a good estimation of a real problem is to know how the loading has been or will be, then count the numbers of cycles with a specific range and peak load and do test according to this data. To do this kind of test a big part is to determine the loading condition. Many tests carried out around the world are made with constant peak load and constant range. These types of testing is accepted for fatigue testing due to the problems with collecting data for more exact testing and it have been seen that this type of testing gives good results.

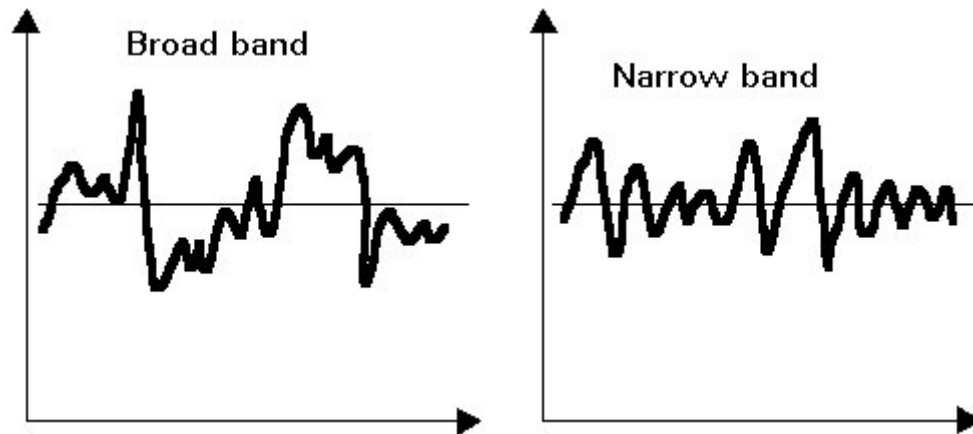


Figure 4-12. Different loading types (from *Advanced Introduction to Fatigue*)

The effect of a change in load range means that the endurance changes which is described in chapter 4.4.2.

4.3.3. Peak load

Peak load (P_{\max}) is the maximum load applied in a load cycle referred to as F_p in Figure 4-12. The peak load affects the life of a structure, but it does not affect the rate of degradation. More about this in chapter 4.4.3

4.3.3.1. Unidirectional and reverse loading

Unidirectional load is a load where both peak load and trough load have the same sign. Reverse loading is a load where peak load and trough load have different sign (see Figure 4-11). For steel only fatigue loading in tension is causing cracks in the material. The effect of reverse loading is that the specimen can take a higher number of cycles than a specimen exposed to unidirectional loading. For a shear stud the effect will be that cracks will arise on both sides of the shear stud as shown in Figure 4-13.



Figure 4-13. Example of Unidirectional and reverse loading (intro fatigue)

4.4. Fatigue testing

As described in the previous chapter, fatigue life is governed by many factors and the combined effects of these factors are very difficult to predict. The safest way to obtain design data is therefore to perform fatigue tests on components under realistic conditions.

One problem with fatigue testing is the large scatter of data. The distribution of test results will typically be log normal or Weibull distributed. This scatter is due to differences in test specimens.

There are two types of fatigue testing: endurance testing and residual strength testing. As described in Introduction the main scope of this report is to determine the residual strength of shear connectors. For sake of completeness a short introduction to endurance testing is also given.

4.4.1. Endurance testing

Endurance testing focuses on the endurance of a structure or component, i.e. how long the test specimen will last under cyclic loading.

In most endurance tests the peak load (P_{\max}) is kept constant and a cyclic load of constant loading range (R) is applied to the specimen (see Figure 4-11). After N cycles the strength of the specimen has reduced to that of the peak load (P_{\max}), and failure occurs. The number of cycles to failure is called the endurance, E .

As mentioned before, the life of a component subjected to cyclic loading can be described as consisting of an initiation and a propagation phase, that is $E = N_{\text{init}} + N_{\text{prop}}$. In many components it is assumed that the initiation phase is very long and once cracks have started to propagate they propagate quickly, so $N_{\text{prop}} \ll E$.

Since the propagation phase is so short, the loss of strength is thought to take place only in the very end of the life of the specimen, and therefore the peak load does not affect the fatigue life as much as the loading range does, see also Figure 4-11 above.

Many steel design standards assume that the endurance is dependent only on the range, and that the peak load gives no effect on the endurance because of the presence of residual stresses that are close to the yield stress. In the case where shear studs have been welded to a steel beam, the residual stresses in the beam are less important, since cracks are initiated by the welding procedure.

Most results from endurance tests are plotted in so called S-N diagrams, see Figure 4-14. In such curves S is either the range of the cyclic load R or some other variable, such as the ratio of the peak load to the static strength, P_{\max}/D_{smax} , or peak load. N is the number of cycles to cause failure, i.e. the endurance, E .

When both axis are logarithmic the test data can be fitted to Basquins equation:

$$S \cdot N^m = \text{Constant}$$

where N is the endurance and m is the slope, see Figure 4-14.

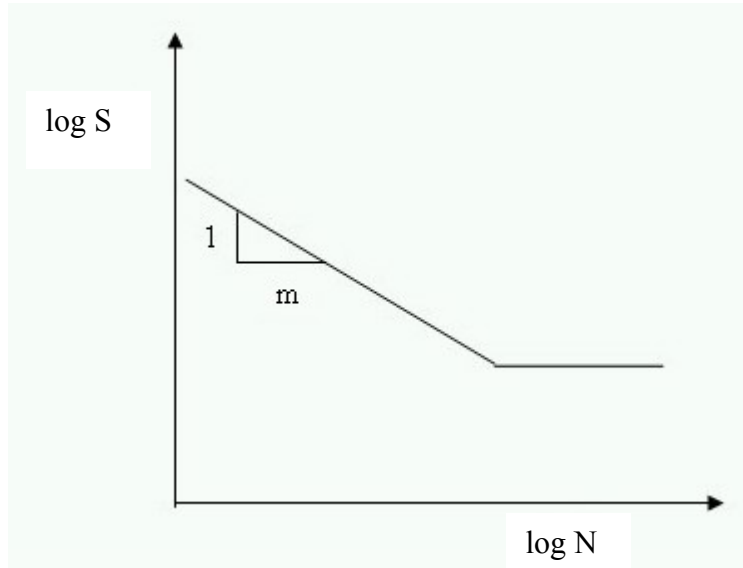


Figure 4-14. Schematic S - N diagram.

The value of m is a matter of discussion. According to Oehlers & Bradford (1995) and Johnson (2000) this mainly depends on how the scatter of test results is minimized. If the test data is schematically represented by the ellipse in Figure 4-15, minimizing by use of the least square method around x (that is $\log N$) would give the curve A-B and the slope $m = 5$. Minimizing around y (that is $\log S$) gives the curve C-D and the slope $m = 8$.

Oehlers & Bradford and Johnson all advocate minimization around x , since N is actually the dependant variable. As will be seen in chapter 5, Design codes, the use of $m = 5$ or $m = 8$ is not even the same throughout different parts of Eurocode.

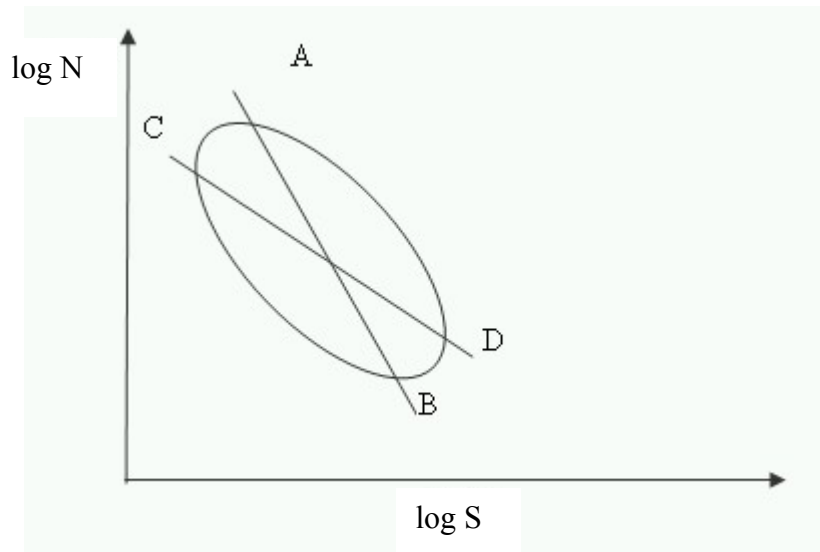


Figure 4-15. Schematic representation of test result scatter.

To show the effect of a change in the range, some common values of m_e for different materials are used. m is normally 3 for welded steel components, 5 or 8 for shear studs and 20 for plain concrete. If the endurance when applying the range R_e is N_e , the endurance of the range $2R_e$ is N_{inc} and the endurance of the range $R_e/2$ is N_{dec} .

Material	$R = R_e$	$R = 2R_e$	$R = R_e/2$
Welded steel	Endurance = $N_{e,steel}$	$N_{inc} = N_{e,steel} \cdot 0,125$	$N_{dec} = N_{e,steel} \cdot 8$
Shear studs, $m = 5$	Endurance = $N_{e,stud5}$	$N_{inc} = N_{e,stud5} \cdot 0,03125$	$N_{dec} = N_{e,stud5} \cdot 32$
Shear studs, $m = 8$	Endurance = $N_{e,stud8}$	$N_{inc} = N_{e,stud8} \cdot 0,00391$	$N_{dec} = N_{e,stud8} \cdot 256$
Concrete	Endurance = $N_{e,concrete}$	$N_{inc} = N_{e,concrete} \cdot 9,5 \cdot 10^{-7}$	$N_{dec} = N_{e,concrete} \cdot 1048576$

4.4.2. Accumulated damage

During the life of a structure it is most likely to be subjected to a cyclic load with variable amplitude (range) as shown in Figure 4-12. For each amplitude the endurance is known (or can be found from experiments), and so the ratio of the number of cycles applied to a component, N , and the endurance, E , is known as the fatigue damage or used life. The sum of the fatigue damage for different amplitudes is known as the accumulated damage or accumulated used-life, and was proposed by Miner (1945).

This can be written as

$$\sum_{k=1}^{k=z} \frac{N_k}{E_k} \leq A \quad \text{Eqn. 4-9}$$

where z denotes the total number of different amplitudes (ranges), N_k is the number of cycles of range R_k and E_k is the endurance of the component to the range R_k . In most cases $A = 1$, but sometimes a value less than 1 is used, e.g. to allow for experimental scatter. The accumulated damage formula is useful when the loading history of a structure is known.

In Handboken BYGG a weakness of the above formula is mentioned: it does not take into account the order in which different ranges of load is applied. According to Handboken BYGG tests have shown that a large range followed by smaller range gives higher endurance than the opposite.

4.4.3. Residual strength based procedures

In the endurance based testing procedure a fluctuating load is applied and after a number of cycles of a certain range the component fails at the peak load. This peak load is lower than the static strength, which clearly indicates that the strength of the component has decreased during the dynamic loading, but not when.

In the residual strength based procedure, a certain number of cycles of a certain range are applied to the component, and then the component is loaded to failure. From this a so called failure envelope, a curve describing the loss of static strength, see Figure 4-16a and b, can be achieved.

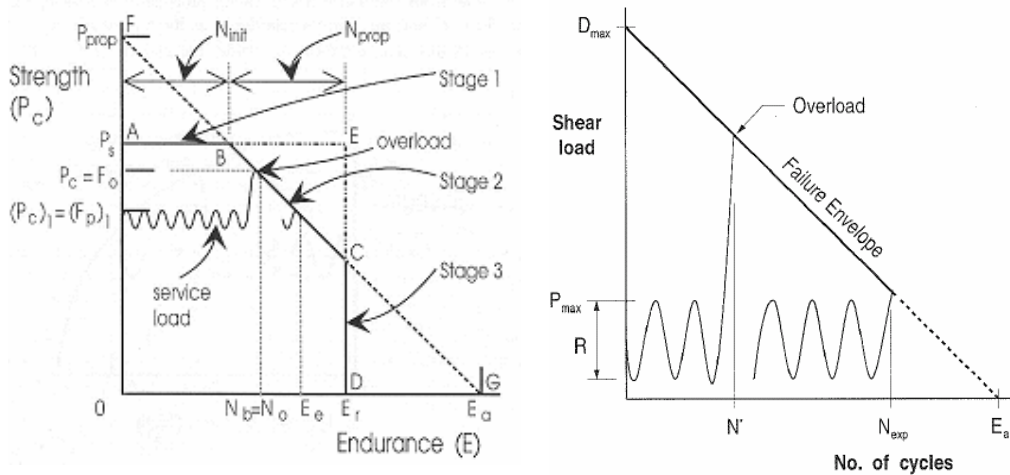


Figure 4-16a) Linearised residual strength envelope (from Oehlers & Bradford).b) Failure envelope of stud shear connector.

In general the failure envelope can be idealized into a tri-linear shape and the different parts of the curve can be seen as the initiation part and the propagation part, like

Figure 4-16a. During the initiation part the static strength is almost unchanged, as the crack is not big enough to affect the static strength. During the propagation part the cracks are growing bigger, decreasing the static strength.

During the life of a structure it is subjected to a certain service load, but most likely it will also be subjected to much higher loads a couple of times during its service life. The structure is of course designed to resist these high loads, but the service cyclic loading reduce the strength of the structure and this may cause fracture in the late life of the structure. The failure envelope and an overload following the normal service life are shown in Figure 4-16a and b.

The rectangular failure envelope shown in Figure 4-11 is an extreme form of the tri-linear failure envelope, as the propagation part is almost non-existent. Stud shear connectors give another extreme form of failure envelope. As mentioned earlier the life of a welded component consists of only two parts; the propagation part and failure. Oehlers (1990) showed that the static strength of stud shear connectors start to reduce immediately under cyclic loading and reduce almost linearly, as shown in Figure 4-16b. This is the path F-C-D in Figure 4-16a, when $P_{prop} = D_{max}$, and the result of a non-existent initiation phase.

According to Oehlers (1990), the maximum shear load that is applied to a connector does not affect the fatigue damage. That is; the rate of degradation of the static strength is not affected, but the life will of course be, as a high peak load will be reached sooner and hence give a lower endurance.

A parameter often used in the comparison between different tests is the asymptotic endurance, E_a , (e.g. when the range is constant between tests and the peak load is differed). This is a theoretical parameter describing the point where the failure envelope cross the N-axis. This is of course not possible in reality, since $E_a > N_e$ and the test specimen will always fracture at the peak load applied.

From the experimental results and statistical analysis, the asymptotic endurance E_a was found to be

$$E_a = 10^{\left(3.12 - \frac{0.70}{\sqrt{n}}\right)} \left(\frac{R}{D_{max}}\right)^{-5.1} \quad \text{Eqn. 4-10}$$

(from Oehlers & Bradford).

Usage of the accumulated damage theory gives the following equation

$$\sum_{k=1}^{k=z} \frac{N_k}{E_{a_k}} = 1 - \frac{P_{max}}{D_{max}}$$

where z is the total number of load ranges. When the used life is known the static strength can be calculated, and thus the maximum overload after a certain number of cycles is known.

5. Design codes

This chapter includes the following parts:

Short introduction to design, where the basis of design is shortly described.

Eurocode, in which the static and fatigue design of shear stud connectors according to Eurocode is presented.

Swedish code, in which the static and fatigue design of shear stud connectors according to BSK 99, BKR 94, BRO 2002 and BV BRO is presented.

Design in British Bridge Code and Peak Load model.

Comparison between design in different codes, in which the design of shear stud connections according to the different standards is compared.

5.1. Short introduction to design

Design codes are used to ensure the safety and function of a structure during its whole life. The design codes are based on both empirical and theoretical experience, and differ from one country to another.

The requirements to fulfil is divided in two different design states,

- the ultimate limit state: to ensure the load bearing capacity and safety against failure for the most extreme loads that can be expected during the life of the structure
- the serviceability limit state: to ensure the function of the structure (e.g. the deformation of a bridge or the maximum crack width) during normal conditions.

All standards used in this report are based on the partial factor design method.

The resistance of a structure is divided by a partial coefficient taking into account the insecurities within the material and geometry of the structure, and so the resistance R can be described as $R = g(a, f, \gamma)$

where

a is the area of the structure

f is the strength of the material

γ is the partial coefficient

The magnitudes of variable loads are commonly normal-distributed during a period of e.g. a year or a century. The characteristic value, Q_k , is set as upper 2 % fractal, which means the characteristic or higher values statistically arises once in 50 years. ψ is a value ($\psi < 1$) which gives the mean value of the normal distribution function, $Q_k \cdot \psi$. The normal-distribution of a variable load is shown schematically in figure 5-1.

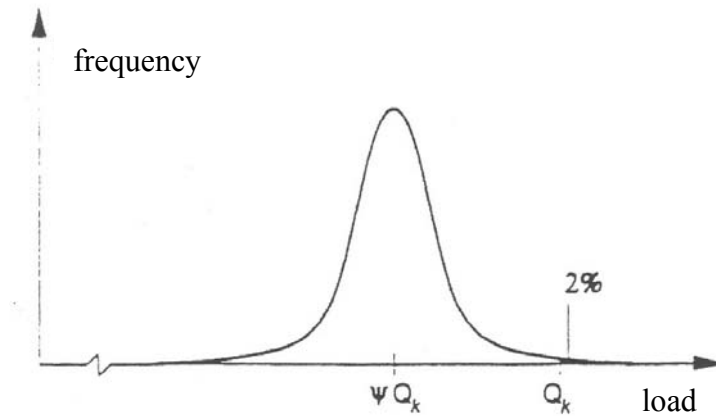


Figure 5-1. Normal distribution of variable load.

When a structure is subjected to a combination of loads, the total effect is described as

$$S = \gamma_f Q_1 + \gamma_f \psi_2 Q_2 + \gamma_f \psi_3 Q_3 + \dots \quad \text{Eqn. 5-1}$$

where:

S is the design load effect acting on the structure

$Q_1, Q_2, Q_3 \dots$ are the different loads acting at the same time

ψ is the load reduction factor, $\psi < 1$

γ is the partial coefficient, $1 < \gamma < 1,25$

For a combination of loads, one load must be taken as the main load using the characteristic value and the rest of the loads are used with their mean values.

The characteristic value of the strength of a material, f , is defined as the lower 5 % fractal of the normal-distribution, and the design strength is the characteristic value divided by partial safety factors.

In the ultimate limit state the requirement is that $R > S$.

In the serviceability state γ_f is 1,0 for all loads, and the requirements is for example that maximum deflection should be lower than allowed by code.

The design of static and fatigue loading of stud shear connectors are described according to three different design codes:

- Eurocode (European pre-standard, for road and railroad bridges).
 - Bro 2002 (Swedish code for road bridges)
 - BV Bro (Swedish code for railway bridges)
- } Based on BSK 99

The design in the British Bridge Code and the design proposed by Oehlers is also presented.

5.1.1. Static resistance of stud shear connectors

The static design is based on the ultimate limit state, and therefore the extreme values are used. This load is not likely to occur more than once in the lifetime of a structure.

5.1.2. Fatigue design

Common for all standards is that only heavy lorries are considered in fatigue design, this is because cars and light lorries mostly give rise to stresses below the fatigue limit, that is the stress limit below which fatigue failure will not occur.

As mentioned in chapter 4 Fatigue, Oehlers & Bradford (1995) and Johnson (2000) relate the discrepancy in the value of m (the slope of the S-N curve) not to the scatter in test results, but to a lack of agreement between authors on how regression analysis of test data should be done. This can clearly be seen when comparing the different standards. According to Johnson (2000) a low value of m means that most fatigue damage is done by the high-frequency low-stress-range loading, e.g. typical loaded lorries on a bridge. If m is high the exceptionally heavy loads matter.

5.2. Eurocode

The Eurocode project was started by the Commission of the European Community (CEC) in 1975 to harmonize the technical specifications and eliminate the technical obstacles to trade. There are 10 parts of this European Standard (EN), each for different kinds of structural design. In this report the following parts of Eurocode have been used: prEN 1991-2: (Eurocode 1: Actions on structures – Part 2: Traffic loads on bridges), EN 1993-2 (Eurocode 3: Design of steel structures – Part 2: Rules for bridges), EN 1993-1-9 (Eurocode 3: Design of steel structures – Part 1.9: Fatigue strength of steel structures), prEN 1994-2 (Eurocode 3: Design of composite steel and concrete structures – Part 2: Rules for bridges).

For shear studs there are several requirements that have to be fulfilled. If these are not fulfilled, the resistance might be lower than assumed according to the code. It is assumed that the following requirements from prEN 1994-2 are fulfilled:

Ductile connectors (with a slip capacity of at least 6 mm) have to be used. To prevent separation, the shear connector should be designed to resist a nominal ultimate tensile force of at least 0,1 times the design ultimate shear resistance of the connectors.

The dimensions of the studs should be:

- height of stud $> 3d$
- diameter of head $\geq 1,5d$
- depth of head $\geq 0,4d$
- for elements in tension or subjected to fatigue loading $d < t_{\text{flange}}$ (thickness of the flange of the steel element)

where

d is the diameter of the stud

There are also requirements of the minimum distance between the stud shear connectors.

The important assumptions made in the fatigue design are

- a) the stresses are calculated for the serviceability limit state
- b) stress ranges due to frequent loads are limited to $\Delta\sigma \leq 1,5 f_y$ and $\Delta\tau \leq 1,5 f_y/\sqrt{3}$
- c) the number of cycles is $N \geq 10^4$ cycles

5.2.1. Road bridges

For road bridges the loading cases to be considered are set in prEN 1991-2. There are a number of loading cases for static load, all including point loads representing lorries and evenly distributed loads representing cars.

For the fatigue design of road bridges five loading cases are presented in prEN 1991-2. Fatigue load model 1 and 2 are intended to be used to check whether the fatigue life may be considered as unlimited when a constant stress amplitude fatigue limit is given, and therefore they are appropriate for steel.

5.2.2. Railway bridges

For railway bridges the loading cases are somewhat different than in road bridges, mainly because the dynamic effects due to the multiple axis following each other in a train. The loading cases to be considered are obtained in prEN 1991-2.

In static design the extreme loading during the whole life of the structure has to be accounted for, and this has to be increased because of the dynamic effects.

In fatigue design the dynamic factor is reduced to the assumed average effect during a lifetime of 100 years, which is the design life of railways in Eurocode.

5.2.3. Static strength of stud shear connectors

From prEN 1994-1, chapter 6.6 the following design resistance of stud shear connectors are given:

$$P_{Rd} = \frac{0,8 \cdot f_u \cdot \pi \cdot d^2 / 4}{\gamma_v} \quad \text{Eqn. 5-2}$$

or

$$P_{Rd} = \frac{0,29 \cdot \alpha \cdot d^2 \sqrt{f_{ck} \cdot E_{cm}}}{\gamma_v} \quad \text{Eqn. 5-3}$$

whichever is smaller,

$$16 < d < 25 \text{ mm}$$

$$\alpha = 1 \quad \text{for } h/d > 4$$

f_u specified ultimate tensile strength of the material of the stud, but not greater than 500 N/mm²

f_{ck} characteristic cylinder compressive strength of the concrete

γ_v 1,25 (safety factor for shear)

h_{sc} is the overall nominal height of the stud.

Both of these equations have been used in many countries for a long time.

According to “Studie av Eurocode 4 – Samverkanskonstruktioner” equation (5.2) describes fracture through the shank of the stud, where the shear stresses on the average is 80 % of the ultimate tensile strength of the material.

Equation (5.3) is in the same form as the equation according to Ollgaard, Slutter and Fischer presented in chapter 3.2.3. As described in chapter 3.2.3 this is the case where the concrete crushes and the shear stud bends.

According to Johnson & Anderson (1993) the constant in EC4 was derived from push test results to be 0,26, but since the mean number of studs per specimen was only six, and the lateral restraint was usually less stiff than in the concrete flange of a composite beam, it was increased to 0,29. The constant according to Ollgaard, Slutter and Fisher is 0,39 ($0,5 \cdot \pi / 4$)

5.2.4. Fatigue strength of stud shear connectors

The fatigue design of shear studs given in Eurocode takes no account of the static shear strength of the stud or of the maximum shear force applied.

In prEN 1993-2 the following definition of the fatigue stress spectra is given:

The reference stress range σ_P for determining the damage effects of the stress range spectrum should be obtained from

$$\sigma_P = |\sigma_{P,\max} - \sigma_{P,\min}| \quad \text{Eqn. 5-4}$$

The damage effects of the stress range spectrum may be represented by the damage equivalent stress range related to $2 \cdot 10^6$ cycles:

$$\sigma_{E2} = \lambda \Phi_2 \sigma_P \quad \text{Eqn. 5-5}$$

where λ is the damage equivalence factor as defined in prEN 1993-2-9.5;

Φ_2 is the damage equivalent impact factor

For railway bridges the value of Φ_2 should be obtained from EN 1991-2. For road bridges Φ_2 may be taken as equal to 1,0, because it is included in the fatigue load model.

The calculation of the damage equivalent factors λ is a lengthy procedure. λ differ from road bridges to railway bridges and is defined as

The damage equivalence factor λ for road bridges up to 80 m span should be obtained from:

$$\lambda = \lambda_1 \cdot \lambda_2 \cdot \lambda_3 \cdot \lambda_4 \quad \text{Eqn. 5-6}$$

where λ_1 factor for different types of girder that takes into account the damage effect of traffic and depends on the length of the critical influence line or area

λ_2 factor that takes into account the traffic volume;

λ_3 factor that takes into account the design life of the bridge;

λ_4 factor that takes into account traffic on other lanes;

λ_{\max} maximum λ -value taking account of the fatigue limit

The definition of λ for railway bridges is similar, but the values are somewhat different.

The design fatigue strength of stud shear connectors is given in both prEN 1994-2 (composite structures) and prEN 1993-1-9 (steel structures), but the design values given are not the same. The design according to these codes is:

5.2.4.1. Design according to prEN 1994-2:

In chapter 6.8 the following design is given:

The fatigue strength curve of an automatically welded headed stud in accordance with 6.6.3.1 is shown in Fig 6.25 [this figure presents an S-N diagram of slope m] and given for normal weight concrete by:

$$(\Delta \tau_R)^m N_R = (\Delta \tau_C)^m N_C \quad \text{Eqn. 5.7}$$

where:

$\Delta \tau_R$ is the fatigue strength

$\Delta\tau_C$ is the reference value at 2 million cycles with $\Delta\tau_C$ equal to 90 N/mm²

m is the slope of the fatigue strength curve with the value $m = 8$

N_R is the number of stress-range cycles.

According to this design, the number of cycles to failure at a specific range or the allowed range at a specific number of cycles can be calculated.

The fatigue assessment should be made by checking the criterion:

$$\gamma_{Ff} \Delta\tau_{E,2} \leq \Delta\tau_C / \gamma_{Mf,s} \quad \text{Eqn 5.8}$$

where:

$\Delta\tau_C$ is the reference value of fatigue strength at 2 million cycles according to prEN 1994-2-6.8.3

For verification of stud shear connectors based on nominal stress ranges the equivalent constant stress range $\Delta\tau_{E,2}$ for 2 million cycles is given by:

$$\Delta\tau_{E,2} = \lambda_v \Delta\tau \quad \text{Eqn 5.9}$$

where:

λ_v is the damage equivalent factor depending on the loading spectrum and the slope m of the fatigue strength curve;

$\Delta\tau$ is the stress range due to fatigue loading.

For bridges the damage equivalent factor λ_v for headed studs in shear should be determined from $\lambda_v = \lambda_{v,1} \lambda_{2,v} \lambda_{v,3} \lambda_{v,4}$ Eqn 5.10

For road bridges of span up to 100 m the factor $\lambda_{v,1}=1,55$ should be used. The factors $\lambda_{v,2}$ to $\lambda_{v,4}$ should be determined in accordance with 9.5.2 (4) to (7) of EN 1993-2 but using exponents 8 and 1/8 in place of those given, to allow for the relevant slope $m = 8$ of the fatigue strength curve for headed studs, given in 6.8.3.

For railway bridges the factor $\lambda_{v,1}$ should be taken from Figure 6.27. The factors $\lambda_{v,2}$ to $\lambda_{v,4}$ should be determined in accordance with N3.1.6 of Annex N of EN 1992-2 but using instead of the exponent k_2 the exponent $m = 8$ for headed studs.

5.2.4.2. Design according to prEN 1993-1-9

The design in prEN 1993-1-9 is slightly different. Here the reference value is defined by detail category, which for stud shear connectors is 80, corresponding to 80 N/mm². The following design procedure is given in prEN 1993-1-9:

$$\Delta\tau_R^m N_R = \Delta\tau_C^m 2 \cdot 10^6 \text{ with } m = 5 \text{ for } N \leq 10^8 \quad \text{Eqn 5.11}$$

$$\text{where } \Delta\tau_L = \left(\frac{2}{100} \right)^{1/m} \Delta\tau_C \quad \text{Eqn 5.12}$$

[$\Delta\tau_C$ is the reference value at 2 million cycles with $\Delta\tau_C$ equal to 80 N/mm² as described above]

and $\Delta\tau_L$ is the cut off limit, below which fatigue will not occur]

As mentioned in chapter 4 and chapter 5.1.1, the value of the slope, m , is a matter of discussion. In EC 4 m was chosen to 8, and in EC 3 to 5. This certainly gives difference in expected life. The difference in reference value will also give effect on the expected life.

$$\text{It shall be verified that } \frac{\gamma_{Ff} \Delta\tau_{E,2}}{\Delta\tau_C / \gamma_{Mf}} \leq 1,0 \quad \text{Eqn 5.13}$$

When no data for $\Delta\tau_{E,2}$ are available the verification format in Annex A.1 [Annex A.1 in EC 3] should be used.

The design value of nominal stress range should be determined from

$$\gamma_{Ff} \Delta\tau_{E,2} = \lambda_1 \cdot \lambda_2 \cdot \lambda_3 \cdot \lambda_4 \cdot \dots \cdot \lambda_n \cdot \Delta\tau(\gamma_{Ff} Q_k) \quad \text{Eqn 5.14}$$

where $\Delta\tau$ ($\gamma_{Ff} Q_k$) is the stress range caused by the fatigue loads specified in EN 1991

λ_i are damage equivalent factors depending on the spectra as specified in the relevant parts of EN 1993

In Annex A.1 the following can be read:

In using the design stress range spectra by applying γ_{Ff} factors to the stress ranges $\Delta\sigma_i$ and the design S_d -N-curves by applying γ_{Mf} factors to the characteristic S_k -N-curves ($\Delta\sigma_C / \gamma_{Mf}$) the damage summation

$$D_d = \sum \frac{n_{Ei}(\gamma_{Ff} \Delta\sigma_i)}{N_{Ri}(\Delta\sigma_C / \gamma_{Mf})} \quad \text{Eqn 5.15}$$

may be performed, where

$n_{Ei}(\gamma_{Ff} \Delta\sigma_i)$ is the number of cycles associated with the stress range ($\gamma_{Mf} \Delta\sigma_i$)

$N_{Ri}(\Delta\sigma_C / \gamma_{Mf})$ is the number of cycles corresponding to the design S_d -N-curve $\Delta\sigma_C / \gamma_{Mf}$ on the level $\Delta\sigma_i / \gamma_{Ff}$

Failure may be assumed when

$$D_d \geq 1,0 \quad \text{Eqn 5.16}$$

Equation A.1 is recognized as the accumulated damage equation according to Palmgren and Miner.

5.3. Swedish code

The code for steel design in Sweden is called BSK99 and is based on BKR 94 which is the standard code for all design. BSK 99 is the base code for design of steel structures. For design of special structures like bridges additional codes are used, where the different load cases and other specific details are defined. In this chapter only the parts for shear connectors are considered.

5.3.1. BSK 99

BSK 99 gives standard for calculating the strength of steel structures. The standard for calculating shear connectors is given below.

Certain rules have to be fulfilled to ensure the strength of shear connectors. These are given in BRO 2002 and not in BSK 99.

5.3.1.1. Static design

Static design according to BSK99 is pure shear in the shear stud. The formula used for design of shearing bolts is used.

$$F_{rd} = 0,6 \cdot A \cdot f_{bud} \quad \text{Eqn 5.17}$$

A is the area of the shear stud

$$f_{bud} = \frac{f_{buk}}{1,1 \cdot \gamma_n} \quad \text{Eqn 5.18}$$

γ_n is a safety parameter, 1,2 for shear studs

f_{buk} is the characteristic yield strength

5.3.1.2. Fatigue design

Fatigue design in BSK 99 is based on the theory of elasticity. It is concluded that parts subjected to stress ranges of 25 MPa or lower does not have to be considered in design for fatigue. BSK 99 considers only the stress range in design which means that the peak load does not affect the fatigue design.

The following equations are used for design of shear studs.

For only normal stresses:

$$\sigma_{rd} \leq f_{rd} \quad \text{Eqn 5.20}$$

$$\text{where } f_{rd} = \frac{f_{rk}}{1,1 \cdot \gamma_n} \quad \text{Eqn 5.21}$$

σ_{rd} is the difference of maximum and minimum stress applied to the component

f_{rd} is the design stress range

For only shear stresses:

$$\tau_{rd} \leq f_{rvd} \quad \text{Eqn 5.22}$$

$$\text{were } f_{rvd} = 0,6 \cdot f_{rd} \quad \text{Eqn 5.23}$$

$$\text{and for bolts class 8.8 and 10.9 } f_{rvd} = 0,9 \cdot f_{rd} \quad \text{Eqn 5.24}$$

For multi axial stresses eqn. 4.1 and the following equation:

$$\sqrt{\frac{\sigma_{rd\parallel}^2}{f_{rd\parallel}^2} + \frac{\sigma_{rd\perp}^2}{f_{rd\perp}^2} + \frac{\tau_{rd\parallel}^2}{f_{rvd\parallel}^2} + \frac{\tau_{rd\perp}^2}{f_{rvd\perp}^2}} \leq 1,10 \quad \text{Eqn 5.25}$$

in some cases the multi axial stresses are considered in the value of C for calculation of f_{rk} .

$$f_{rk} = C \left(\frac{2 \cdot 10^6}{n_t} \right)^{1/3} \quad \text{Eqn 5.26}$$

C is a constant that consider notch effects and what part (e.g. weld, shear connectors etc) the design is made for (for shear studs C = 63).

n_t is the number of cycles of stress the part is subjected to.

If the stress ranges vary another demand have to be for filled.

$$\sum \left(\frac{n_i}{n_{ti}} \right) \leq 1,0 \quad \text{Eqn 5.27}$$

Were n_i is the numbers of cycles with a certain stress range (σ_{ri}) and n_{ti} is the number of cycles for constant stress range for the characteristic resistance for σ_{ri} .

For typified stress collective the characteristic fatigue resistance can be calculated from the variable κ

$$\kappa = \frac{\min \sigma_r}{\max \sigma_r} \quad \text{Eqn 5.28}$$

where σ_r is the range.

From table 6:524 in BSK99 the characteristic fatigue resistance is given according to κ .

For high values of κ the resistance is low and for low values of κ the resistance is high.

Consider the following example:

- a) A bridge is designed to resist 10^6 passages of a load which gives constant stress range, $\kappa = \frac{\min \sigma_r}{\max \sigma_r} = 1$. This gives a resistance of $F_{rd} 13,7 \text{ kN}$.
- b) A bridge is designed to resist 10^6 passages of a load which give $\kappa = \frac{\min \sigma_r}{\max \sigma_r} = 5/6$. This gives a resistance of the shear studs $F_{rd} = 16 \text{ kN}$.

5.3.2. BRO 2002 (Swedish code for road bridges)

The requirements of the dimensions of the shear studs are:

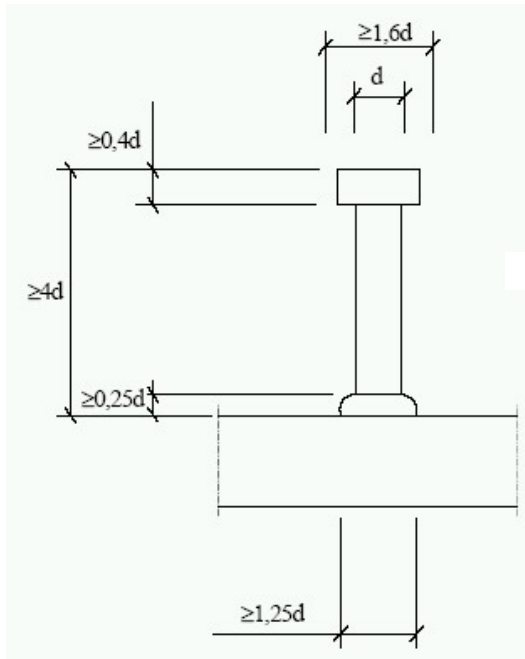


Figure 5-2. Requirements according to BRO 2002.

Design of Swedish road bridges is performed according to BRO 2002 which is based on the BSK 99, as mentioned earlier. An example of road bridge calculation according to BRO 2002 is given in Appendix E. The design procedure is explained and the number of shear studs required for different lengths are shown. BRO 2002 is published by the Swedish road administration as a complement to BSK 99 for bridge design. In BRO 2002 the fatigue strength of a shear stud is given in Table 5-1. The values in the table are calculated according to BSK 99.

Table 5-1. The table show shear stud resistance for security class 3 and for fatigue $\kappa=1$

n_t [Number of cycles]	Diameter of shear stud [mm]	F_{rd} [kN]	F_{hrd} [kN]
10^5	19	77	22
	22	100	30
	25	127	38
$4 \cdot 10^5$	19	77	14
	22	100	19
	25	127	24

5.3.3. BV BRO (Swedish code for railroad bridges)

BV BRO is a complement to BRO 2002, BV BRO is the standard for railway bridges and is published by the Swedish railway administration. The big difference between these two standards is that BV BRO only allows composite action in serviceability limit stage and not on ultimate limit stage. BV BRO's assumption gives it a more conservative assumption of the resistance of the bridge. Like in BRO 2002 the resistance for shear studs is calculated according to BSK 99 given in a Table 5-2.

Table 5-2. The table show shear resistance for security class 3 and $N = 10^6$.

Diameter of shear stud [mm]	F_{rd} [kN]	F_{hrd} $\kappa=2/3$ [kN]	F_{hrd} $\kappa=5/6$ [kN]
19	77	15	12
22	100	20	16
25	127	26	21

5.4. Design in British Bridge Code and Peak Load model

In Johnson (2000) the model for fatigue design in the British Bridge Code (BS) is described. Unlike Eurocode the BS consider the static shear strength and is given by

$$N_e (R/D_{max})^m = 10^k \quad \text{Eqn 5.29}$$

where

N_e is the endurance of a uni-directionally loaded specimen

m is the slope of the S-N curve, $m = 8$

k is a constant, $k = 1,29$

The "Peak Load model" based on the work by Oehlers is also presented in Johnson(2000), and this model also consider the maximum shear force applied, P_p :

$$N_f (R/D_{\max})^m = 10^k \quad \text{Eqn 5.30}$$

where the endurance is $N_e = N_f [1 - (P_{\max}/D_{\max})]$

$m = 5,1$ and

$$k = 3,12 - 0,70/\sqrt{n} \quad \text{Eqn 5.31}$$

5.5. Comparison between design in different codes

The design given in Eurocode and BSK 99 can be written as

$$N_e (\Delta\tau)^m = 10^k \quad \text{Eqn 5.32}$$

and the values of m and k are

EC 4: $m = 8$ and $k = 21,93$

EC 3: $m = 5$ and $k = 15,82$

BSK 99: $m = 3$ and $k = 11,70$

In the work done by Oehlers (in Johnson (2000)) the regression for EC 4 gives the value $m = 5$ and $k = 15,8$, which are the values used in EC 3.

Johnson (2000) conclude that for $P_p/P_R \leq 0,6$ the peak load has a fairly small influence. According to Johnson (2000), in drafting ENV 1994-2 it was assumed although $P_{p,k}$ is less than $0,6 P_{R,k}$ but this is not specified as a limit, which Johnson advocate.

The peak load is, as mentioned before, not taken into account in any standard considered here.

In diagram 5-1 the design shear range of shear studs is shown as a function of the number of cycles. This is done for EC 3, EC 4 and BSK 99.

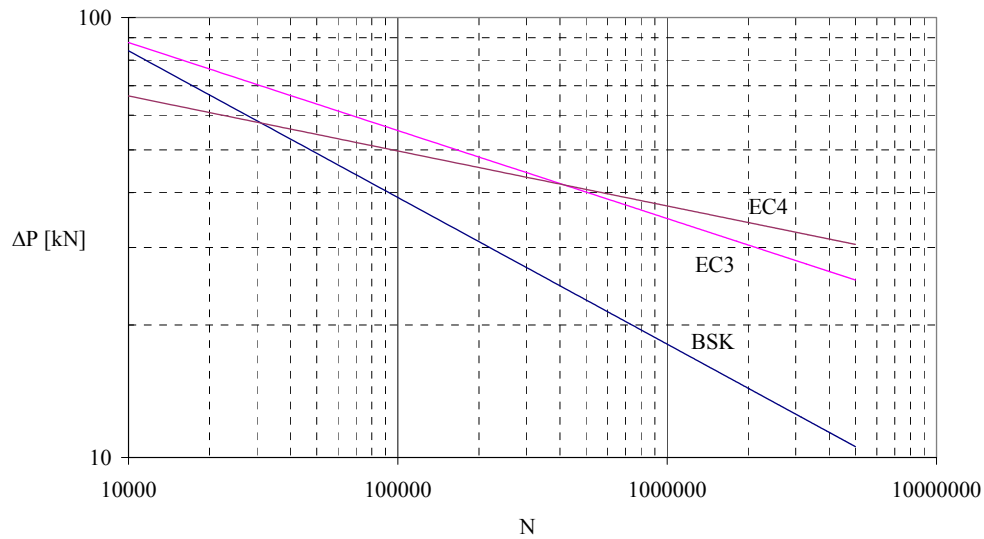


Diagram 5-1. Comparison between fatigue resistance according to BSK 99, EC3 and EC4

A comparison was made between the standards, to show the difference in expected life. The values used in the comparison were taken from the experimental study as:

$$R = 35,5 \text{ kN}$$

$$P_{\max} = 107,5 \text{ kN}$$

$$D_{\max} = 178,75 \text{ kN}$$

Table 5-3. Comparison between endurance according to different codes.

Code	R	P_{\max}	D_{\max}	m	k	A	N_e	k	m
EC 3	x			x	x	x	930110	15,82	5
EC 4	x			x	x	x	1471143	21,93	8
BSK 99	x			x	x	x	615347	11,7	3
Peak Load model	x	x	x	x	x		1128106	2,87	5,1
Tests at LTU							4900000		

6. Experimental studies

The experimental studies were performed at Testlab, a laboratory at the Department of Civil and Environmental Engineering at Luleå University of Technology. The push-out tests performed were five static, one endurance test and four residual strength tests.

6.1. General about test set-up

As mentioned in chapter 3.3 there are various testing arrangements used for push-out test to measure resistance of headed stud shear connectors under static and fatigue loading. Standard for the push-out test set-up, Figure 6-1, is given in Eurocode 4, part 1-1. This is done in order to avoid problems that arise from different testing arrangements and to make comparisons possible between tests.

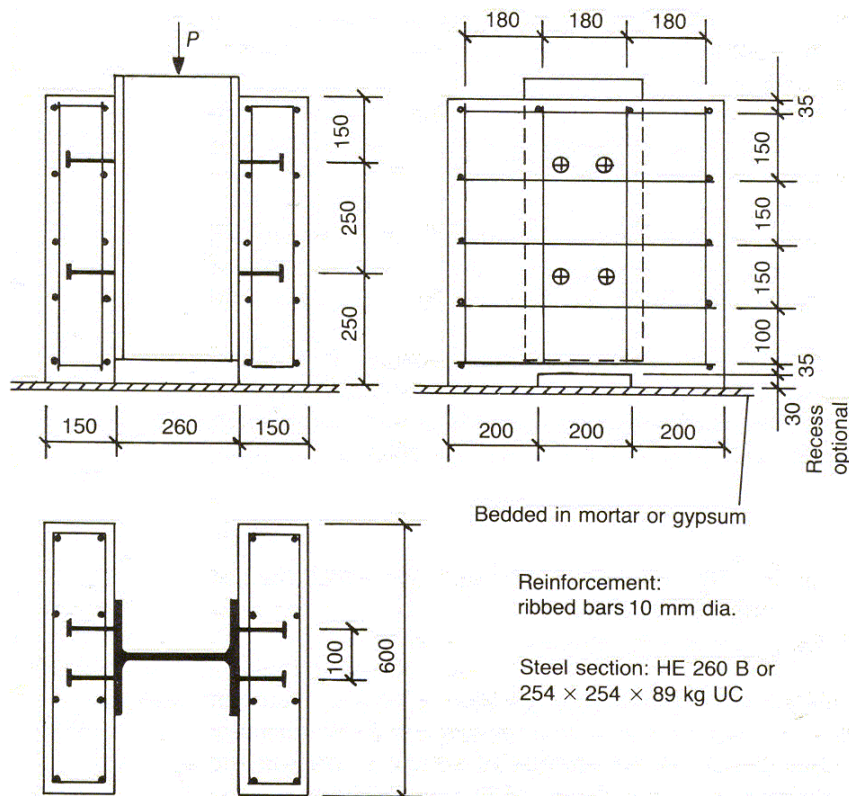


Figure 6-1. Test setup due to EC4

In EC 4 the separation of the concrete slabs and the steel beam is prevented, but the horizontal forces are not known from the test set-up shown in Figure 6-1.

In order to measure the horizontal force a small modification in the test set-up was made. The supports are modified to allow horizontal movement and the force is measured using steel rods connected to load cells, see Figure 6-2. To fit these the concrete slabs were extended 110mm.

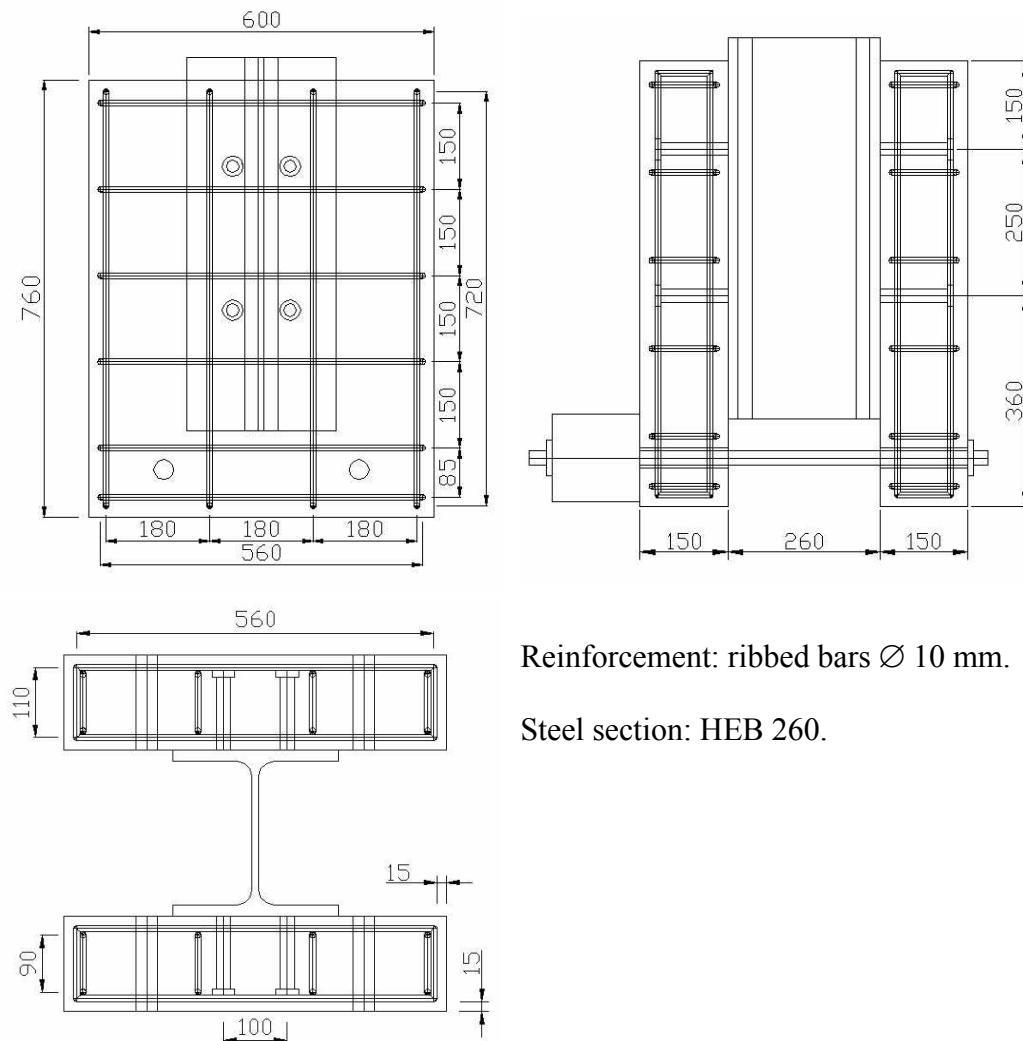


Figure 6-2. Modified specimen

The testing device and one push-out specimen is shown in Figure 6-3.

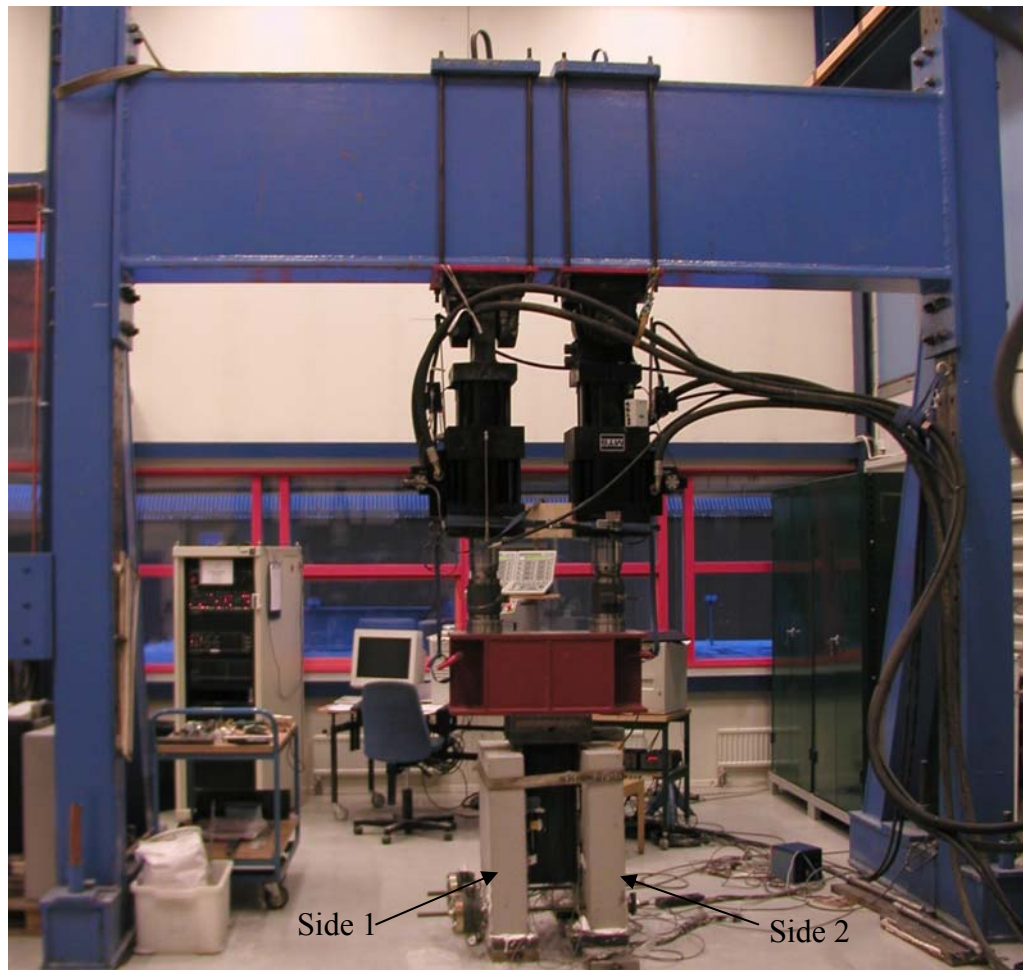


Figure 6-3. Testing device.

6.1.1. Preliminary support set-up

The preliminary test set-up is shown in Figure 6-4. The supports consisted of a steel roll welded on top of a steel plate. This was done in order to control the exact position of the reaction force and the forces in the steel rods (horizontal forces). On side one the steel plate was put in gypsum on the floor. On side two the steel plate was put on a layer of Teflon which made horizontal movement possible. Under the Teflon layer was another steel plate, put in gypsum on the floor.

The first two static tests were performed with such setup.

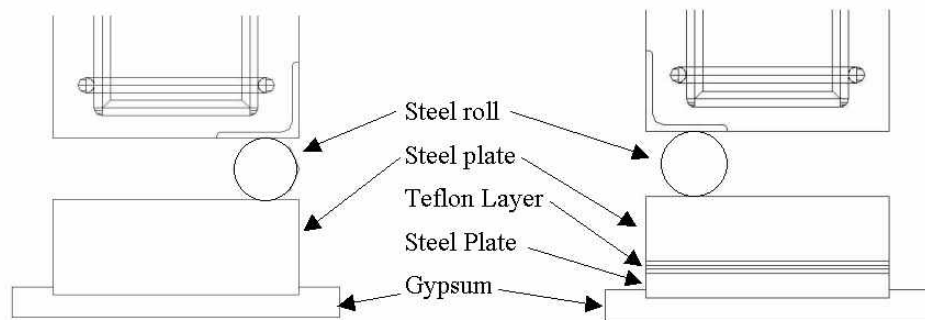


Figure 6-4. Detail of preliminary support set-up.

Problems with crushing of the concrete above the concentrated supports (see Figure 6-5) appeared in the preliminary tests, before the maximum force in the push-out test was achieved. Due to this the support-setup was modified to the standardized described below.



Figure 6-5. Crushing of concrete

6.1.2. Standardized support set-up

The remaining tests were performed with the standardized support conditions, see Figure 6-6.

In accordance with EC 4 only 200 mm on each side of the concrete slab is placed in gypsum, and the mid 200 mm is free.

In order to assemble the test specimen in a horizontal position, it was attached to the load cylinders and lowered into the gypsum.

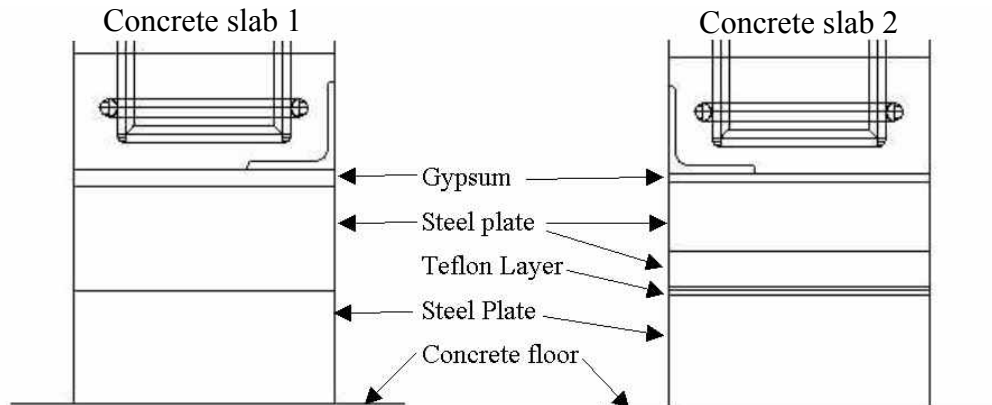


Figure 6-6. Detail of the standardized support set-up

6.2. Manufacturing of specimens

Cutting of the steel beam and welding of the headed shear studs were made at a workshop, BrisabAB in Piteå. They are certified according to requirements of Banverket for welding of headed shear studs in bridge constructions, see appendix F.

A formwork made out of wood and stable plywood was used to cast the concrete slabs. In accordance with EC 4 the concrete slabs were cast in a horizontal position, see Figure 6-7, to resemble the casting of a bridge deck. To cast the second side the formwork was removed from side one and assembled on side two. To get as little as possible difference in the concrete strength only three days passed between the two castings. The concrete was delivered by a local concrete manufacturer. The first side of all slabs were cast at the same time and from the same concrete mixture and the same procedure was carried out for the second side. Therefore the concrete strength is thought to be the same for all specimens, but may differ between the two slabs.



Figure 6-7. Specimens ready for the first casting

6.2.1. Concrete properties

The concrete mixture was: crushed stone with maximum grade 16 mm, Portland limestone cement, water/cement ratio 0,6.

In order to know the concrete strength of the push-out specimens, concrete cubes (150·150·150mm) were cast from the same concrete delivery as the concrete slabs. Half of the cubes were stored in water for four days and the rest beside the push-out specimens, and then all were stored in room temperature along with the push-out specimens. The cubes were tested after 52 days, at the beginning of the first push-out test. In order to see how the concrete strength increases in time a concrete test was also carried out after 146 days, when the last push-out specimen had been tested. The concrete was tested for compressive strength, f_{ck} , and for tensile strength, f_{ctk} . The test results are shown in Appendix C and in Table 6-1 a summary of the compressive strength is given. The compressive strength is strongly related to the strength of the test specimen and the tensile strength can be of interest. The concrete test was carried out as the standard test for concrete.

Table 6-1. Compressive strength of 150x150x150 mm concrete cubes.

		52 days	146 days
casting	storage	σ_{mean} [MPa]	σ_{mean} [MPa]
1	air	38,1	41,6
1	water	43,5	46,7
2	air	49,4	56,9
2	water	59,0	59,6

6.2.2. Characteristics of headed shear studs

The studs were manufactured by Köster & Co GmbH in Bogense, Denmark.

Nominal material characteristics for headed shear studs according to DIN EN 10204 are:

Tensile strength 350 MPa

Yield strength 450 MPa

Elongation 15 %

These values are used in the calculations below.

The weld collars of the headed studs were not perfect; the height of the weld collars was uneven around many studs. Based on detail inspection of welds following estimations can be given:

- About 60 % of the welds were even.

- 38 % missed $\frac{1}{4}$ or less of the weld collar (mostly on one side).
- 2 % missed $\frac{1}{4}$ - $\frac{1}{2}$ of the weld collar.

According to BRO 2002 and EC 4 the weld collars should comply with requirements given in chapter 5. Since the welding procedure were the same as the procedure used in bridge construction it is expected that similar weld quality exist in bridge beams. Photographs were taken before casting to make a complete documentation of the state of the specimens.

6.2.3. Reinforcement

The reinforcement is according Figure 6-2. The reinforcement was bent and assembled in Tibnor AB in Luleå.

Nominal yield strength for the reinforcement was 420 MPa and the tensile strength 500 MPa.

Steel profiles, L 50.50.5, 500mm long were cast into the inner side of each concrete slab to avoid crushing of the concrete in contact with concentrated reaction forces. As can be seen in Figure 6-4 and Figure 6-5 this profiles were not stiff enough to prevent local crushing of the concrete.

6.3. Testing procedure

The static tests were made in accordance with EC 4-1-1 presented below.

The first two steps in the testing procedure is to assure that the chemical bond between steel and concrete is broken, so that all load is taken by dowel effect of the shear studs. In the results from the experimental study presented herein the slip during these first two steps are not taken into account since this was very small.

The expected static resistance was calculated according to the formula by Oehlers & Johnson presented in chapter 3.3.2.2:

$$D_{\max} = \left(5,3 - \frac{1,3}{\sqrt{n}} \right) A_{\text{sh}} f_u^{0,65} f_c^{0,35} \left(\frac{E_c}{E_s} \right)^{0,40}$$

where

$A_{\text{sh}} = 380 \text{ mm}^2$, $f_{\text{ck}} = 30 \text{ MPa}$, $f_u = 450 \text{ MPa}$, $E_c = 32 \text{ GPa}$, $E_s = 210 \text{ GPa}$ and $n = 8$, which gives

$$D_{\max} = 151,2 \text{ kN}$$

The expected static resistance of a push-out specimen is

$$(D_{\max})_{\text{push}} = 151,2 \cdot 8 = 1,21 \text{ MN}$$

6.3.1. Static tests

The following procedure was used for static tests:

1. The test specimen was loaded to 40 % of the expected static resistance, that is 500 kN, in 60 seconds.
2. The load was cycled 25 times between 5 % (60 kN) and 40 % (500 kN) of the expected static resistance. The frequency used was $f = 0,25$ Hz.
3. The specimen was loaded to failure at the deformation rate 0,01 mm/s (this includes the deformation of the testing device). The aim was to prevent failure in less than 15 minutes.
4. The testing procedure was terminated when the load had dropped to 20 % below the maximum load.

6.3.2. Fatigue testing and residual test

The size of the range and the peak load had to be determined for the cyclic loading. In BRO and BV BRO the maximum design range is 30 kN/shear stud (for 100000 cycles). In tests found in reference, the range of about 20-25 % of the static strength have been used (see Oehlers (2000), Hanswille et al (2004)). That was the reason to choose the range of 20 %, that is 35,5 kN, in tests performed at LTU.

According to Johnson (2000) most tests performed have been with a peak load of $\leq 0,6 \cdot P_{\text{static}}$. Johnson advocate a limit for the peak load to $0,6 \cdot P_{\text{static}}$ in Eurocode. He also conclude that the peak load has a fairly small influence on the fatigue life if below this value.

The peak load in the fatigue loading is set to $0,6 \cdot D_{\text{max}}$. This was done for two reasons:

- A practical reason to get a shorter lifetime of the specimens
- To complement the existing results.

The following procedure was used for fatigue tests:

1. The test specimen was loaded to 40 % of the expected static resistance, that is 500 kN, in 60 seconds.
2. The load was cycled 25 times between 5 % (60 kN) and 40 % (500 kN) of the expected static resistance. The frequency used was $f = 0,25$ Hz.
3. The dynamic loading was started at a frequency of $f = 2$ Hz. The load was cycled between 40 % of the mean resistance of the static tests (570 kN) and 60 % (860 kN). The number of cycles was different in each test.
4. The dynamic test was stopped at the number of cycles chosen.
5. The specimen was loaded to failure at the deformation rate 0,01 mm/s (this includes the deformation of the test rig).

6. The testing procedure was terminated when the load had dropped to 20 % below the maximum load.

One test specimen was subjected to dynamic loading until the failure, and thus the endurance was found.

6.4. Measurement

The slip between steel beam and the concrete slab was measured by eight LVDTs and two laser gauges, see Figure 6-8, they were placed as in Figure 6-9. The LVDTs were placed on the flanges of the steel beam, at the same level as of the shear studs. The laser gauges were placed between the two rows of stud connectors, one on each side of the beam.

The force/displacement was applied by two hydraulic activators where the displacement and force were measured.

On each steel rod a load cell was placed to measure the horizontal forces. The steel rods were pre-stressed to approximately 20 kN in all tests except test 4s.

Two different measuring schemes were used:

1. All channels were measured at a frequency of $f = 50$ Hz. All data saved to database.
2. Laser gauges, force and stroke of the hydraulic activators and horizontal force were measured at the frequency of 50 Hz. Only the maximum and minimum value for every period of eight cycles was saved to database.

During static testing scheme 1 was used. During fatigue testing scheme 2 was used. Once a day, during fatigue testing, at an interval of approximately 170 000 cycles, scheme 1 was used to measure about 100 cycles. When the residual strength of the push-out specimen was tested scheme 1 was used.

The reason for the above procedure was that the amount of data saved using scheme 1 was very large and that the endurance of the LVDTs was thought to be about 200 000 cycles.

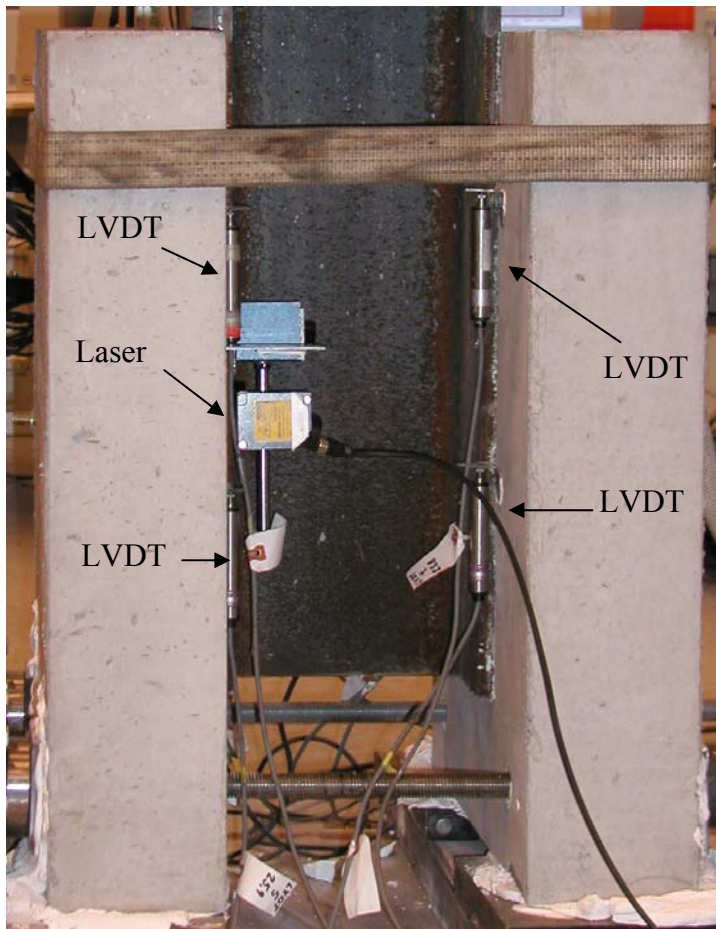


Figure 6-8. Position of devices for the slip measurement

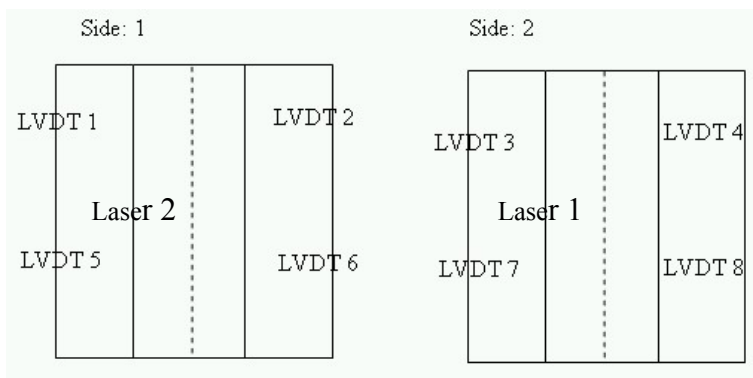


Figure 6-9. Placing of LVDT:s and laser gauges..

6.5. *Results of static tests*

The first five push-out specimens were tested with static load until the test specimen failed. These tests were carried out to get the static resistance of the test specimen, and the failure modes for this type of loading are described in chapter 3.

The tests were preceded until the shear studs on one ore both sides had failed.

Results from all tests are available in Appendix A, in this chapter only a summary is given.

All failures were shear failures of the stud shank.

6.5.1. *Summary of the static tests*

In Figure 6-10 the slip-load curves of all static tests are plotted. The slip shown is the mean of the side/sides where the studs were broken.

Table 6-2 shows the maximum load from all static tests, D_{max} . The horizontal forces in the steel rods increase the friction between the steel and the concrete slabs, thus increasing the resistance. The increase is thought to be about 20 % of the horizontal force. The corrected resistance, D_{corr} , is also shown in

Table 6-2. Some comments about the test are also given in the table.

The elastic load (maximum load giving an elastic behaviour of the shear studs) and the “elastic coefficient” have been determined from figure 2, 6, 8, 10 and 12 in Appendix 6-1. These are also shown in Table 6-3.

The horizontal forces of all static tests are plotted versus total force in Figure 6-11. The horizontal forces from the beginning of each test and the increase are shown in Table 6-4.

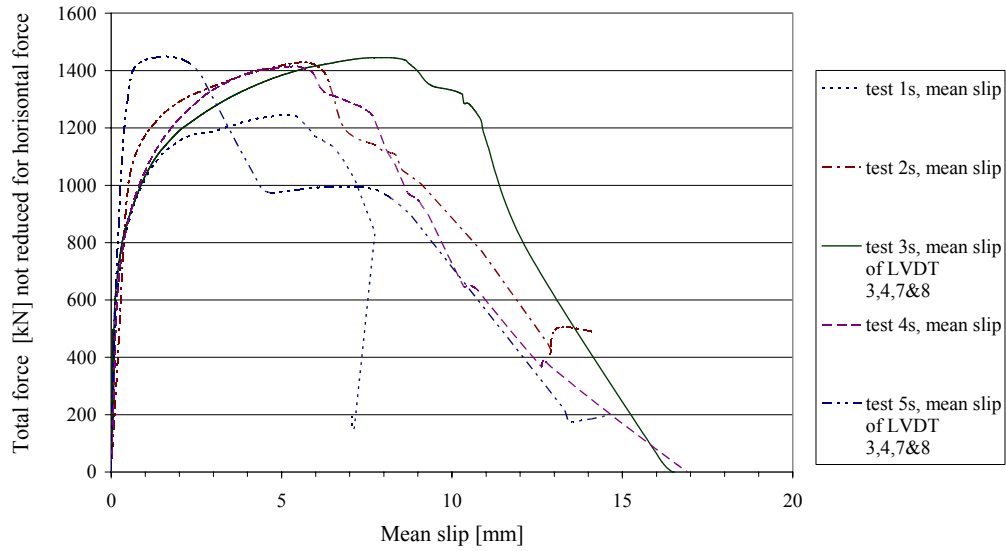


Figure 6-10. Slip-load curves of all static tests.

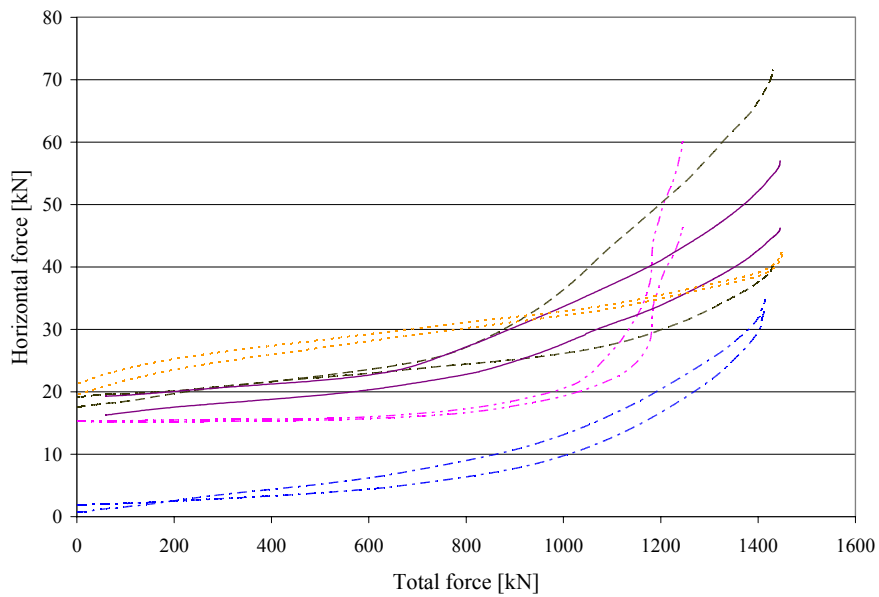


Figure 6-11. Total force-horizontal force for all static tests.

Table 6-2. Resistance of static tests.

Test	D _{max} [kN]	D _{corr} [kN]	Min slip [mm]	Max slip [mm]	Comments
1	1245	1217	3,2	5,1	Concrete crushing side 1 - the final failure is on side 2
2	1430	1408	4,7	7,1	Concrete failure - new test set-up. Result quite reliable
3	1445	1425	6,5	7,9	-
4	1415	1401	5,1	5,8	-
5	1449	1432	1,6	2,3	Accidental high load \approx 1000 kN before testing started

Table 6-3. Elastic coefficient of studs.

Test	Elastic load	Max slip at E.L.	Min slip at E.L.	Max elastic coefficient [kN/mm]	Min elastic coefficient [kN/mm]
1	580	0,14	0,12	4140	4830
2 – concrete crush	520	0,11	0,07	4730	7430
2	950	0,47	0,39	2020	2440
3	540	0,09	0,067	6000	8060
4	500/600	0,21	0,11	2380	5450
5	815/640	0,45	0,14	1810	4570

Table 6-4. Horizontal forces in static tests.

test	start 1 [kN]	start 2 [kN]	at fracture H ₁ [kN]	at fracture H ₂ [kN]	increase H ₁ [kN]	increase H ₂ [kN]	Total increase [kN]	maximum load [kN]	mean increase/ maximum load
1	15,35	15,33	46,46	60,27	31,11	44,94	76,05	1244	0,0306
2	17,55	19,14	71,5	40,25	53,95	21,11	75,06	1430,22	0,0262
3	16,67	19,96	46,23	56,99	29,56	37,03	66,59	1445,34	0,023
4	0,68	1,96	34,7	33,27	34,02	31,31	65,33	1414,77	0,0231
5	19,58	21,35	41,86	42,64	22,28	21,29	43,57	1449,45	0,015
mean of all							65,32	mean of all	0,0236

The mean resistance of the specimen has to be known when performing fatigue testing, and was thus calculated. The results from test 1 was not taken into account, since the crushing of concrete of side 1 was thought to have given a rise in the forces of the shear studs on side 2, giving failure at a lower load than would be the case without crushing of the concrete. Test number 5 was not used, since it had not yet been performed.

$$D_{\max} = \frac{1430 + 1445 + 1415}{3} = 1430 \text{ kN}$$

$$D_{\text{corr}} = \frac{1408 + 1425 + 1401}{3} = 1411 \text{ kN}$$

The corrected value was not used when the peak load for the dynamic tests was settled.

6.6. Results of endurance and residual strength tests

One fatigue test to failure was made to find the endurance of the push-out specimen.

Four residual strength tests were made after $4 \cdot 10^5$, $1,0 \cdot 10^6$, $1,2 \cdot 10^6$ and $2 \cdot 10^6$ cycles.

6.6.1. Observed Failure modes for cyclic loading

In order to characterise the failure models for the shear studs the modes observed are characterised of one of three models described here.

Failure of type 3 is crack initiation at the stud shank/weld interface, and crack propagation towards the middle of the shank. The crack is in all cases propagating down, towards the flange. When the area of the shank becomes too small the crack propagates (forced fracture) through the rest of the shank, towards the shank/weld interface, along the line to 3 in Figure 3-14. The failure can be seen in Figure 6-12.

Failure of type 1 is crack initiation and propagation like mode A but when the area becomes too small to handle the forces on the stud the crack propagates (forced fracture) in the flange along line 1 in Figure 3-14 as shown in Figure 6-12.

Failure of type 2 has the same crack initiation and crack propagation as mode A and mode B. When the area of the shank becomes too small to handle the forces applied on the stud the crack propagates (forced fracture) along line 2 in Figure 3-14, as shown in Figure 6-12.

In some cases the cracks have been initiated at the flange/shank interface, probably due to poor welds. These cracks then propagated down into the flange and the forced fracture made these cracks propagate to the weld/shank interface as shown in Figure 6-12, called type 4.

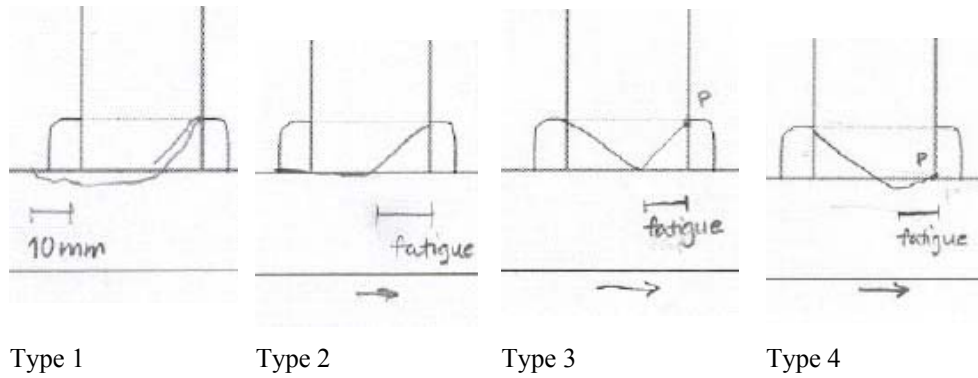


Figure 6-12. Failure modes of endurance and residual strength testing.

6.6.2. Endurance test

The slip of the laser gauges during the whole test is shown in Figure 6-13. The lower curves are slip between steel and concrete and the upper curves shows the horizontal forces. Figure 6-14 shows load - slip curves for 4 whole cycles at different stages of life.

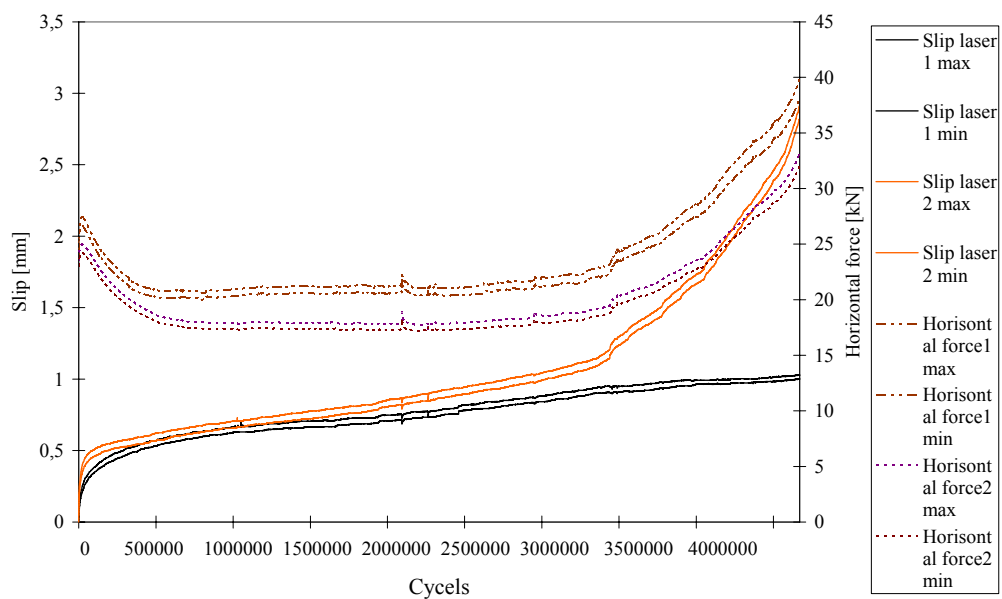


Figure 6-13. Slip diagram of endurance test.

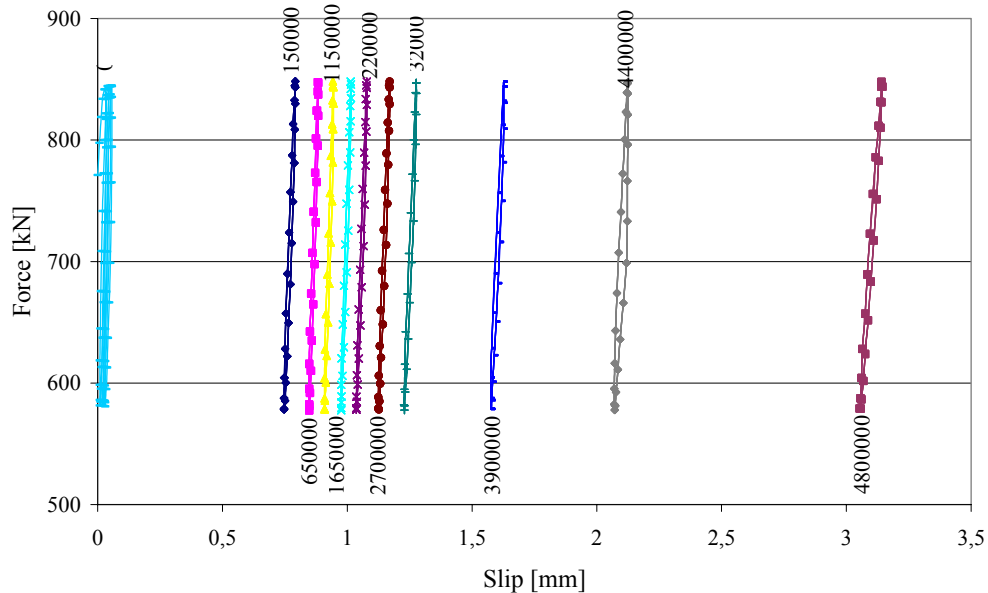


Figure 6-14. Slip measured for 4 cycles at different stages of life.

As can be seen in these figures the initial slip behaviour is non-linear, but after approximately $2 \cdot 10^5$ cycles it can be approximated as linear. At about $3,5 \cdot 10^6$ cycles the slip of laser 2 and the horizontal forces started to increase more rapidly. Failure occurred at $4,9 \cdot 10^6$ cycles.

The failures of the endurance test were two of type 1 and two of type 3.

6.6.3. Summary of residual strength tests

A complete description of the residual strength tests is given in Appendix B. Herein only a summary is given.

Table 6-5 show the residual strengths. The maximum load reduced for horizontal force and max and min slip is also given. Figure 6-15 show the slip curves during the fatigue loading for all residual strength tests and the endurance test.

The slip-load curves during the residual strength test is shown in Figure 6-16.

Failure modes for residual strength tests are summarised in Table 6-6 and sketches of each stud is shown in Appendix D.

Table 6-5. Results from residual strength tests.

Test	Number of cycles	D_{\max} [kN]	D_{corr} [kN]	zero = start of static		zero = start of dynamic	
				Min slip [mm]	Max slip [mm]	Min slip [mm]	Max slip [mm]
1	400 000	1329	1316	4,3	4,8	4,8	5,3
2	1 000 000	1295	1269	3,9	4,8	4,5	5,8
3	1 200 000	1277	1258	4,3	5,2	4,5	6,0
4	2 000 000	1313	1294	4,0	4,9	4,7	5,7

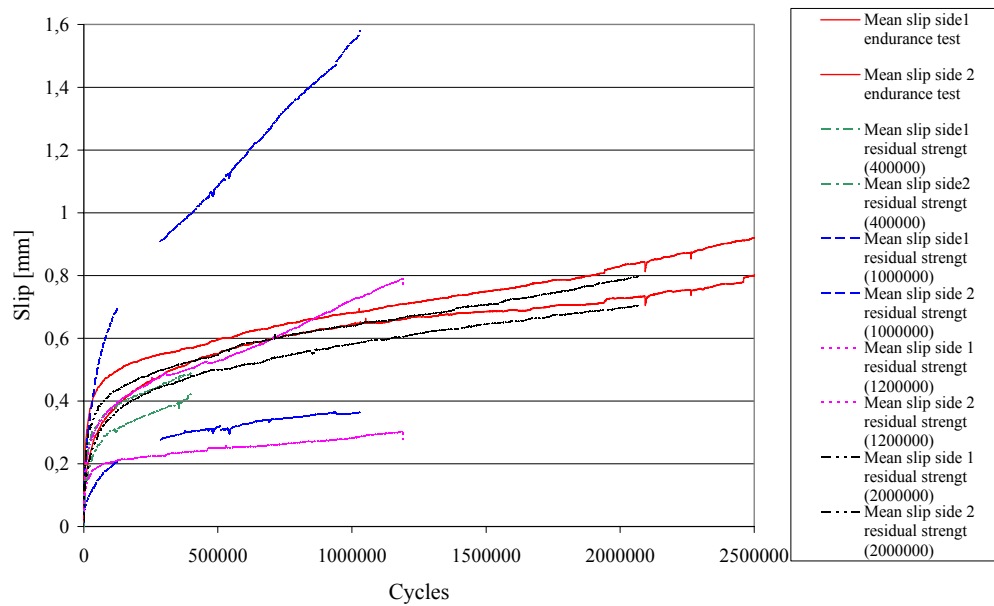


Figure 6-15. Mean slip of lasers in fatigue tests and endurance test.

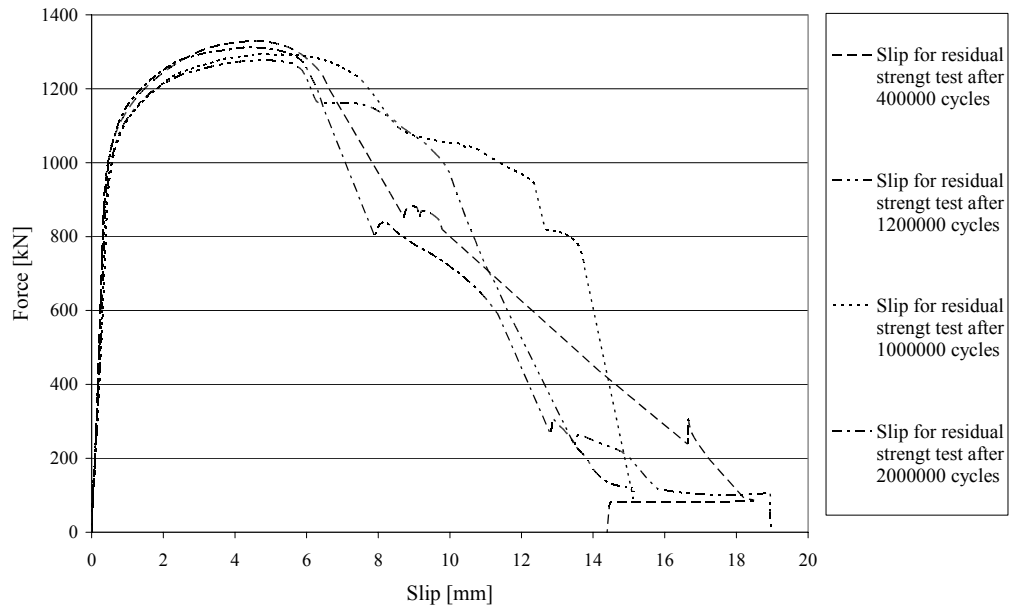


Figure 6-16. Static loading after fatigue.

Table 6-6. Failure modes of residual strength tests.

No. cycles	No. shear studs failed	Type 1	Type 2	Type 3	Type 4
$4 \cdot 10^5$	4			4	
$1 \cdot 10^6$	4			4	
$1,2 \cdot 10^6$	8			6	2
$2 \cdot 10^6$	8		1	7	

7. Discussion

In this chapter the results of the experimental study performed in this project and results by others are discussed. The following parts are included:

Static tests where the results from the static tests are evaluated.

Residual strength tests where the results from the endurance and residual strength tests are evaluated and compared to the results of other researchers.

7.1. Static tests

The results of the static tests are necessary to describe the residual strength because it provides the start point on the failure envelope curve.

7.1.1. Slip for static tests

The slip in the static testing can be seen in Figure 6-10 and in Appendix A the slip for each test is shown. The slip show god similarity between the tests, but test no 1 and test no 5 differ from the others due to the problems during testing described earlier. Test no 2 shows a straighter curve than no 3 and no 4 this is due to problems with support set up.

The maximum loads for the different tests show have small scattering and only test 1 differs, and this is probably due to crushing of the concrete at the support. Tests no 2 and no 5 were first loaded and then released and loaded to failure. The small difference in static load between tests no 2, no 3, no 4 and no 5 indicate that this pre-loading did not influence the maximum capacity.

7.1.2. Horizontal force for static tests

From Table 6-4 can be seen that the increase in horizontal force is almost the same for all tests, independent of the start value. The increase for test no 3 and test no 4 are identical compared to the maximum load applied. Tests no 1, no 2 and no 5 differ more due to problems during testing and are less reliable. The slip in test no 5 was only about 1/3 of the slip in tests no 2 to no 4 and the horizontal force about 2/3.

7.1.3. Comparison between test results and theoretical prediction

In order to get an overview of the results from the static tests, the experimental results are compared to design standards and the calculation model (Oehlers & Johnson) in Table 7-1. The values used in this table are $f_u = 450$ MPa, $f_c = 47,5$ MPa, $E_c = 36$ GPa, $E_s = 210$ GPa (nominal values for steel, values from concrete tests for concrete).

Table 7-1. Comparison between test results and characteristic strength obtained according to Oehlers & Johnson and design codes.

	Static resistance / shear stud [kN]	P_{mean} set as 1
Test result (based on P_{mean})	178,75	1
Test result (based on $P_{\text{mean, reduced}}$)	176,38	0,99
Oehlers & Johnson	186,1	1,04
BSK 99 (Bro 2002 and BV BRO)	132	0,74
Eurocode 3 and 4	136,8	0,77

7.2. Residual strength tests

One objective in this thesis was study the reduction of residual strength, this is done here.

7.2.1. Residual strength test and asymptotic endurance

Experimental results from residual strength tests, endurance test and static tests and best fitting linear regression line are shown in Figure 7-1.

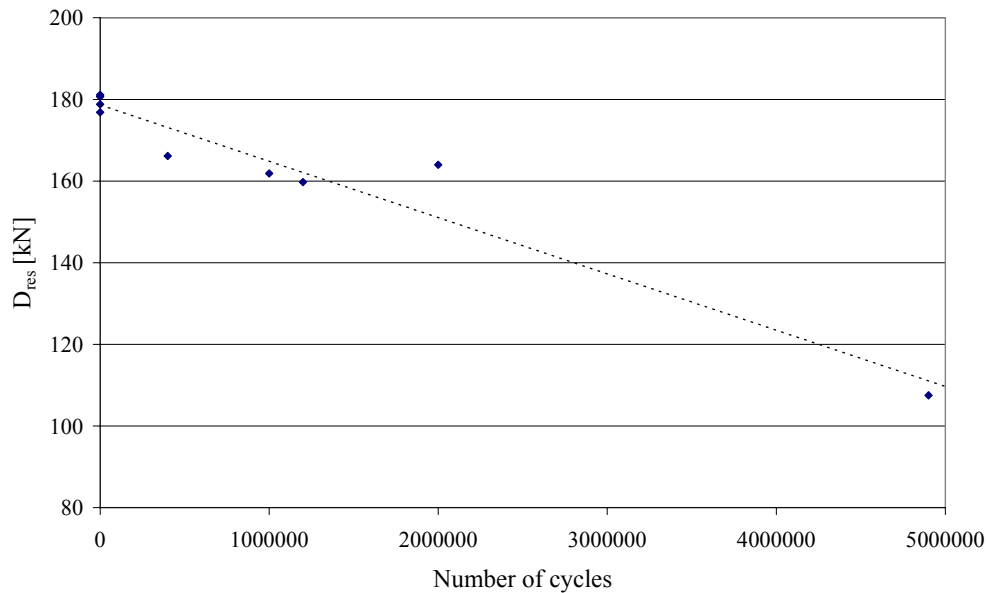


Figure 7-1. Residual strength from tests performed at LTU.

7.2.1.1. Evaluation of E_a according to Oehlers et al (1999)

The regression analysis by Oehlers (1990) gave the following equation for asymptotic endurance, E_a (see also chapter 2):

$$N = E_a \cdot \left(1 - \frac{D_{\text{residual}}}{D_{\text{max}}} \right) \quad \text{Eqn. 7-1}$$

This was applied on the experimental results from LTU, Oehlers (1990) and Hanswille (2004). For each result in a series of tests E_a was calculated using two points; static strength and residual strength. This method was used for evaluation by Oehlers et al (1999). For each series the standard deviation and mean of E_a was calculated, see Table 7-2. In the tests from LTU and Oehlers each value represents one single test result, but in the tests by Hanswille each value is the mean value from three test results.

Table 7-2. Asymptotic endurance of research results from LTU, Hanswille et al(2004) and Oehlers(1990).

Test series	d [mm]	R	P _{max}	D _{max} [kN]	D _{residual} [kN]	N (10 ⁶)	E _a (10 ⁶)	mean E _a (10 ⁶)	Standard deviation (10 ⁶)
LTU	22	0,2 D _{max}	0,6 D _{max}	178,8	166	0,40	5,66	12,82	6,88
					162	1,00	10,59		
					160	1,20	11,29		
					164	2,00	24,24		
					108	4,90	12,29		
Hanswille et al, series 1	22	0,2 D _{max}	0,44 D _{max}	205	154	1,98	7,97	11,39	3,54
					129	5,58	15,05		
					91	6,20	11,15		
Hanswille et al, series 2	22	0,25 D _{max}	0,71 D _{max}	184	174	0,38	7,07	5,46	1,47
					154	0,84	5,15		
					131	1,20	4,17		
Hanswille et al, series 3	22	0,25 D _{max}	0,44 D _{max}	201	133	1,22	3,62	7,28	3,17
					123	3,52	9,07		
					89	5,10	9,15		
Oehlers	12	0,25 D _{max}	0,29 D _{max}	54,33	15,6	1,25	1,75	2,24	0,43
					15,6	1,51	2,11		
					46,1	0,25	1,65		
					43,6	0,50	2,53		
					40,1	0,75	2,86		
					30	1,03	2,29		
					26,5	1,25	2,44		
Oehlers endurance test	12	0,25 D _{max}	0,83 D _{max}	54,33	44,9	0,57	3,30	2,33	0,66
			0,66 D _{max}		35,9	0,72	2,12		
			0,50 D _{max}		26,9	1,09	2,15		
			0,50 D _{max}		26,9	0,90	1,77		

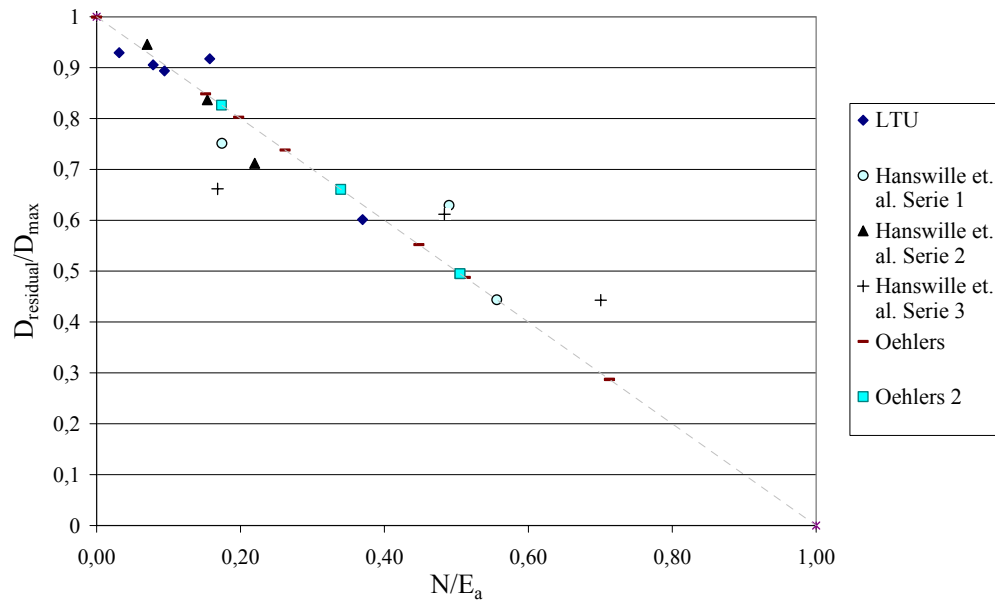


Figure 7-2. Linearly decreasing residual strength.

Table 7-3. Range and peak load for tests shown above.

	R	P _{max}
LTU	0,2 D _{max}	0,6 D _{max}
Hanswille series 1	0,2 D _{max}	0,44 D _{max}
Hanswille series 2	0,25 D _{max}	0,71 D _{max}
Hanswille series 3	0,25 D _{max}	0,44 D _{max}
Oehlers	0,25 D _{max}	0,29 D _{max}
Oehlers 2	0,25 D _{max}	Varying

Oehlers et al (1999) and, as mentioned before, Oehlers (1990) concluded a linear decrease of the residual strength. Observations made by Hanswille et al (2004) indicates crack initiation at about 10-20 % of the fatigue life, and thus not a linearly decreasing residual strength.

Using the evaluation technique presented here, by normalizing each test group with corresponding mean value of E_a , a tendency of linearly decreasing residual strength can be obtained.

7.2.1.2. Evaluation of E_a from test series

An alternative evaluation of the tests considering each test in group for it self follows.

For each series of test a linearization by least square method was made, see Figure 7-3. The equations given by this linearization is shown in Table 7-4 and E_a is calculated for each series.

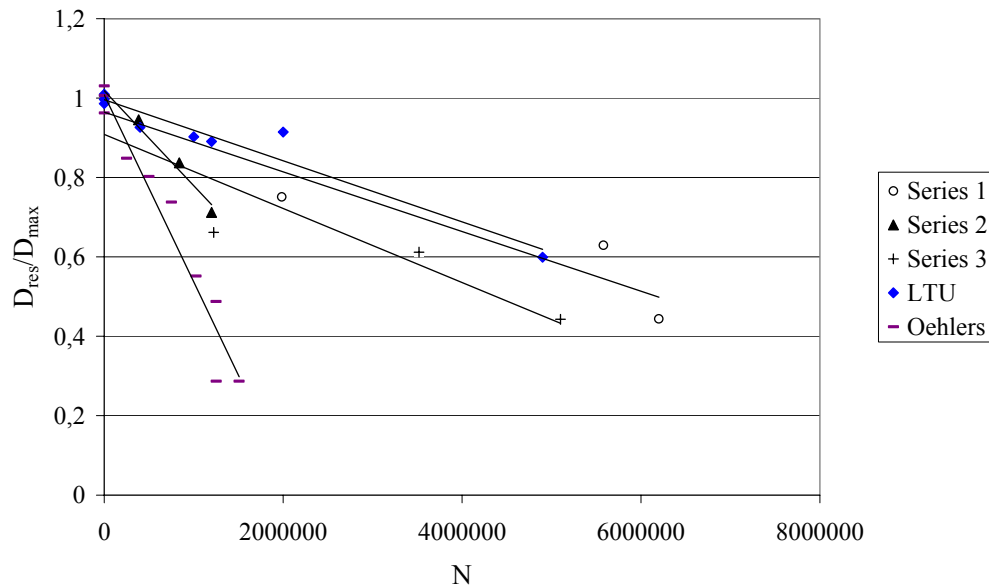


Figure 7-3. Test series with lines adopted to results.

Table 7-4. Equation describing fatigue life and asymptotic endurance.

	Equation, $D_v = D_{res}/D_{max}$	$E_a [10^6]$
LTU	$D_v = 0,9960 - 7,69 \cdot 10^{-8} \cdot N$	12,95
Hanswille series 1	$D_v = 0,9646 - 7,51 \cdot 10^{-8} \cdot N$	12,84
Hanswille series 2	$D_v = 1,018 - 2,39 \cdot 10^{-7} \cdot N$	4,26
Hanswille series 3	$D_v = 0,9088 - 9,34 \cdot 10^{-8} \cdot N$	9,73
Oehlers	$D_v = 1,0083 - 4,71 \cdot 10^{-7} \cdot N$	2,14

7.2.1.3. Observation for residual strength tests

From chapter 7.2.1.1 and 0 the following observations are made:

- The asymptotic endurance seems to depend on the range. Test specimens loaded with high range show a tendency of shorter fatigue life. Table 7-2 indicate that peak load does not influence E_a . Test with the same range and

different peak load gives approximately the same asymptotic endurance for the same diameter.

- The shank diameter influence E_a . The smaller bolts used by Oehlers has shown a more rapid decrease of residual strength and shorter life than bolts of larger for the shank diameter subjected to the same range.

The residual strength can be approximate by the linearly decreasing equation derived according to Oehlers (1990).

$$D_{\text{residual}} = D_{\text{max}} \left(1 - \frac{N}{E_a} \right) \quad \text{Eqn. 7-2}$$

$$R = 0,2 \cdot D_{\text{max}} \text{ gives } E_a = 12,9 \cdot 10^6.$$

As mentioned in chapter 5 BV BRO does not allow composite action in ULS. In BRO 2002 and Eurocode it is assumed that the residual strength is high enough to allow composite action in design in ULS.

In Table 7-5 characteristic ranges for different number of cycles according to EC, BV BRO and BRO 2002 are shown. BRO 2002 limits characteristic static strength to 132 kN and since composite action is allowed in ULS this value are considered the residual strength at all stages of life. The same design procedure is used in EC 3 and 4, but the characteristic static/residual strength is 136,8 kN. BV BRO does not allow for composite action in ULS and so the residual strength is taken to be zero.

Comparing the residual strength of the tests from LTU to those given in the codes suggest that the residual strength is 15-18 % higher than characteristic for ranges similar or smaller.

Figure 7-4 show equation 7.2 plotted for $R = 0,2D_{\text{max}} = 35,5$ kN, characteristic values according to EC 3 for $R = 34,9$ kN and BRO 2002 for $R = 39,6$ kN. As seen in the figure, the strength of a shear connector is higher than suggested in EC 3 and BRO 2002. The use of modified version of equation 7.2 would be a more accurate design model, but EC 3 can be considered an acceptable simplification. Arguments to support the assumption in BV BRO have not been found. For the largest range allowed when design life is 106 cycles, 26,4kN, the residual strength would be considerably higher than the static strength given in EC (136,8 kN).

Table 7-5. Comparison between residual strength and range in tests and codes, without safety factors.

Code	D_{\max} [kN]	Cycles					
		10^5		4×10^5		10^6	
		R [kN]	D_{res} [kN]	R [kN]	D_{res} [kN]	R [kN]	D_{res} [kN]
BRO2002	132	39,6	132	25,08	132	18,1*	132*
BV BRO, $\kappa=2/3$	132	55,9	0	-	0	26,4	0
EC 3	136,8	55,2	136,8	42	136,8	34,9	136,8
EC 4	136,8	49,8	136,8	41,8	136,8	37,2	136,8
Test at LTU	178,5	-	-	35,5	166,1	35,5	161,9

* Calculated according to BSK99, see chapter 4.

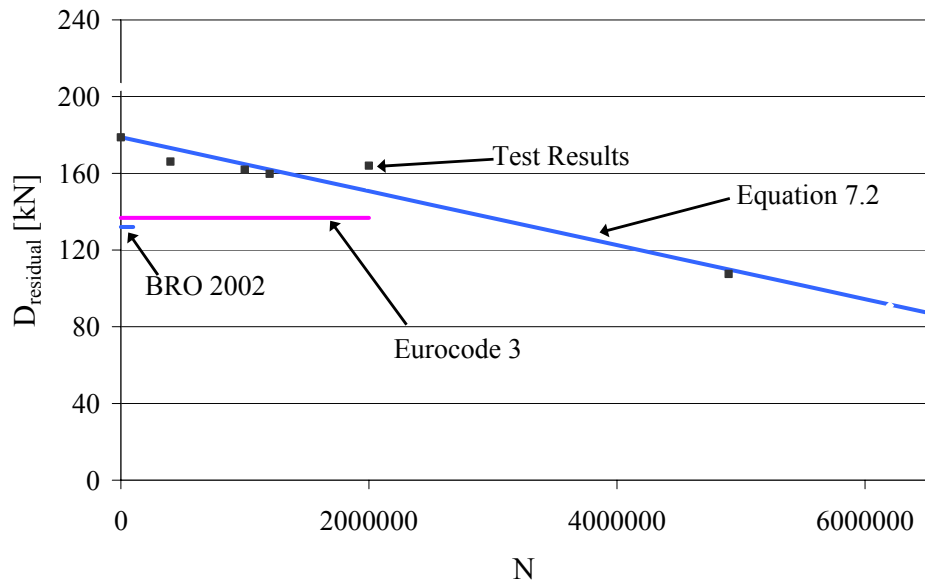


Figure 7-4. Comparison between residual strength according to EC 3, BRO 2002 and equation proposed at LTU for $R = 35,5$ kN.

7.2.2. Slip

The mean slip from all fatigue tests is shown in Figure 7-5. For each curve the slope has been approximated for the straight part. The approximation curve is also shown in the figure. The approximation curve was visually adapted to the test result by choosing a point in the beginning of the straight part and one point in the end. The start point

was therefore not chosen at the same cycle in different tests. The slip growth/cycle (δf) has been calculated and is shown in Table 7-6. Since side 1 of test 2 is deformed much more than the other tests, test 2 is omitted in the second calculation of the mean value.

The slip growth is thought to be of use as a check. It is clear that the slip growth is constant after the initial deformation. In push-out tests of 22 mm diameter studs, performed at LTU with a range of $0,2D_{\max}$, the initial deformation was of 0,3-0,6 mm and the slip growth about $2,2 \cdot 10^{-7}$ mm/cycle.

Slip growth for a composite bridge is also thought to be constant after the initial deformation, but value presented above is not likely valid.

Oehlers et al (1999) found that the slip growth starts to increase rapidly after approximately 50 % of the asymptotic endurance. In the single endurance test performed at LTU this point was approximately 30 % of E_a (see Figure 6-13). This increase indicates that the fatigue life is in its final stage, which could be useful to estimate the condition of a bridge and avoid fatigue failure.

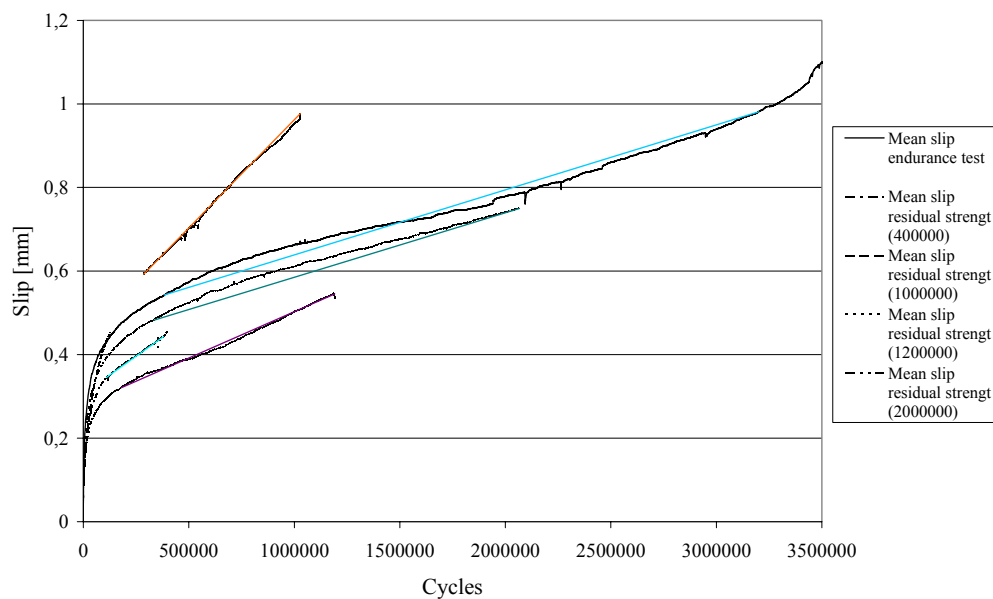


Figure 7-5. Mean slip of lasers during fatigue test and approximate curves describing the mean slip

Table 7-6. Slip/cycle for fatigue tests

test	number of cycles	slip/cycle [mm/cycle]	initial slip [mm]
1	400 000	3,60E-07	0,35
2	1 000 000	5,18E-07	0,59
2	1 000 000 - side 1	9,07E-07	0,59
2	1 000 000 - side 2	1,29E-07	0,59
3	1 200 000	2,22E-07	0,32
4	2 000 000	1,54E-07	0,48
endurance	Endurance	1,56E-07	0,54
mean of all		2,82E-07	0,46
mean of all but 1 000 000		2,23E-07	0,42

Calculation models for slip growth has been proposed by for example Taplin & Grundy (1997, 1995) and Oehlers & Coughlan (1986). The model by Oehlers & Coughlan was derived for 116 push-tests of different diameters and could be expected to be valid. The value achieved was

$$\delta_f = 1,70 \cdot 10^{-5} \cdot \frac{R}{D_{\max}}^{4,55} = 1,12 \cdot 10^{-8}$$

for $R/D_{\max} = 0,2$ (same as in tests performed at LTU). This slip is much smaller than the slip achieved at LTU and the reason for this difference (about 20 times) is uncertain.

7.2.3. Failure modes

The failure mode observed in tests carried out at LTU is seen in Figure 6-12. These modes are all very similar; type 1, 2 and 3 only differs in what way the forced fracture takes. Type 4 was only observed once and this mode is very similar to the other failure modes, but due to poor welding the fatigue crack starts at the interface between flange and stud shank. Hanswille et al (2004) observed similar failure modes.

All failures occurred in the shank of the stud shear connectors. This means that the results obtained are reliable for deriving residual strength of shear studs.

8. Conclusions

The following conclusions were made:

- The residual strength is linearly decreasing and the decreasing rate is dependent only on range. The following equation can be used to derive the residual strength:

$$D_{\text{residual}} = D_{\text{max}} \left(1 - \frac{N}{E_a} \right)$$

where $E_a = 12,9 \cdot 10^6$ for $R = 0,2 \cdot D_{\text{max}}$ and $d = 22\text{mm}$.

- Bolt diameter affect the fatigue life. Comparison between tests by Hanswille (22 mm studs) and Oehlers (12,7 mm studs) for the same range ($0,25D_{\text{max}}$) show that smaller diameter gives a shorter fatigue life.
- The design according BV BRO, where composite action is not allowed in ULS, is not supported by arguments found in this thesis. There is considerable residual resistance after high cyclic preloading.
- The results are reliable for shear studs since failure occurred in the shank of the stud in all tests. Failure modes were identical to those described in previous research reports.

Further investigations needed:

- Compare tests performed with $R = 0,2 \cdot D_{\text{max}}$ to those of $R = 0,25 \cdot D_{\text{max}}$ for $P_{\text{max}} < 0,6 \cdot D_{\text{max}}$ to further investigate the influence of range on residual strength.
- Perform more residual strength tests in the last stage of fatigue life to elucidate the linear form of the failure envelope.

9. References

- Banverket (1999). BV BRO – Banverkets ändringar och tillägg till Vägverkets BRO 94, Utgåva 5.
- Boverket (1998). BKR 94 – Boverkets konstruktionsregler. BFS 1998:38. ISBN 91-7147-455-2.
- Boverket (1999). BSK 99 – Boverkets handbok om stålkonstruktioner. ISBN 91-7147-527-3.
- Broek, D. (1982). *Elementary engineering fracture mechanics*. 3d rev edition. The Hague: Martinus Nijhoff Publishers. ISBN 90-247-2580-1.
- EC 1, Eurocode 1 (2002). prEN 1991-2: (Eurocode 1: Actions on structures – Part 2: Traffic loads on bridges). CEN (Comité Européen de Normalisation), Brussels.
- EC 3, Eurocode 3 (2002). prEN 1993-2: (Eurocode 3: Design of steel structures – Part 2: Rules for bridges). CEN (Comité Européen de Normalisation), Brussels.
- EC 3, Eurocode 3 (2002). EN 1993-1-9 (Eurocode 3: Design of steel structures – Part 1.9: Fatigue strength of steel structures). CEN (Comité Européen de Normalisation), Brussels.
- EC 4, Eurocode 4 (2003). prEN 1994-2 (Eurocode 4: Design of composite steel and concrete structures – Part 2: Rules for bridges). CEN (Comité Européen de Normalisation), Brussels.
- Gurney, T. R. (1979). *Fatigue of welded structures*. 2nd edition. Cambridge: Cambridge University Press. ISBN 0-521-22558-2.
- Hallam, M.W. (1976). *The behaviour of stud shear connectors under repeated loading*. Boston: British Library. Research report no R281.
- Höglund, T. (1994) *Handboken BYGG*. K18, Dimensionering av stålkonstruktioner. Solna: Svensk Byggtjänst. ISBN 91-38-12820-9
- Institutionen för Väg- och vattenbyggnad. *Grundläggande konstruktionslära*. Luleå.
- Johnson, R. P. & Anderson, D. (1993). Designer's handbook to Eurocode 6. Part 1.1: Design of composite steel and concrete structures. Wiltshire: MHL Typesetting Ltd. ISBN 0-7277-1619-5.
- Johnson, R. P. (2000). Resistance of stud shear connectors to fatigue. *Journal of Constructional Steel Research*. Vol 56, p 101-116.
- Johnson, R.P. & Oehlers, D.J. (1996) Integrated static and fatigue design or assessment of stud shear connections in composite bridges. *The Structural Engineer*. 74 (14), p 236-240.
- Mainstone, R.J. & Menzies, J.B. (1967). Shear connectors in steel-concrete composite beams for bridges. *Concrete*. September 1967, p 291-302.

- Oehlers, D.J. & Coughlam, C. G. (1986). The shear stiffness of stud shear connections in composite beams. *Journal of Structural Steel Research*. 1986 (6), p. 273-284.
- Oehlers, D. J. & Johnson, R. P. (1987). The strength of stud shear connections in composite beams. *The Structural Engineer*. 65B (2), p. 44-48.
- Oehlers, D. J. & Bradford, M. A. (1995). *Composite steel and concrete structural members*. Oxford: Elsevier Science Ltd. ISBN 0-08-041919-4.
- Oehlers, D.J., Seracino, R. & Yeo, M.F. (1999). *Reverse cycle fatigue tests on stud shear connectors*. Research report No. R165, University of Adelaide. ISBN 0-68396-811-2.
- Oehlers, D.J. (1990). Deterioration in strength of stud connectors in composite bridge beams. *Journal of Structural Engineering*. 116 (12), p 3417-3431.
- Oehlers D.J. (1990). Methods of estimating the fatigue endurance of stud shear connections. IABSE Proceedings P-145/90, IABSE Periodica 3/1990, p 65-84.
- Popov, E. P. (1990). *Engineering mechanics of solids*. New Jersey: Prentice-Hall, Inc. ISBN 0-13-279258-3.
- Rolfe, S. T. & Barsom, J. M. (1977). *Fracture and fatigue control in structures*. New Jersey: Prentice-Hall Inc. ISBN 0-13-329953-8.
- Stålbyggnadsinstitutet. (1994). *Studie av Eurocode 4 – Samverkanskonstruktioner*. Rapport 177:1. Stockholm: NsT Kopia. ISBN 91-7127-010-8.
- Taplin, G & Grundy, P (1995). The incremental slip behaviour of stud shear connectors. Proceedings of the Fourteenth Australasian Conference on the Mechanics of Structures and Materials, Hobart.
- Taplin, G & Grundy, P (1997). Incremental slip of stud shear connectors under repeated loading. *International Conference Composite Constructions*. Innsbruck, p. 145-150.
- Taplin, G & Grundy, P (1999). Steel concrete composite beams under repeated load. Sixteenth Australasian Conference on the Mechanics of Structures and Materials, Sydney, December 1999
- Veljkovic, M. (2001) Behaviour of shear studs under repeated load – pre-study report. Luleå. Department of Civil Engineering. Publication No.2001:01.
- Vägverket (2002). BRO 2002 - Vägverkets allmänna tekniska beskrivning för nybyggande och förbättring av broar Bro 2002. ISSN 1401-9612.
- Upphovsman. (År). Lecture 12.2: Advanced Introduction to Fatigue. URL: <http://www.bwk.kuleuven.ac.be/bwk/materials/Teaching/master/wg12/t0200.htm>. (2004-02-19).

Appendix A

Test 1s

Description and comments

As described in chapter 6 the support in this test consisted of two rolls, one of which was free to slide and one which was steady. Between the steel rolls and the concrete slabs, thin steel plates were placed in order for load to spread as intended in EC4. The rolls were placed 25 mm from the inner edge of the concrete slab. At first the steel rods were pre-stressed at about 50 kN, but since horizontal cracks could be seen on the outside of the concrete slabs this value was reduced to about 20 kN.

During the test procedure noise indicating cracking started to come from the test specimen at about 1000 kN. Right before fracture cracking of the concrete at side 1 was observed (see figure 6-4 in chapter 6), and soon after this fracture occurred as the shear studs of side 2 was sheared off.

Results

$$(D_{\max})_{\text{push}} = 1245 \text{ kN}.$$

The slip at the maximum load can be seen as three different curves at the approximate deformations of

Slip on side 1 [mm]				Slip on side 2 [mm]			
Left		Right		Left		Right	
LVD1 1	LVD1 5	LVD1 2	LVD1 6	LVD1 3	LVD1 7	LVD1 4	LVD1 8
3,2	3,2	3,7	3,7	5,1	5,1	5,1	5,1

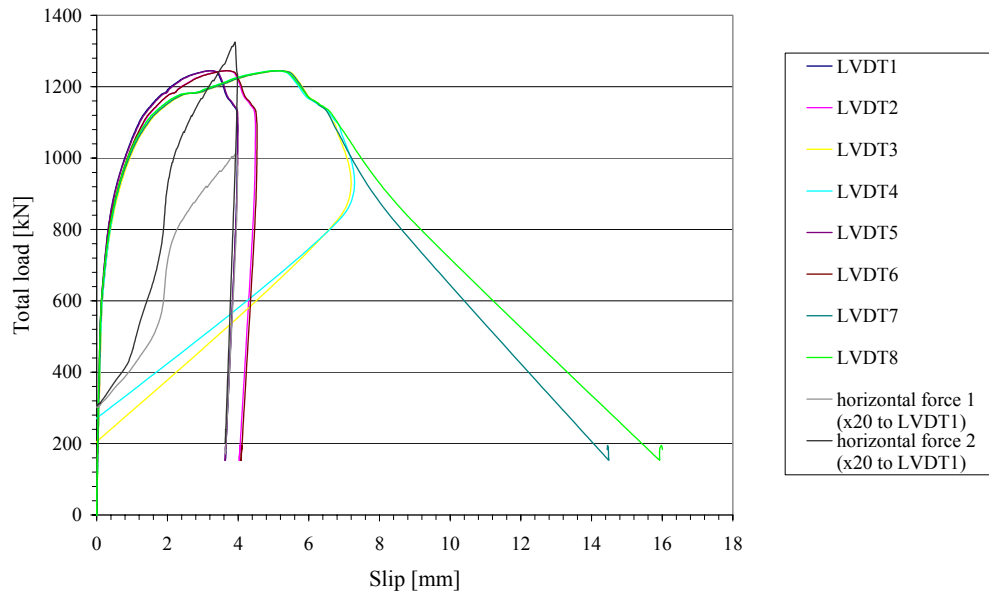


Figure A. 1 Slip-load diagram of test 1s.

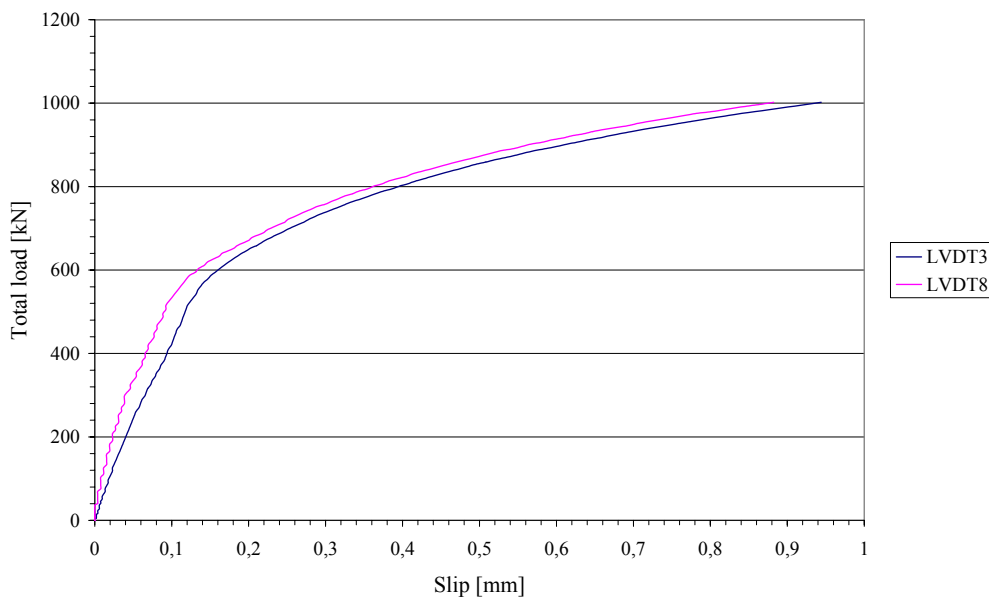


Figure A. 2 Enlarged load-slip diagram used to estimate tangent stiffness of the shear stud.

Test 2s

Description and comments

In this test, the rolls were placed 15 mm from the inner edge of the concrete slab. The steel bar was pre-stressed till about 20 kN. At about 950 kN, crushing of the concrete could be seen above the support-steel rods. The crushing occurred at both sides. At about 1150 kN, the test specimen could not resist any more load. The slip-load curve of this loading is shown in figure 3. The load was removed and the failure was analysed. As seen in figure 4 the L-bar tilted, enlarging the compressive and shear forces in the concrete.

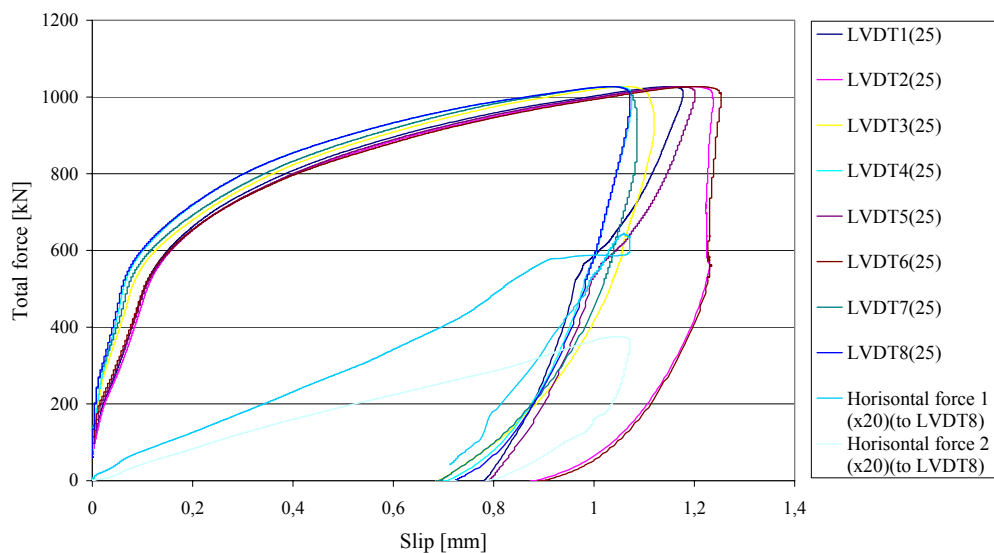


Figure A. 3. Slip-load diagram of test 2s, concrete failure. Observe the scale



Figure A. 4 Concrete crush of test specimen 2.

Since the failure was not the anticipated, and the shear studs were not yet expected to have failed, the test set-up was changed according to chapter 6 and a new test was performed on the same specimen.

This time the applied force and slip between the steel and concrete increased during deformation, until the specimen could not resist any more load.

When the maximum load had been reached, deformation was continued during decreasing load, until the studs of both sides was sheared off.

Results

$$(D_{\max})_{\text{push}} = 1430 \text{ kN}.$$

The slip at the maximum load can be seen as three different curves at the approximate deformations of

Slip on side 1 [mm]				Slip on side 2 [mm]			
Left		Right		Left		Right	
LVDT 1	LVDT 5	LVDT 2	LVDT 6	LVDT 3	LVDT 7	LVDT 4	LVDT 8
6,2	6,2	7,1	7,1	6,2	6,2	4,7	4,7

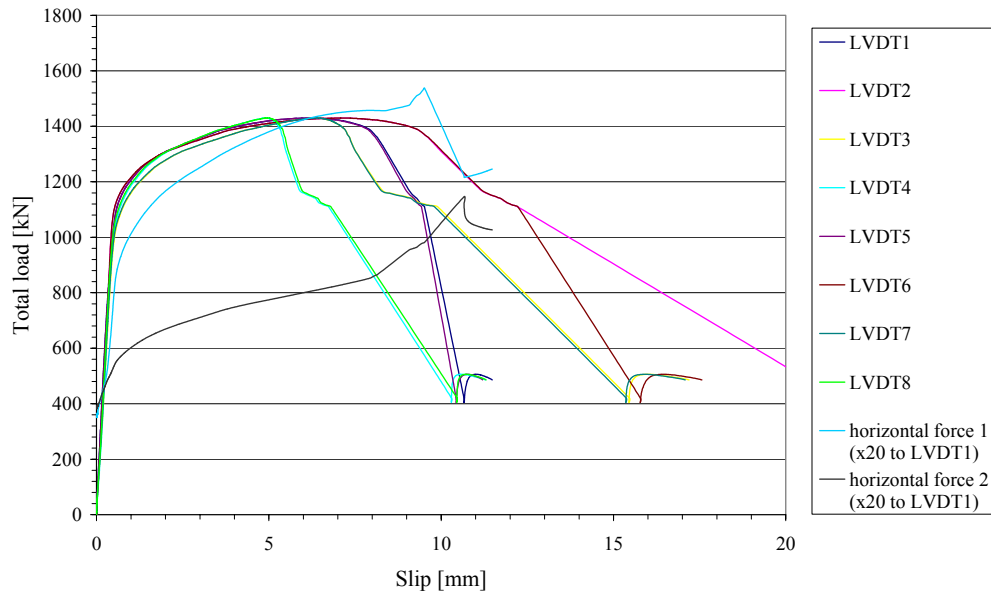


Figure A. 5 Slip-force diagram of test 2s

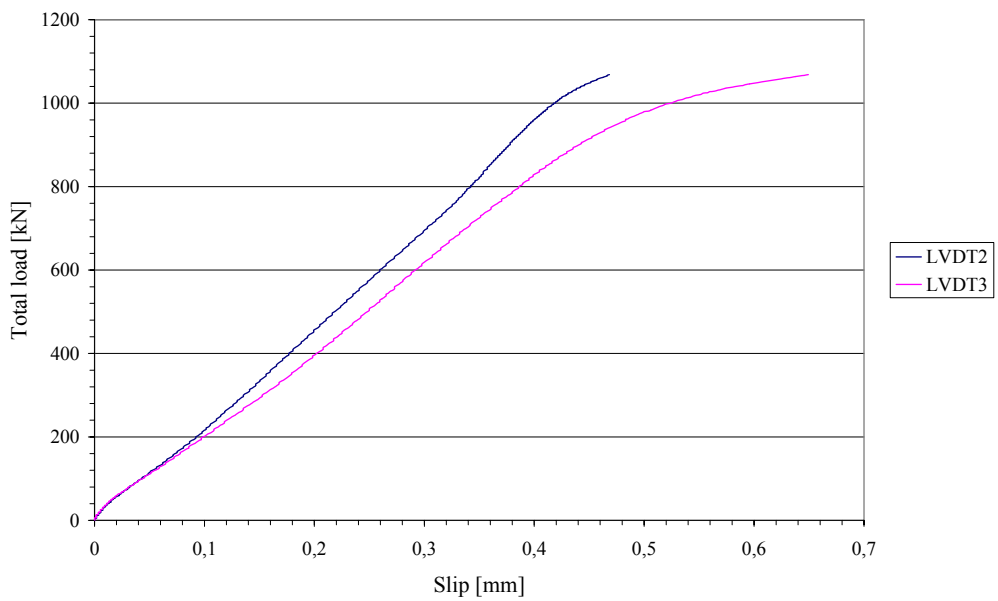


Figure A. 6 Enlarged load-slip diagram used to estimate tangent stiffness of the shear stud.

Test 3s

Description and comments

In this test a new test set-up was used, see chapter 6. The steel rods were pre-stressed till about 20 kN.

In this test the shear studs of both sides were sheared off.

Results

$(D_{\max})_{\text{push}} = 1445 \text{ kN}$.

The deformation at the maximum load can be seen as two curves at the approximate deformations of

Slip on side 1 [mm]				Slip on side 2 [mm]			
Left		Right		Left		Right	
LVDT 1	LVDT 5	LVDT 2	LVDT 6	LVDT 3	LVDT 7	LVDT 4	LVDT 8
7,9	7,9	6,5	6,5	7,9	7,9	7,9	7,9

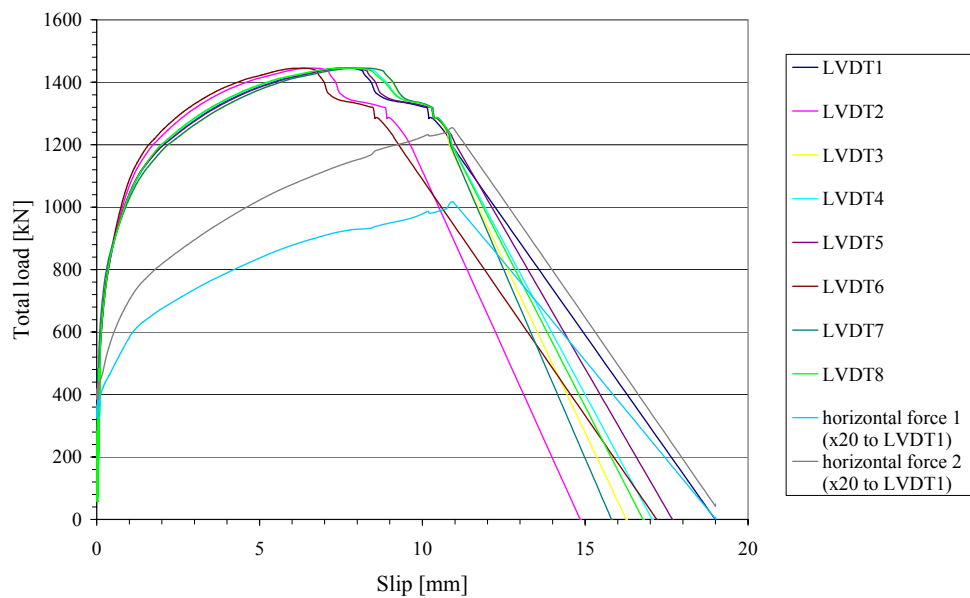


Figure A. 7 Slip-force diagram of test 3s.

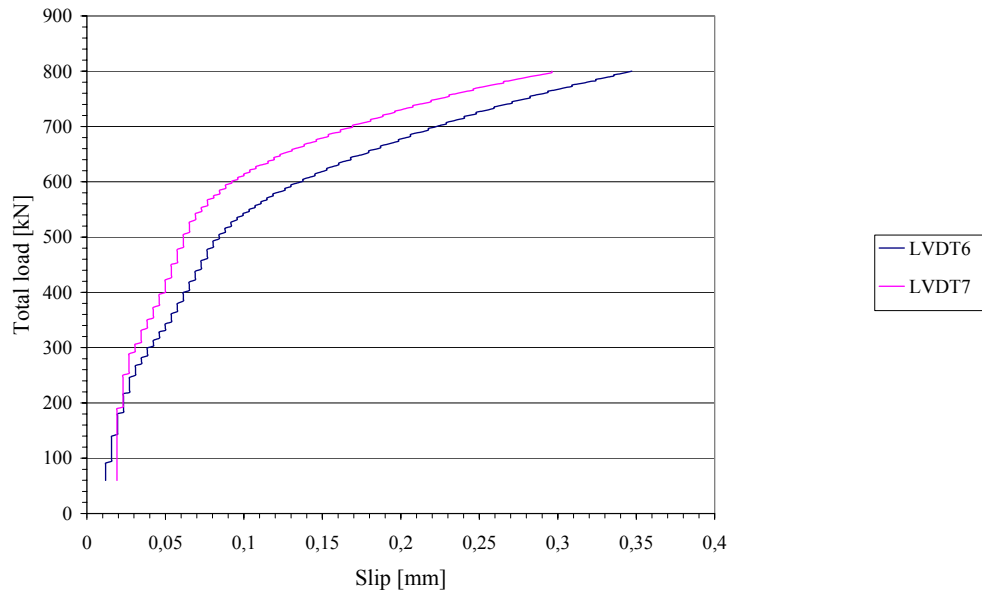


Figure A. 8 Enlarged load-slip diagram used to estimate tangent stiffness of the shear stud.

Test 4s

Description and comments

This test was performed as test 3, but the pre-stressing of the steel rods was reduced to about 1 kN.

In this test the shear studs of both sides were sheared off.

Results

$(D_{\max})_{\text{push}} = 1415 \text{ kN}$.

The slip at the maximum load can be seen as two curves at the approximate deformations of

Slip on side 1 [mm]				Slip on side 2 [mm]			
Left		Right		Left		Right	
LVDT 1	LVDT 5	LVDT 2	LVDT 6	LVDT 3	LVDT 7	LVDT 4	LVDT 8
5,1	5,1	5,1	5,1	5,8	5,8	5,1	5,1

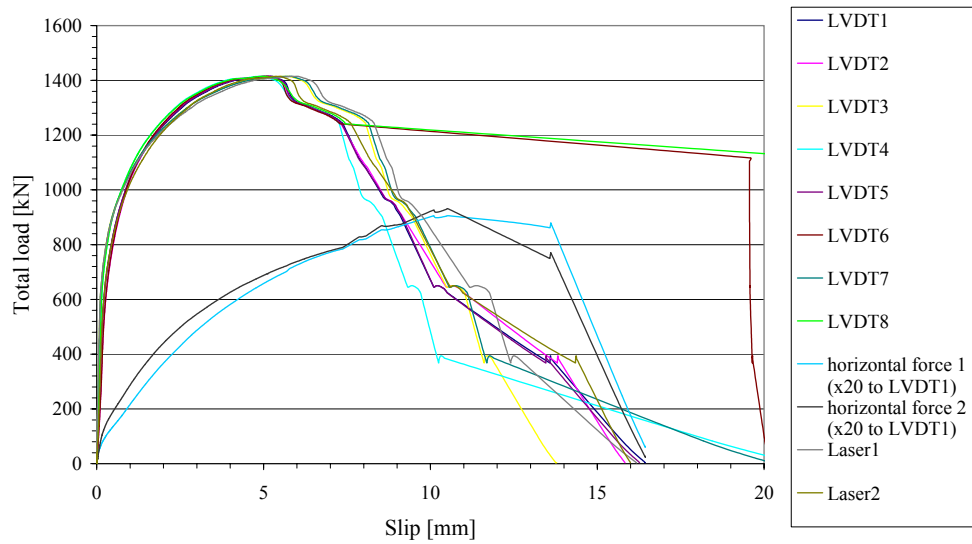


Figure A. 9 Slip-load diagram for test 4s.

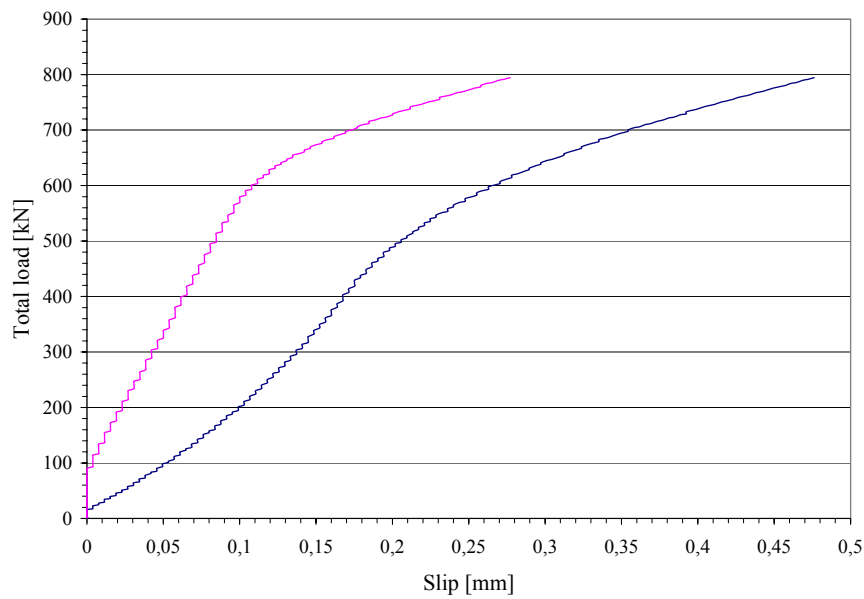


Figure A. 10 Enlarged load-slip diagram used to estimate tangent stiffness of the shear stud.

Test 5s

Description and comments

The test set-up was as in the previous two tests. When a dynamic test should be started, the load happened to be applied extremely fast (1350 kN in just a couple of seconds) and because of this the results from the test would not be reliable. Therefore it was decided to perform another static test, using this test specimen.

The small slip is probably due to the accidentally applied load. Unfortunately the measurement had not yet been started when this load was applied so the deformation was not measured.

In this test the shear studs of side 2, with LVDT 3, 4, 7 and 8, were sheared off.

Results

$(D_{\max})_{\text{push}} = 1449 \text{ kN}$.

The slip at maximum load can be seen as two curves at the approximate deformation of

Slip on side 1 [mm]				Slip on side 2 [mm]			
Left		Right		Left		Right	
LVDT 1	LVDT 5	LVDT 2	LVDT 6	LVDT 3	LVDT 7	LVDT 4	LVDT 8
2,3	2,3	2,3	1,6	1,6	1,6	1,6	1,6

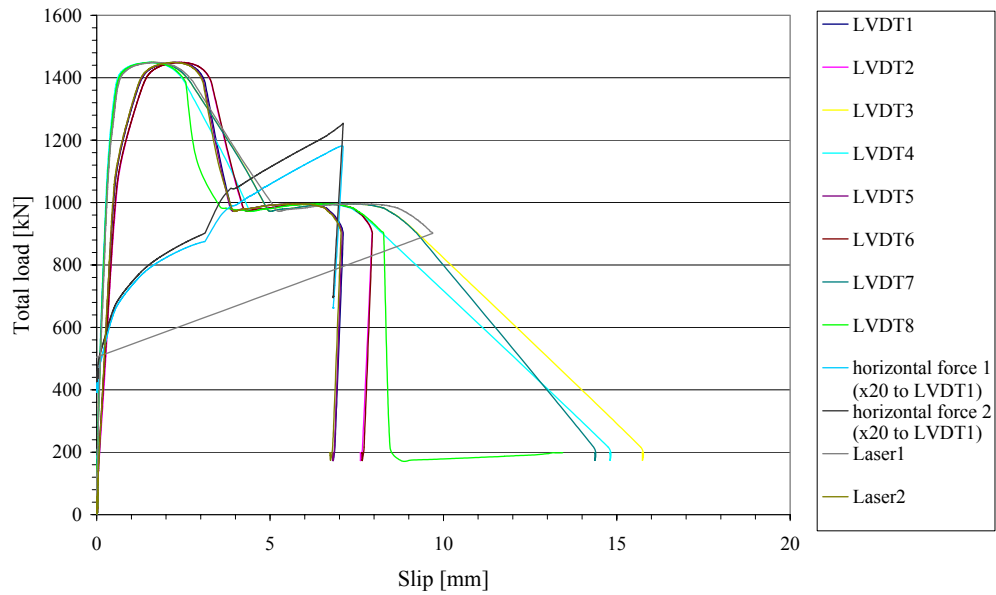


Figure A. 11 Slip-load diagram of test 5s.

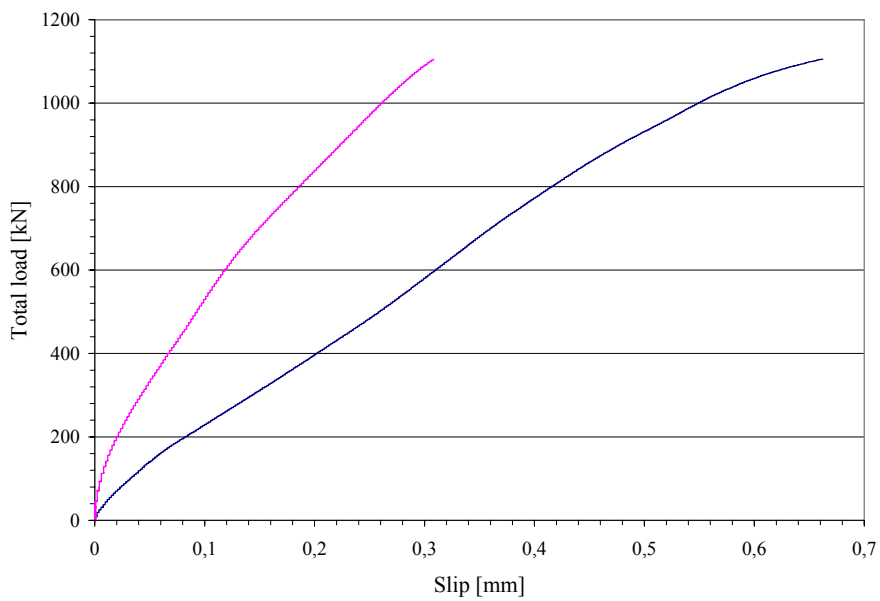


Figure A. 12 Enlarged load-slip diagram used to estimate tangent stiffness of the shear stud.

Appendix B

Test 1d

Description and comments

The number of cycles was set to 400 000, and the slip during the whole test is shown in Figure B. 1. After the fatigue loading the test specimen was loaded statically to fracture.

Results

$(D_{\text{residual}})_{\text{push}} = 1329 \text{ kN}$.

The slip-force diagram is shown in Figure B. 2. The slip at the maximum load can be seen as two curves, with a slip of

Side 1					Side 2				
Left			Right		Left			Right	
LVDT 1	LVDT 5	Laser 2	LVDT 2	LVDT 6	LVDT 3	LVDT 7	Laser 1	LVDT 4	LVDT 8
4,8	4,8	4,8	4,8	4,8	4,8	4,8	4,8	4,3	4,3

when start is set to the beginning of the residual strength loading. The slip during dynamic loading was about 0,5 mm.

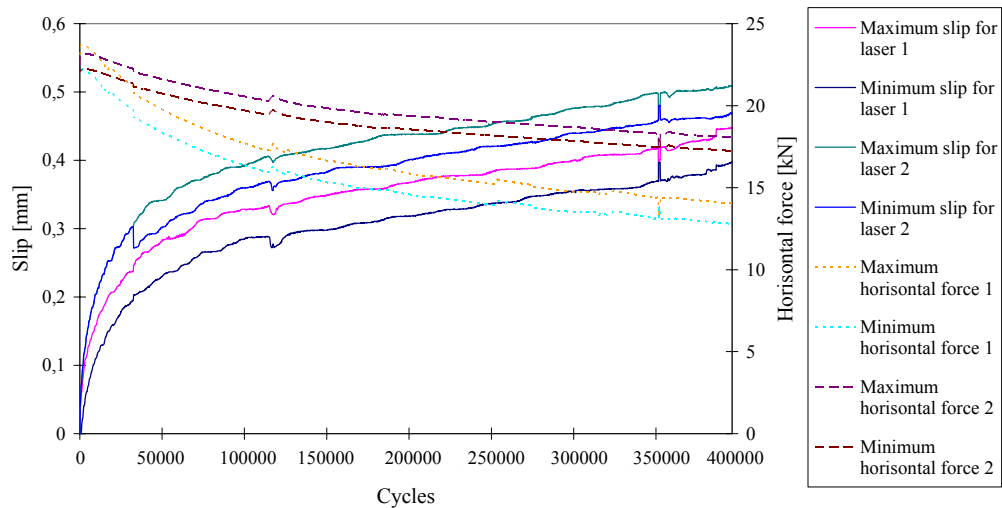


Figure B. 1 Slip of lasers during fatigue loading.

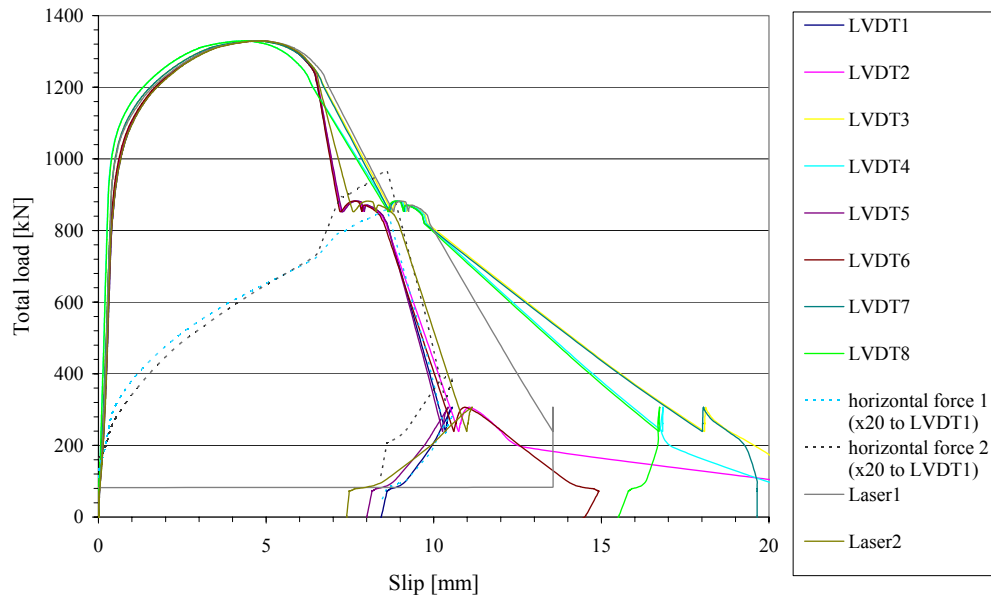


Figure B. 2. Slip-load diagram of residual strength test.

Test 2d

Description and comments

The number of cycles was 1 200 000, the slip during the test is shown in Figure B. 3.

The slip-load curve is shown in Figure B. 4.

Results

$(D_{\text{residual}})_{\text{push}} = 1329 \text{ kN}$. The slip at maximum load can be seen as three curves with a slip of

Side 1					Side 2				
Left			Right		Left			Right	
LVDT 1	LVDT 5	Laser 2	LVDT 2	LVDT 6	LVDT 3	LVDT 7	Laser 1	LVDT 4	LVDT 8
4,9	4,9	-	5,2	5,2	4,3	4,3	-	4,3	4,3

when start is set to the beginning of the residual strength loading. The slip during dynamic loading was 0,2-0,8 mm.

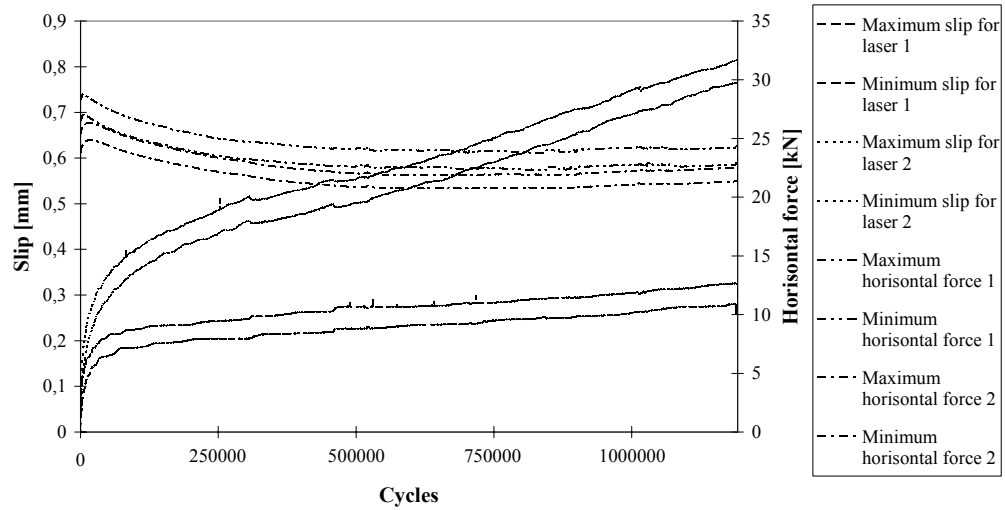


Figure B. 3 Slip of lasers during fatigue loading.

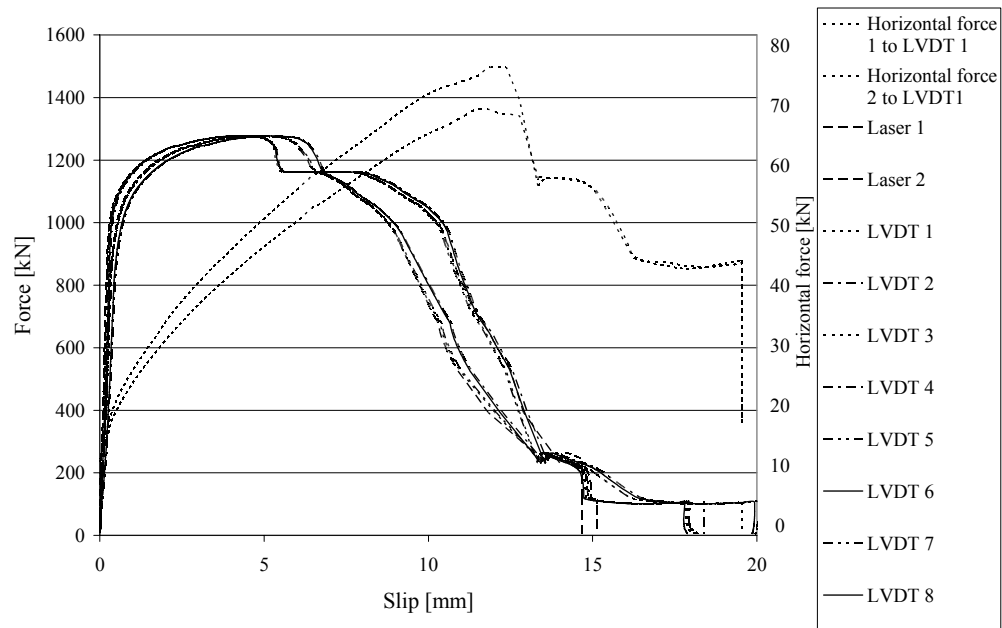


Figure B. 4. Slip-load curve during residual strength testing.

Test 3d

Description and comments

The number of cycles was 2 000 000 and the slip curve during fatigue loading is shown in Figure B. 5.

The slip-load diagram is shown in Figure B. 6.

Results

$$(D_{\text{residual}})_{\text{push}} = 1312,7 \text{ kN}$$

Side 1					Side 2				
Left			Right		Left			Right	
LVDT 1	LVDT 5	Laser 2	LVDT 2	LVDT 6	LVDT 3	LVDT 7	Laser 1	LVDT 4	LVDT 8
4,9	4,9	4,9	4,3	4,3	4,0	4,0	4,0	4,3	4,3

when start is set to the beginning of the residual strength loading. The slip during dynamic loading was 0,5-0,8 mm.

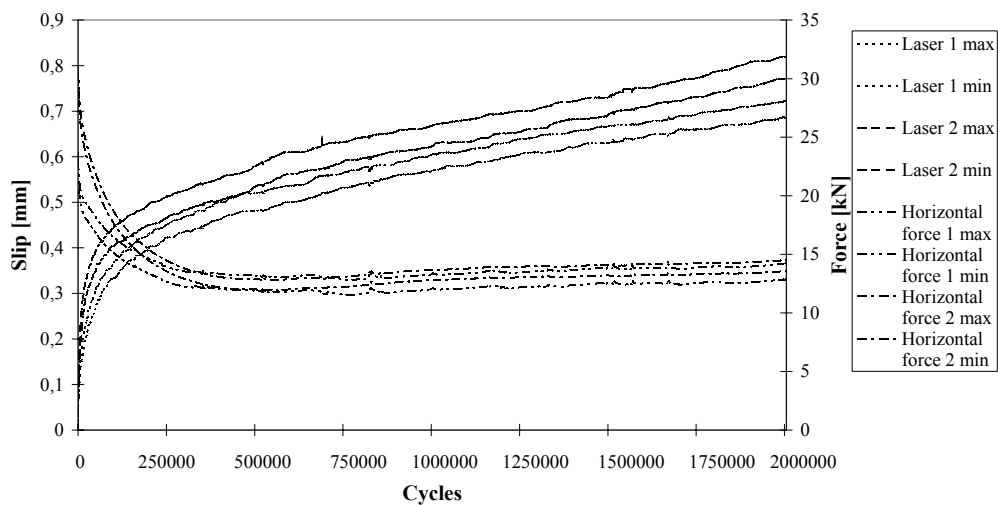


Figure B. 5. Slip of lasers during fatigue loading.

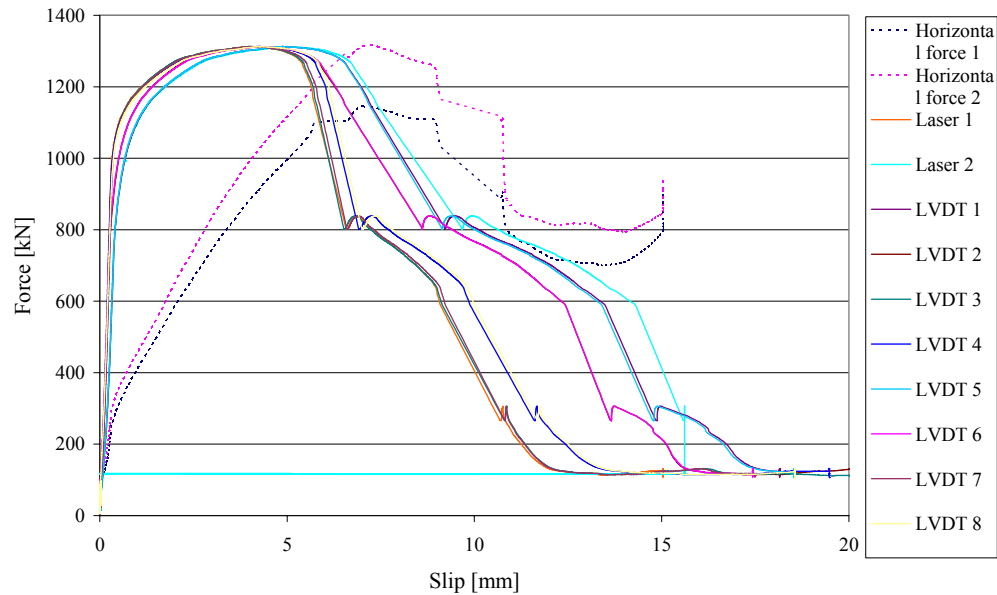


Figure B. 6. Slip-load curve of residual strength test.

Test 4d

Description and comments

The number of cycles was 1 000 000 and the slip curve during fatigue loading is shown in Figure B. 7. The load-slip curve is shown in Figure B. 8.

Results

$$(D_{\text{residual}})_{\text{push}} = 1295 \text{ kN}$$

The maximum slip at fracture can be seen as two curves with a slip of

Side 1					Side 2				
Left			Right		Left			Right	
LVDT 1	LVDT 5	Laser 2	LVDT 2	LVDT 6	LVDT 3	LVDT 7	Laser 1	LVDT 4	LVDT 8
3,8	3,8	3,8	3,8	3,8	4,8	4,8	4,8	4,8	4,8

when start is set to the beginning of the residual strength loading. The slip during dynamic loading was 0,2-1,0 mm.

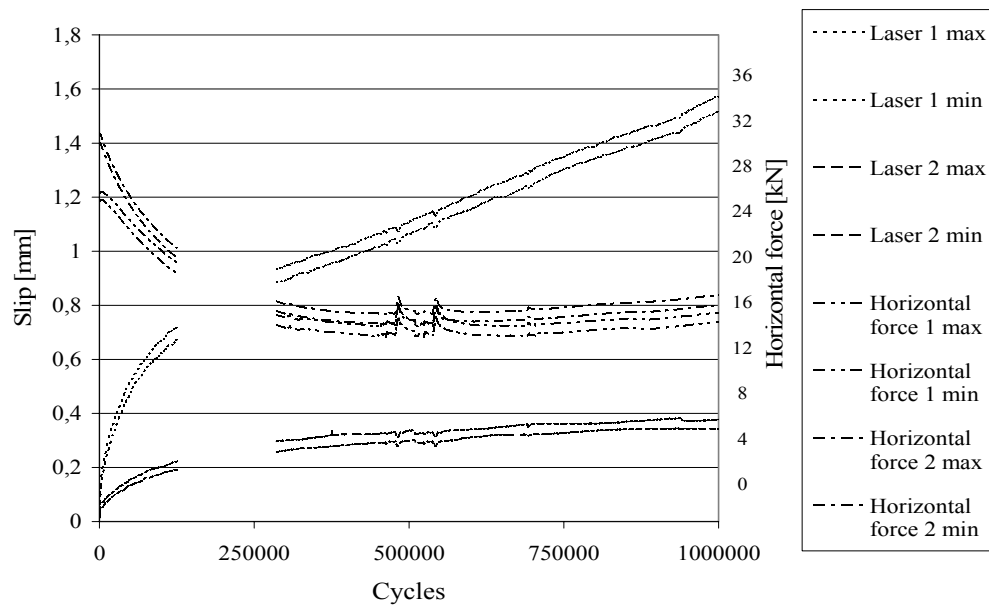


Figure B. 7 Slip of lasers during fatigue loading.

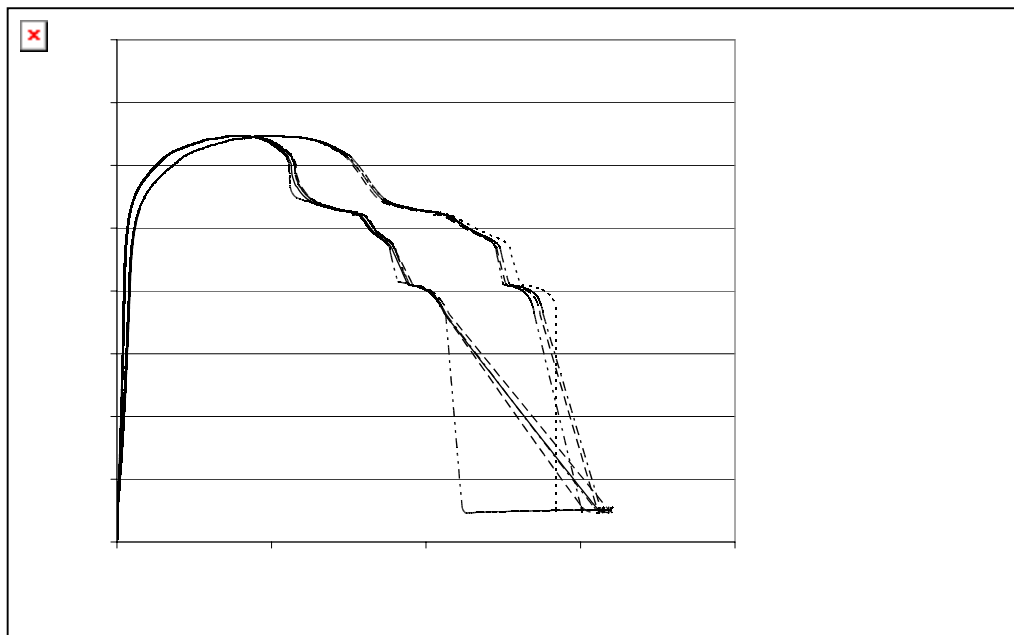


Figure B. 8 Slip-load curve of residual strength test.

Appendix C

Table C.-1. Compressive strength, f_{ck} , of concrete cubes, results from 11/11, 52 days after casting.

Test nr	casting	storage	B	l	H	F [kN]	σ [MPa]	σ_{mean} [MPa]	
2	1	Water	151,3	151,5	150,6	985	43	43,5	mean 1
3	1	Water	151	152	150,4	1011	44		40,8
5	2	Water	150,3	148,8	150	1302	58,2	58,95	mean 2
6	2	Water	150,7	149	150,1	1340	59,7		54,15
8	1	Air	152,6	149,6	150,3	843	37	38,1	Mean of 1 & 2
9	1	Air	151	151,3	151	896	39,2		
									47,48
11	2	Air	150,7	152	150,5	1113	48,6	49,35	
12	2	Air	152,1	152,1	150,6	1159	50,1		

TableC.-2. Tensile strength, f_{ctk} , of concrete cubes, results from 11/11, 52 days after casting.

Test nr	casting	storage	B	l	h	F [kN]	σ [MPa]
1	1	Water	150,6	152,3	150,1	170	7,44
4	2	Water	151,7	149	150,5	168	7,49
7	1	Air	152,3	150,1	150,1	132	5,86
10	2	Air	151,7	152,4	149,9	152	6,65

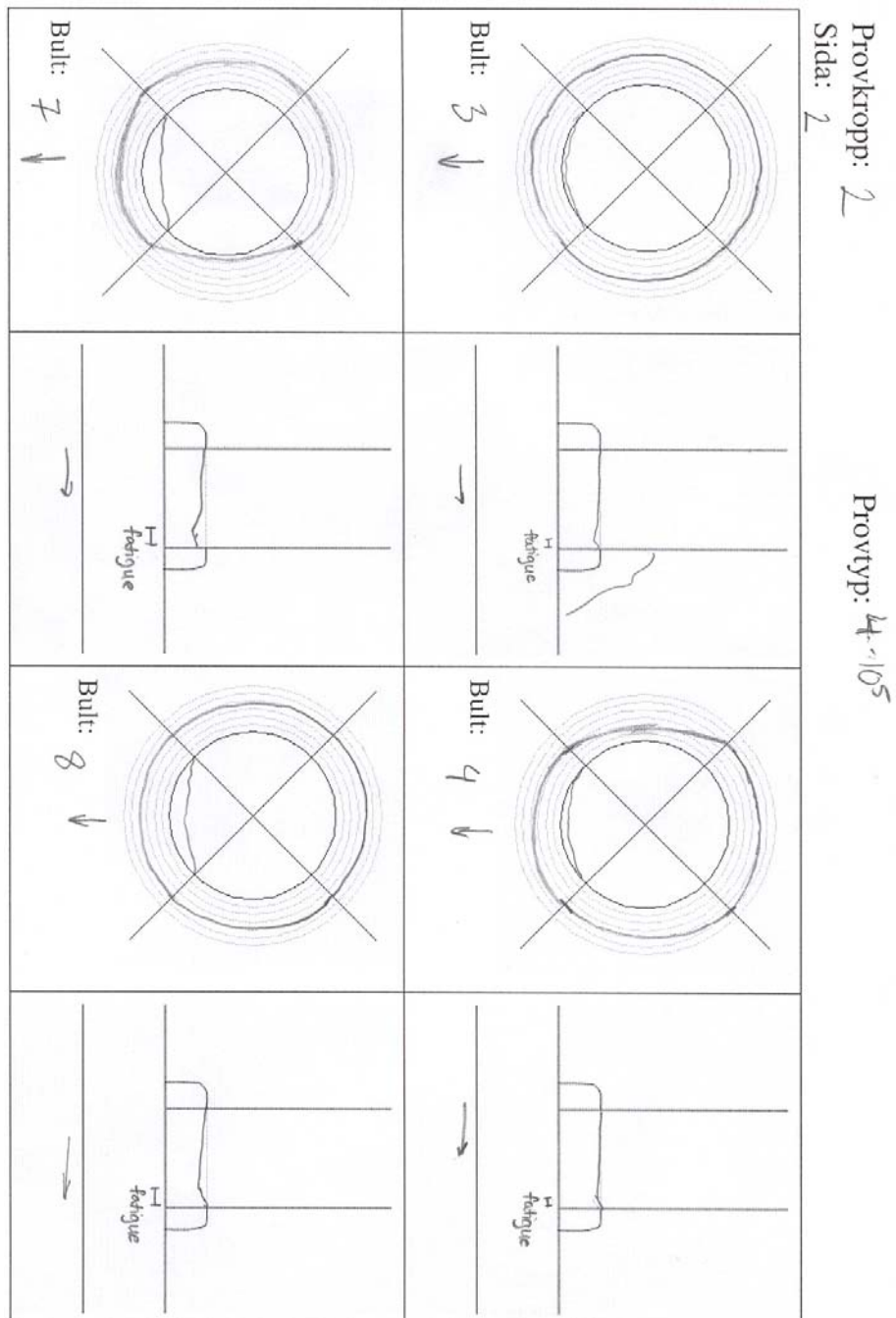
Table C -3. Compressive strength, f_{ch} , of concrete cubes, results from 16/3, 146 days after casting.

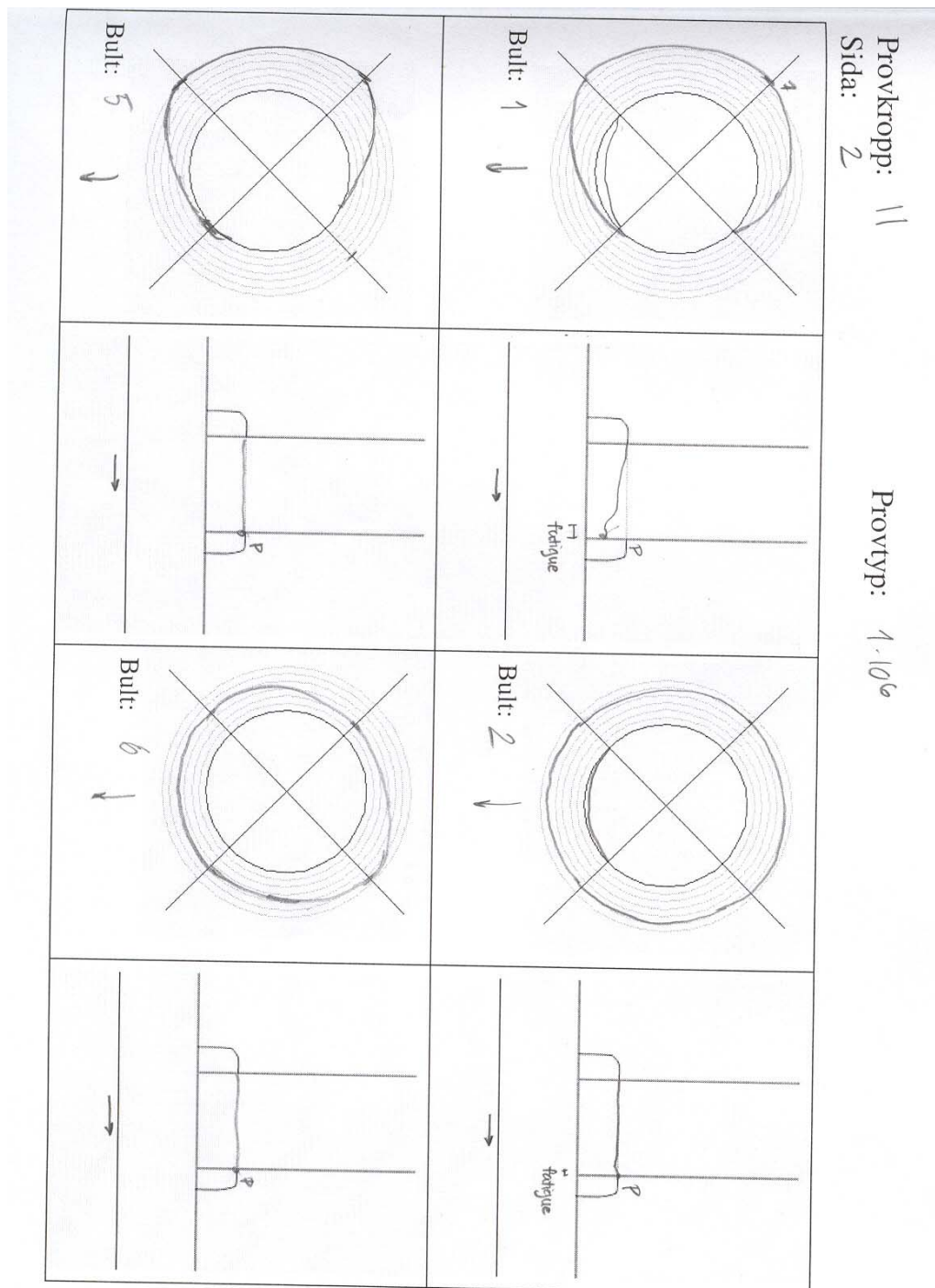
Test nr	casting	storage	B	l	H	F [kN]	σ [MPa]	σ_{mean} [MPa]	
1	1	luft	149,8	151	150,3	878	38,8	41,6	mean 1
2	1	luft	150,6	148,9	150,1	997	44,5		44,2
4	2	luft	151,8	151,5	150,5	1292	56,2	56,9	mean 2
5	2	luft	151,3	152,2	150,6	1329	57,7		58,3
7	1	H2O	152,2	151,8	150,3	1091	47,2	46,7	Mean of 1 & 2
8	1	H2O	151,3	152,1	150,4	1062	46,1		
									51,2
10	2	H2O	151,3	152,6	150,7	1374	59,5	59,6	
11	2	H2O	153,4	150,5	151,6	1376	59,6		

Table C -4. Tensile strength, f_{ctk} , of concrete cubes, results from 16/3, 146 days after casting.

Test nr	casting	storage	b	l	h	F	σ [MPa]
3	1	Air	152,9	151,3	150,1	142	6,25
6	2	Air	152,3	152,4	150,3	136	5,94
9	1	Water	151,3	152,5	150,9	157	6,82
12	2	Water	152,2	151,2	150,2	133	5,86

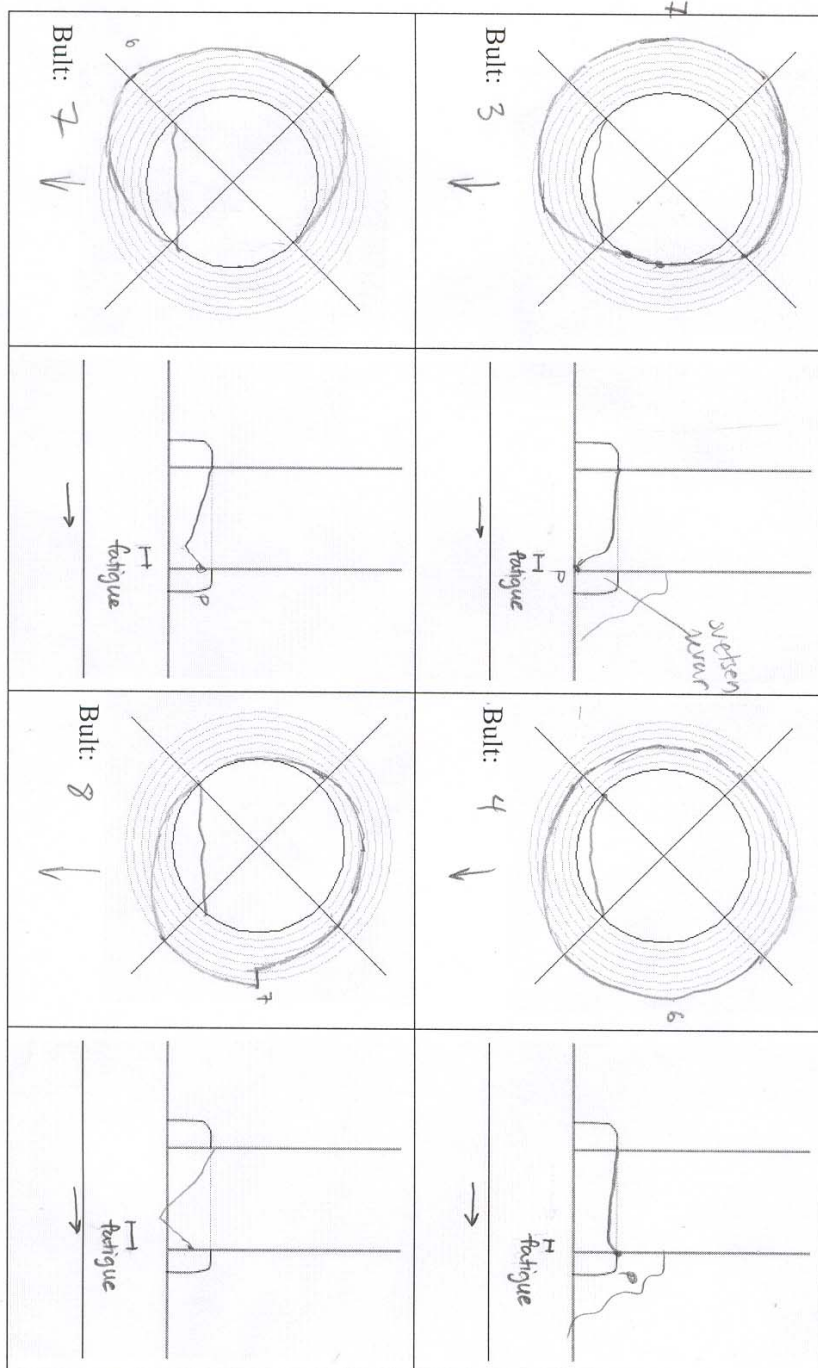
Appendix D

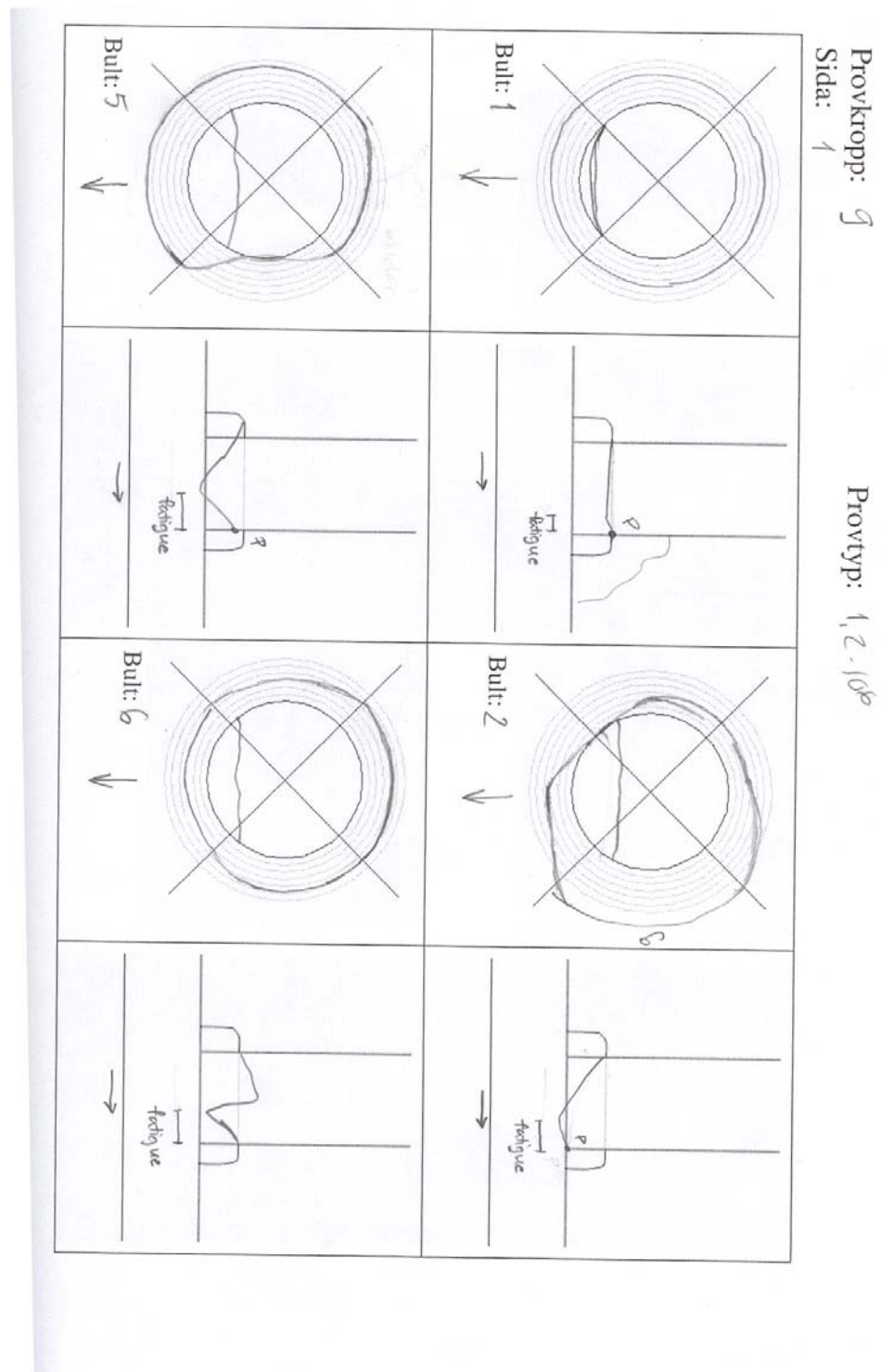




Provkropp: 9
Sida: 2

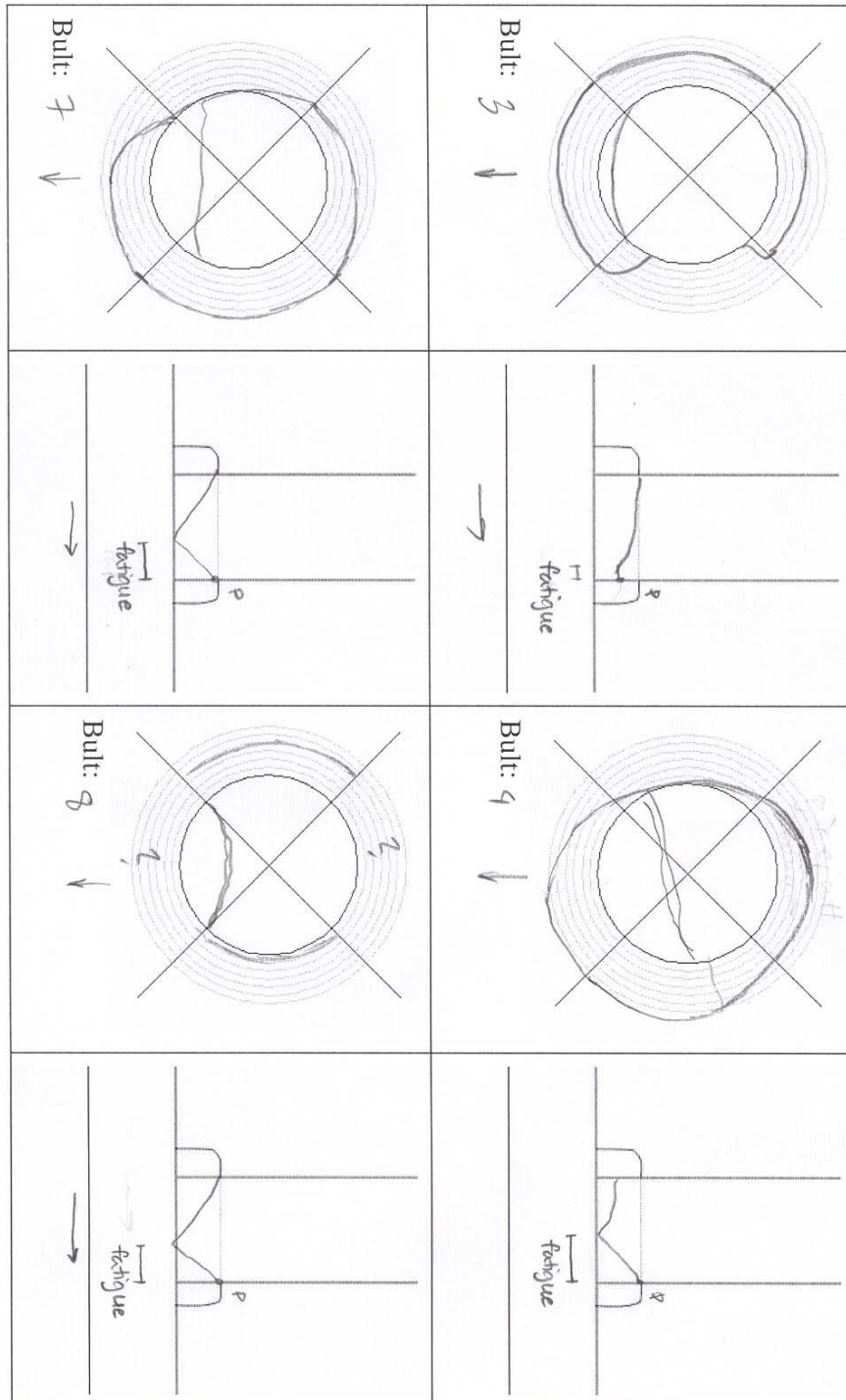
Provtyp: 1/2-106

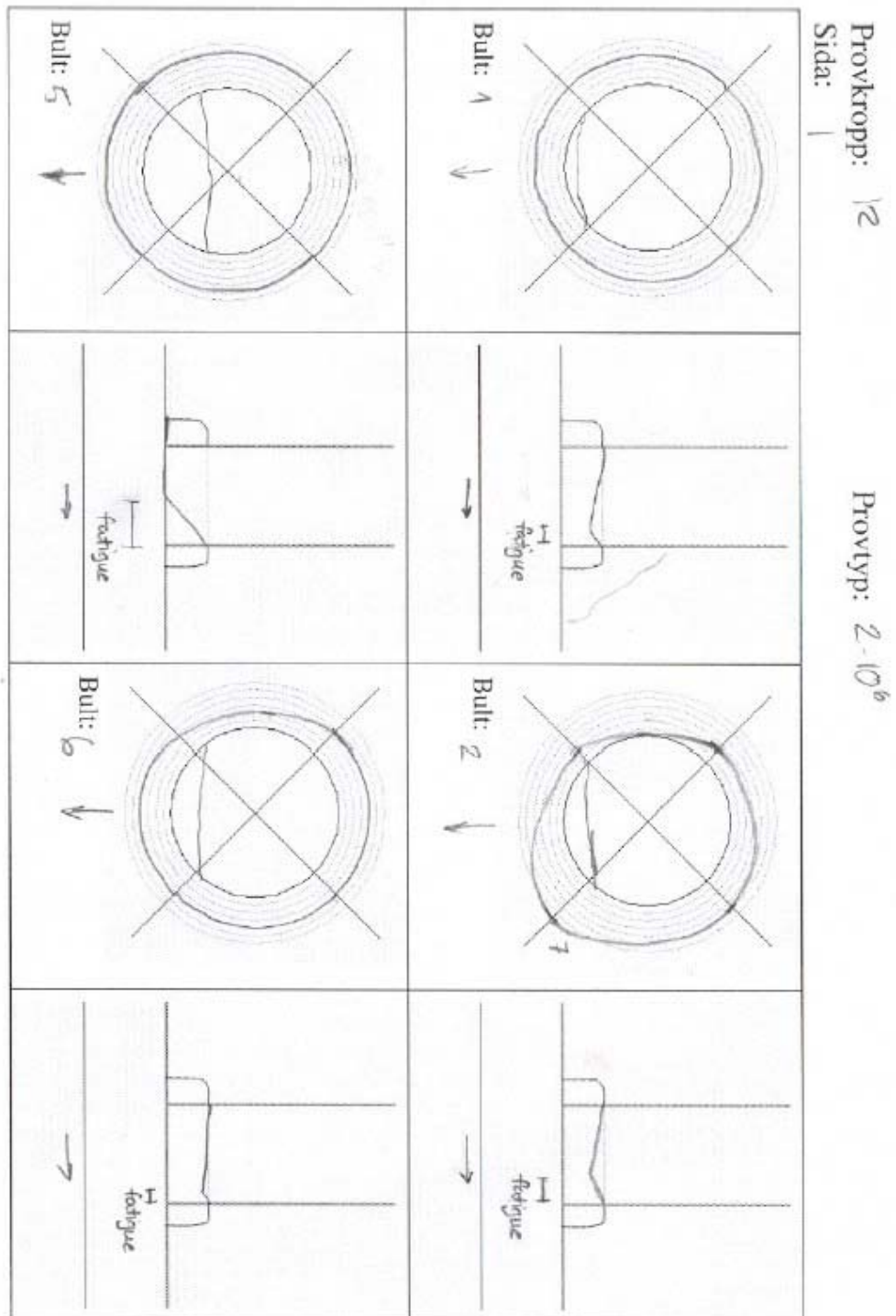




Provkropp: 12
Sida: 2

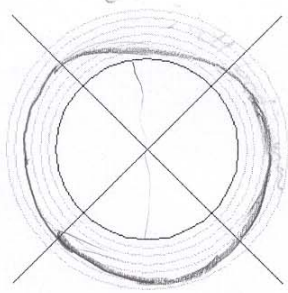
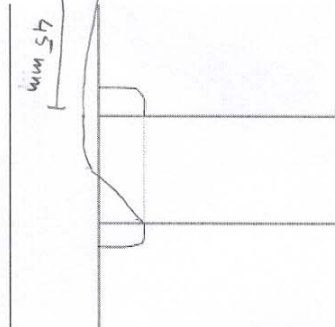
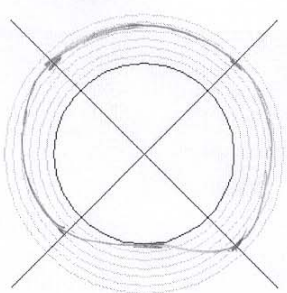
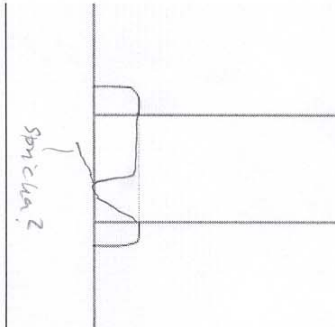
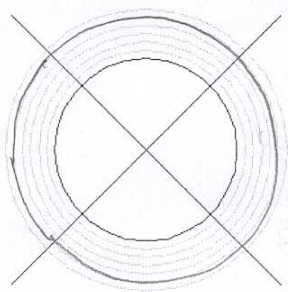
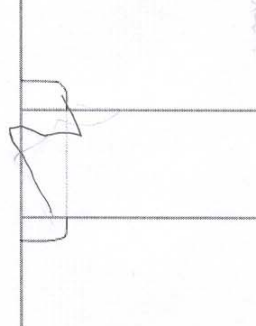
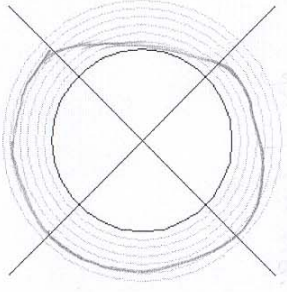
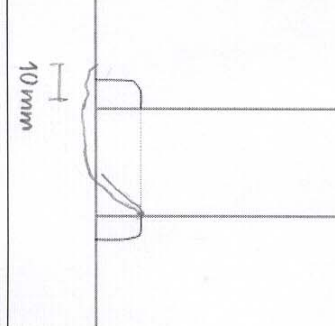
Provtyp: 2-10⁶





Provkropp: 4
Sida: 2

Provtyp: *endurance*

 <p>Bult: 1 ↓</p>	 <p>45 mm ↓</p>	 <p>Bult: 5 ↓</p>	 <p>spricka: 2 →</p>
 <p>Bult: 2</p>		 <p>Bult: 6 ↓</p>	 <p>10 mm</p>

Appendix E

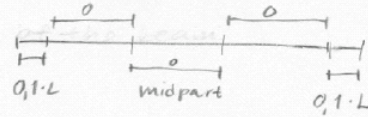
Table E- 1. Number of shear studs required for different length of one span bridge.

Length		Outerpart						Midpart		
		outer 10 %			inner			100 000	400 000	static
		100 000	400 000	static	100 000	400 000	static			
25	no of studs	12	19	22	10	16	12	9	14	15
	design no	22	22	22	12	16	12	15	15	15
	range [kN]	16,36	16,36		23,99	17,99		16,49	16,49	
35	no of studs	10	15	17	8	12	9	7	10	11
	design no	17	17	17	9	12	9	11	11	11
	range [kN]	16,17	16,17		24,43	18,32		16,81	16,81	
45	no of studs	8	12	14	6	10	8	5	8	8
	design no	14	14	14	8	10	8	8	8	8
	range [kN]	15,51	15,51		21,72	17,37		16,72	16,72	
55	no of studs	7	10	11	5	8	6	4	6	6
	design no	11	11	11	6	8	6	6	6	6
	range [kN]	16,36	16,36		24	18		17,64	17,64	

The following procedure have been used in the calculations :

1. Length of bridge were chosen
The width and concrete area have been the same; 13m and 4 m².
2. Eigenweights of concrete and steel, shrinkage, eigenweights of pavement, traffic and fatigue loads were calculated.
3. Shear force and moment were calculated for the three stages:
I/ without composite action for steel and concrete
II/ longtime loading for pavement and shrinkage
III/ shorttime loading for traffic and fatigue loads.
4. The cross section was calculated and checked.
I/ in the stage without composite action the eigenweight of steel and concrete is carried by the steel beam and the upper flange of the steel beam carries $\sim 1/2$ of the load
→ area of upper flange
III/ in this stage the moment from eigenweights, traffic loads shrinkage and temperature
5. The moment of inertia is calculated → the stress → change of cross section → moment of inertia and so on.
6. The web is checked for buckling because of shear and the welds are designed.
7. The shear force from pavement and traffic loads, from moment of eccentric loads are calculated. and the number of
The force from temperature changes and shrinkage is distributed over a length of 10% on each side.
Forces from shrinkage are transferred into the bridge beams by reinforcement and those forces does not affect the shear studs.
This is also true for temperature differences when $T_s > T_c$, but $T_c > T_s$ gives forces in the studs.
All shear forces give the number of studs in ULS.

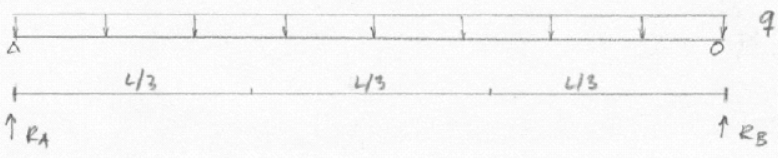
8. The shear force from pavement, and traffic loads, and from moment of eccentric loads gives the number of shear connectors in the parts marked by σ .



In the outer parts the shear force from pavement, traffic, shear from moments of eccentric loads and temperature gives the number of connectors

9. Fatigue loading is governed by special cases in BR0 2002 and the fatigue load for shear connectors are given by traffic load and eccentric loads.
The peak load is given by the range (fatigue load) and pavement. The fatigue loading gives range which is compared to characteristic values in BR0 2002, and the number of connectors required in fatigue is given.
10. The number of connectors are the higher of ULS and fatigue.

max shear force and moment of distributed load, midpart



$R_A = \frac{qL}{2}$

maximum moment is in the middle of the beam, $x = \frac{L}{2}$

$$M_{mid} = R_A \cdot x - \frac{qx}{2} \cdot x = \frac{qL}{2} \cdot \frac{L}{2} - \frac{qL^2}{8} = \frac{qL^2}{4}$$

the maximum shear force in the midpart is in $x = L/3$ where

$$V = R_A - qx = \frac{qL}{2} - \frac{qL}{3} = \frac{qL}{6}$$

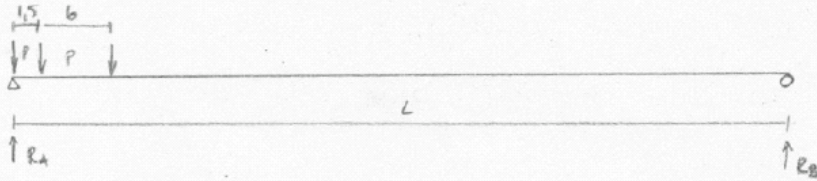
outer parts, $x = L/3$ for moment

$$M_{out} = R_A \cdot x - \frac{qx^2}{2} = \frac{qL}{2} \cdot \frac{L}{3} - \frac{qL^2}{18} = \frac{qL^2}{6} - \frac{qL^2}{18} = \frac{2qL^2}{18} = \frac{qL^2}{9}$$

$x=0$ for shear force

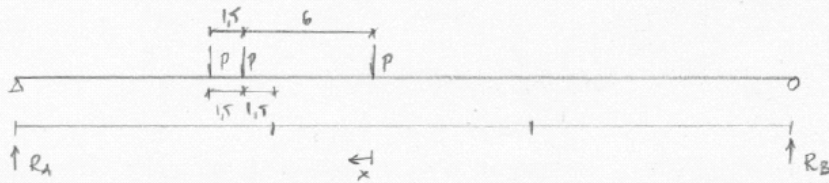
$$V = R_A = \frac{qL}{2}$$

Max shear force and moment for outer parts



Max shear force occur when the forces are above one support.

$$\sum \curvearrowright B : R_A \cdot L - P(3L - 7.5) = 0 \quad R_A = \frac{P(3L - 7.5)}{L}$$



$$\sum \curvearrowright A : -R_B \cdot L + P\left(\frac{L}{3} - 3 + \frac{L}{3} - 1.5 + \frac{L}{3} + 4.5\right) = 0$$

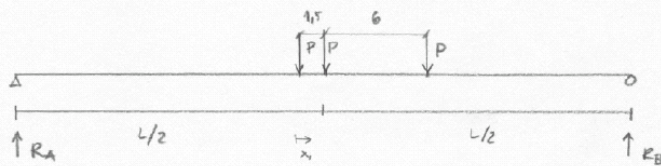
$$R_B = P$$

$$\sum \curvearrowright x : R_B \cdot \left(\frac{2L}{3} - 6 + x\right) - Px = M_1$$

$$P\left(\frac{2L}{3} - 6\right) = M_1$$

Max shear force and max moment of traffic load (point)

Mid part



$$\sum \curvearrowright B: R_A \cdot L - P \left(\frac{3L}{2} + 1.5 - 6 \right) = R_A \cdot L - P \left(\frac{3L}{2} - 4.5 \right) = 0$$

$$R_A = \frac{P \left(\frac{3L}{2} - 4.5 \right)}{L}$$

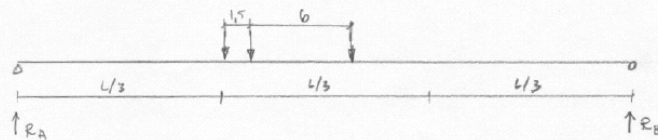
$$\sum \curvearrowright x: R_A \left(\frac{L}{2} - 1.5 + x \right) - P \cdot x - M_1 = 0 \quad M_1 = R_A \left(\frac{L}{2} - 1.5 + x \right) - P \cdot x =$$

$$= \frac{P}{L} \left(\frac{3L}{2} - 4.5 \right) \left(\frac{L}{2} - 1.5 + x \right) - P \cdot x = \frac{P}{L} \left(\frac{3L^2}{4} - \frac{9L}{4} + \frac{3Lx}{2} - \frac{9L}{4} + \frac{27}{4} - \frac{9x}{2} \right)$$

$$= \frac{P}{L} \left(\frac{3L^2}{4} - \frac{9L}{2} + \frac{3Lx}{2} + \frac{27}{4} - \frac{9x}{2} - xL \right) = \frac{P}{L} \left(\frac{3L^2}{4} - \frac{9L}{2} + \frac{Lx}{2} + \frac{27}{4} - \frac{9x}{2} \right)$$

The maximum moment is in the middle of the beam, so $x = 1.5$ which gives

$$M_1 = \frac{P}{L} \left(\frac{3L^2}{4} - \frac{9L}{2} + \frac{3L}{4} + \frac{27}{4} - \frac{27}{4} \right) = P \left(\frac{3L}{4} - \frac{15}{4} \right)$$



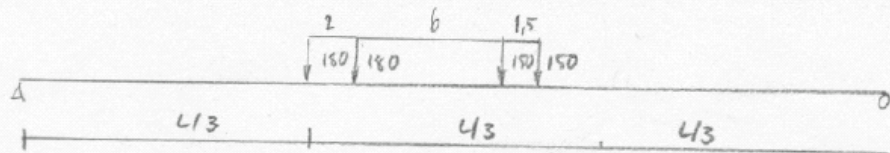
$$\sum \curvearrowright B: R_A \cdot L - P \left(\frac{2L}{3} + 1.5 - 6 \right) = 0 \quad R_A = \frac{P \left(\frac{2L}{3} - 4.5 \right)}{L}$$

The shear force is constant to $L/3$, so the maximum

$$\text{shear force for the midpart is } V = P \left(2 - \frac{15}{2L} \right)$$

Fatigue loading

midpart



$$\sum \vec{B}: R_A \cdot L - 180 \left(\frac{2L}{3} + \frac{2L}{3} - 2 \right) - 150 \left(\frac{2L}{3} - 8 - \frac{2L}{3} - 9,5 \right) = 0$$

$$R_A = \frac{180 \left(\frac{4L}{3} - 2 \right) + 150 \left(\frac{4L}{3} - 17,5 \right)}{L}$$

$$V_{\max} = R_A = 440 - \frac{2985}{L}$$

outer part



$$\sum \vec{B}: R_A L - 180 (2L - 2) - 150 (2L - 8 - 9,5) = 0$$

$$R_A = 360 - \frac{360}{L} + 300 - \frac{2625}{L} = 660 - \frac{2985}{L}$$

Temperature

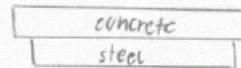
Different temperature in the different parts of a bridge will give rise to forces affecting the shear studs.

According to BR02002 the change of length is calculated as

$$\epsilon_t = \alpha \cdot \Delta T, \text{ where } \alpha = 1,0 \cdot 10^{-5} \frac{1}{^\circ\text{C}}$$

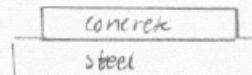
for a steel concrete bridge $\Delta T = \pm 10^\circ\text{C}$.

When $T_{\text{concrete}} > T_{\text{steel}}$



which will have the same effect on the shear studs as the traffic load.

When $T_{\text{concrete}} < T_{\text{steel}}$



which will have the same effect on the shear studs as the shrinkage.

$$F_{\text{Temp}} = \epsilon_t \cdot E \cdot A_c$$

$$M_{\text{Temp}} = F_{\text{Temp}} \cdot y$$

Shrinkage

Concrete is subjected to shrinkage.

The E-modulus for longtimeloading is

$$E_{long} = \frac{E}{3}$$

The maximum shrinkage is 0,025%

The tension required to "hold" the concrete in its original position is

$$\sigma = E_{long} \cdot \varepsilon = \frac{E}{3} \cdot 0,025$$

The neutral axis is somewhere in the steel beam, a value is assumed, the forces and crosssection is calculated and a new value is given...

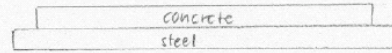
The force to resist the effect of shrinkage is given by

$$F = \sigma \cdot A_{concrete}$$

and the moment introduced by shrinkage is calculated

$$y = |y_{concrete\ middle} - y_g|$$

$$M = F \cdot y$$



Appendix F



sid. 1 (2)

DNV Inspection AB
Neongatan 4B
431 53 Mölndal

Vår ref.
Dennis Bergström

Er ref.
Sixten Andersson

Datum
2002-01-29

Projekt : Provning av svetsbult.

Ref: Förundersökning av svetsade bultar enligt Bro 94, 54.43 samt bilaga 9-9.

Beställning

Vi beställer härmed provning av svetsbult enligt Bro 94, 54.43 samt bilaga 9-9.

Svetsning av bult 22 x 200 är utförd 2002-01-25 under överinseende av oberoende utomstående kontrollant. Böjprovning med slägga av 15 st svetsbult har utförts vid samma tillfälle.

Vi skär 150mm remsor ur provstycket och levererar dessa till er. Remsorna innehåller totalt 35 st svetsbult.

Ert uppdrag

Provberedning
Dragprovning, 5 st
Mekaniserad böjprovning, 30 st
Snitt- slip- och etsning, 30 st
Makroundersökning, 30 st
Upprättande av erforderliga provnings- och resultatprotokoll.

Tidplan

Provningen utförs och redovisas under vecka 206 - 207

Bilagor

Provningsintyg för svetsbult och plåt.
pWPS med svetsvärden.

Adress	Telefon	Fax	Org.nr.	Postgiro	Bankgiro
Mejselvägen 17 94336 Öiebn	+46 911 66705	+46 911 66344	556470 - 1109	742668 - 7	5872 - 7017

BRISAB

INDUSTRI AB

sid. 2 (2)

Ersättning

Pris totalt 30.000,- exkl. moms

Betalningsvillkor

30 dagar efter ankomststämplad faktura

Med vänliga hälsningar

BRISAB Industri AB


Dennis Bergström

Adress	Telefon	Fax	Org.nr.	Postgiro	Bankgiro
Mejselvägen 17 94336 Öjebyn	+46 911 66705	+46 911 66344	556470 - 1109	742668 - 7	5872 - 7017



Procedurprov av svetsbult enligt BRO 94

Företag: Brisab Industri AB
Mejselvägen 17
943 36 ÖJEBYN

Omfattning: Enligt avsnitt 54.43 samt bilaga 9-9

Svetsare: Niklas Nordsten 751001-8935

Datum: 2002-01-25

Produktform: Plåt 30 mm, svetsbult 22x200

Grundmaterial: Plåt 460 NL1

Svetsläge: PA

Svetsutrustning: Kôco 2601 E1

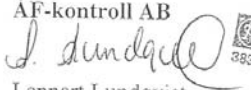
Svetsdata: Brinntid 1 sek. Lyfthöjd 5 mm, Ström 2,0 KA

Arbetstemperatut: +20 °C

Värmebehandling: Ingen

Provning:

Dragprovning:	5 st	Godkänt resultat	bilaga 3:4
Makroprov:	30 st	Godkänt resultat	bilaga 4:4
Böjprov:	30 st	Godkänt resultat	Bilaga 4:4
Bockprov:	15 st	Godkänt resultat	

ÅF-kontroll AB

Lennart Lundqvist

BRISAB

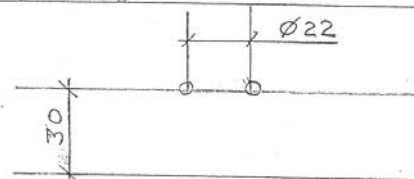
INDUSTRI AB

Datum 2002-01-25

Preliminary Welding Procedure Specification (pWPS)

Plats	Verkstad Öjebyn	Granskare / organ	ÅF-Kontroll AB, Luleå
Tillv. svetsprocedur	15	Metod fogberedning	Slipning
Referensnummer	15 / 00	Metod rengöring	Slipning
WPAR nr.		Grundmaterial	Grupp 2, P 460 NL1 + St.37

Tillverkare	BRISAB Industri AB	Materialtjocklek	P=30mm, svetsbult 22x200
Svetsmetod	Svetsning svetsbult	Ytterdiameter (rör)	
Svetstyp	Automatisk brännsvetsning	Svetsläge	PA
Fogberedning	(se skiss)		

Fogutformning	Svetsföljd
	

Sträng	Metod	Tillsatsmaterial Dimensioner	Ström (A)	Spänning (V)	Strömtyp Polaritet	Trådmättnings- hastighet	Stränglängd /elektrod	Värme- tillförsel
1			2000					

Tillsatsmaterial (namn)		Övrig information	
Skyddsgas / pulver		Pendling	
Gasflöde		Strängbredd	
Rotmejsling / rotstöd		Pulssvetsning	
Förhöjd arbetstemp.		Plasmasvetsning	
Mellansträngstemp.		Brännarvinkel	90 grader
Värmebehandling		Lyfthöjd	5 mm
Utstick	4 mm	Brinntid	1.0 sek
Dämpning	3		

Tillverkare	Granskare / granskande organ
BRISAB Industri AB	ÅF-Kontroll AB, Luleå
Göran Magnusson	Lennart Lundqvist



KONTROLLRAPPORT Test report

 Sida/Page
1/1

Ordernr/Order No	DNV oppdragsgivare/Customer
Rapport# C020231	BRISAB
DNV oppdragsnr/DNV comm No	INDUSTRI AB
99000200	Mejselvägen 17
Tilvirket/Manufacturer	943 36
BRISAB INDUSTRI AB	Oppdragsgivarens referens/Customer's reference
Provningsplats/Test site	
Materiallaboratoriet	
Provningsobjekt/Test objekt	
Föremål/Object	Ritning nr/Drawing No
Trettiofem (35) svetsbultar	pWPS15, datum: 2002-01-15
Övriga uppgifter/Supplementary data	
Provning av svetsbult enligt BRO 94, 54.43 samt bilaga 9-9	

Resultat/Result

Dragprovning enligt EN 10 002-1 utförd den 7/2 2002

Pos #	Prov nr.	T	b / D	a	S0	ReL	ReH	Rp0,2	Rp1,0	Rm
Item #	Test No.									
		*C	mm	mm	mm2	N/mm2		N/mm2		N/mm2
	Krav		min			350				450
	Requirements		max							522
	C020231	+20	22,0							532
	C020231	+20	22,0							522
	C020231	+20	22,0							523
	C020231	+20	22,0							521

Mekaniserad böjprovning utförd den 4/2

Utförd med godkänt resultat

Makroundersökning utförd på böjda bultar

Utförd med godkänt resultat, se bilaga

DNV 120 [EE] 2000-04-25

DNV Inspection

 Datum/Date
2002-02-18

Operatör/Operator




Sixten Andersson

Underskrift/Signature

 Datum/Date
2002-02-18

Nivå/Level

BILAGA 1
TILL RAPPORT #:Date:
2002-02-15Page (of):
1 (1)Rapport-Report #:
C020231

MACRO - EXAMINATION			
Test according to:	Specimen according to:	Requirement:	Date:
EN 1321	EN 1321	BRO 94, 54.43 Bilaga 9-9	2002-02-15
Performance:			
<p>30 st svetsade och böjprovade bultar har makroundersökts enligt BRO 94, 54.43 och bilaga 9-9.</p>			
Result(s):			
<p>Samtliga bultar uppvisade god inbränning och relativt jämn form på smältbadet.</p> <p>Några defekter över acceptansgränserna kunde ej konstateras.</p> <p>Proverna är godkända.</p>			
Handläggare-Handled by:		Kontrollerad av-Controlled by:	
 Arne Gudmundson		 Anders Pettersson	
		 GOTHENBURG	

CEOC

COLLOQUE EUROPÉEN DES ORGANISMES DE CONTRÔLE

Abnahmeprüfzeugnis DIN EN 10 204 - 3.1 A
Inspection Certificate ISO 10 474 - 3.1 A
Certificat de Réception
Certificato Collaudo Materiali

Besteller-Customer-Acheteur-Committente:
Artur Naumann Stahl AG
40508 Düsseldorf

Hersteller-Manufacturer-Fabricant-Produttore:
Salzgitter AG
Werk Ilsenburg
D-38871 Ilsenburg

Prüfgegenstand-Article-Produit-Prodotta:
Grobblech / Heavy plate / Tôle forte

Prüfgrundlagen-Anforderungen-Technical requirements/Demand-Spécifications techniques/Exigences-Norma di controllo/Requisiti:
ADW 1/ W 10/ Vd-TUV 357-1, DIN EN 10029 B 10/91,
DIN EN 10163-2 KL.B Untergruppe 2 10/91, DIN EN 10028-3 04/93

Werkstoff-Material-Matière-Materiale:
P 450 NL1

entsprechend-according to-suivant-secondo:
DIN EN 10028-3

Ausgabe-Edition-Edizione:
04/93

Lieferzustand-State of delivery-Etat de livraison-Stato di fornitura: normalisiert / normalized / normalisé
Erhitzungsart-Melting process-Procédé d'élaboration-Procédimento di elaborazione:
Sauerstoffaufblasverfahren / Basic oxygen process / Procédé de conversion à l'0

Kennzeichnung-Marking-Marquage-Punzonatura:
Werkstoff-Material:
Matière-Matériau: P460NL1
Herstellerzeichen-Brand of the manufacturer-Marque du fabricant-Marshio del produttore:
Erzeugnis-Nr./Sachverständigenstempel
Trademark/Steelgrade/Heat-No/Product-No/
Inspector's stamp
Sigle de l'usine/Vuance de l'acier/N° coulé/
N° produit/Poinçon de l'expert

Stempel des Sachverständigen-Inspector's stamp-Poinçon de l'expert-Punzone dell'esperto:

(TUV)

Umfang der Lieferung-Extent of material delivery-Liste descriptive-Descrizione della fornitura:

Pos.-Nr. Item No Posto-N° N° pos.	Stückzahl Number of Qts Numero pezzi	Gegenstand-Article-Désignation du produit-Tipo di prodotto mm x mm x mm	Schmelz-Nr. Heat No N° Coulee N° Coiata	Probe-Nr. Test No N° d'éprouvette N° di prova
04	1	30,00 x 3000,0 x 12000	34924	353694 1
04	1	30,00 x 3000,0 x 12000	34924	353695 1
04	1	30,00 x 3000,0 x 12000	34924	353697 1

Zusätzliche Angaben-Additional remarks-Autres remarques-Osservazioni:
Die gestellten Anforderungen sind lt. Anlagen erfüllt-The requirements are fulfilled according to annexes.
Les conditions imposées sont satisfaites suivant annexes.
I risultati sono conformi ai requisiti richiesti come da allegati.

Magdeburg
(Ort-Location-Lieu-Località)

26.02.2000
(Datum-Date-Data)

Bezirk 11

Dipl.-Ing. Wehr
(Der Sachverständige-Inspector-L'expert-L'ispettore)

Anlagen-Annexes-Allegati:
1) Ergebnis der Prüfungen-Test results-Risultati des essais-Risultati delle prove
Weitere Anlagen in 1) - Other annexes in 1) - Autres annexes en 1) - Altri allegati in 1)

00 04/03 11:15 FAX 031223250

TERRAMET-STÄLCENTER AB

008

Marke: *svet prave*

CEOC

TÜV NORD GRUPPE
TÜV Hannover/Sachsen-Anhalt

COLLOQUE EUROPÉEN DES ORGANISMES DE CONTRÔLE

Anlage-Annex-Annexe-Allegato: 1

Ergebnis der Prüfungen
Test Results
Résultats des Essais
Risultati delle ProvePrüf-Nr. 129812
Inspection No
Certificat N°
N° di collaudoTeil
Part
Partie
ParteBlatt-Nr. 2/4
Sheet No
Page N°
Pag N°

Mechanische Prüfungen-Mechanical tests-Essais mécaniques-Prove meccaniche

Prüfart-Test type-Type d'essai-Tipo di prova: Probenart-Specimen type-Type de l'éprouvette- Tipo di provetta: Probenzustand-state of delivery of specimen- traitement de l'éprouvette-Stato della provetta:						Zugversuch DIN EN 10002-1 prismatisch normalisiert					Kerbschlagbiegeversuch DIN EN 10045 KV normalisiert					
Probe-Nr. Test No N° d'éprouvette N° di prova	Probenabmessung Dim. of specimen Dim. de l'éprouvette Dim. della provetta	Entnahme Specimen Prélevement Prelevamento	Temperatur Temperature Température Temperatura	Reibung Friction Frottement Attrito	Reibung Friction Frottement Attrito	Reibung Friction Frottement Attrito	Reibung Friction Frottement Attrito	Reibung Friction Frottement Attrito	Reibung Friction Frottement Attrito	Reibung Friction Frottement Attrito	1-J Schlagarbeit-Energie of Impact- Energie de rupture-Energie di rottura Kerbschlagbiegeversuch-impact strength Résistance-Rasistenza 3-J Krit. Bruchanteil-Cryst. proportion- Partie cristalline-Proportione cristalline 4-mm/100 Bréilung-Expansion- 5-J Elongiervermögen-Elongation- Härte (Einheiten)-Hardness- Durezza-Durezza	2-J Schlagarbeit-Energie of Impact- Energie de rupture-Energie di rottura Kerbschlagbiegeversuch-impact strength Résistance-Rasistenza 3-J Krit. Bruchanteil-Cryst. proportion- Partie cristalline-Proportione cristalline 4-mm/100 Bréilung-Expansion- 5-J Elongiervermögen-Elongation- Härte (Einheiten)-Hardness- Durezza-Durezza	3-J Krit. Bruchanteil-Cryst. proportion- Partie cristalline-Proportione cristalline 4-mm/100 Bréilung-Expansion- 5-J Elongiervermögen-Elongation- Härte (Einheiten)-Hardness- Durezza-Durezza	4-J Krit. Bruchanteil-Cryst. proportion- Partie cristalline-Proportione cristalline 4-mm/100 Bréilung-Expansion- 5-J Elongiervermögen-Elongation- Härte (Einheiten)-Hardness- Durezza-Durezza	5-J Krit. Bruchanteil-Cryst. proportion- Partie cristalline-Proportione cristalline 4-mm/100 Bréilung-Expansion- 5-J Elongiervermögen-Elongation- Härte (Einheiten)-Hardness- Durezza-Durezza	
Schmelze-Nr. Heat No N° Coulee N° Colata	Dicke Thickness Epaisseur Spessore	Breite Width Largeur Larghezza	Ort-Location Lieu Direction-Sens Posizione	Reibung Friction Frottement Attrito	Reibung Friction Frottement Attrito	Reibung Friction Frottement Attrito	Reibung Friction Frottement Attrito	Reibung Friction Frottement Attrito	Reibung Friction Frottement Attrito	Reibung Friction Frottement Attrito	1 Werte-Values- Valeurs-Valori	2 Werte-Values- Valeurs-Valori	3 Werte-Values- Valeurs-Valori	4 Werte-Values- Valeurs-Valori	5 Werte-Values- Valeurs-Valori	Bemerkung Remark Remarque Osservaz
1	2	3	4	5	6	7	8	9	10	11	12	13	14	15	16	17
Anforderungen / Requirements / Exigences																
	> 16	≤ 35		Q	G	RT	≥450	≥570	≥17							
	≥ 12	≤150		Q		-050					1	≥11			≥16	450/10
353694	31,3	25,4	K	Q	G	RT	481	644	21							
353694	31,0	25,6	K	Q	G	RT	470	641	20							
353694	8,0	10,0	K	Q	G	-050				1	34	55	42	44	450/10	
353694	8,0	10,0	K	Q	G	-050				1	52	44	42	46	450/10	
353696	31,1	26,2	K	Q	G	RT	482	640	19							
353696	31,0	26,5	K	Q	G	RT	473	650	20							
353696	8,0	10,0	K	Q	G	-050				1	44	41	42	42	450/10	
353696	8,0	10,0	K	Q	G	-050				1	41	56	41	46	450/10	
353697	31,5	26,7	K	Q	G	RT	495	648	19							
353697	30,9	26,5	K	Q	G	RT	504	650	18							
353697	8,0	10,0	K	Q	G	-050				1	54	52	57	54	450/10	
353697	8,0	10,0	K	Q	G	-050				1	42	59	45	49	450/10	

Prüfart-Test type-Type d'essai-Tipo di prova: Probenart-Specimen type-Type de l'éprouvette- Tipo di provetta: Probenzustand-state of delivery of specimen- traitement de l'éprouvette-Stato della provetta:						Warmzugversuch DIN EN 10002-5 zylindrisch normalisiert									
mm	mm					°C	Rp0.2 N/mm²			Z	1	2	3	Ø	
Anforderungen / Requirements / Exigences															
	> 8	≤ 70		Q	O	+400	≥235								
34924			K	Q	O	+400	325								

Magdeburg
(Ort-Location-Lieu-Località)25.02.2000
(Datum-Date-Data)Dipl.-Ing. Wehr
(Der Sachverständige-Inspector-
L'expert-L'ispettore)

28-01-02 09:50 ID=+45 64813696

+45 64813696

KÖCO
KÖSTER & CO

SVETSBILT TILL PROVNING

Köster & Co GmbH

Köster & Co GmbH - Postfach 1364 - D-58242 Ennepetal

KÖSTER DANMARK ApS Ennepetal, 23.01.02

POSTBOX 18

DK 5400 BOGENSE Zeugnis-Nr.: 13004
Certificate No. / Certificat n°

Kundennummer: 23010 Auftragsnummer: 103252
Customer No. / Client No.: File No. / Dossier n°
Bestellnummer: 220 Artikelnummer: 017-0050-001
Order No. / N° de commande: Art. No.
Bestelldatum: 20.12.01 Auslieferungsmenge: 100
Order Date / Quantité livrée
Bestellmenge: 5500 KÖCO - Chargennummer: 4001263
Quantity / Quantité
Artikelbezeichnung: SD Kopfbolzen Werkstoff: S235J2G3+C450
Object / Matière
Abmessung: Ø22x200 mm Lieferbedingung:

Abnahmeprüfzeugnis DIN EN 10204 / 3.1 B
Inspection certificate DIN EN 10204 / 3.1 B
Certificat de réception DIN EN 10204 / 3.1 B

Prüfergebnisse / Test Results / Résultats des essais						
Rm N/mm²	A 5	RP02 / Rel	Ein- schnürung	Kerbschlag- arbeit	Härte	
Zugfestigkeit Tensile strength Résistance à la traction	Dehnung % Elongation Allongement	N/mm² Streckgrenze Yield stress Limite d'élongement	Z %	J Notch Toughness Resilience	HB/HV/HRC Hardness Dureté	
Sollwert >=:	450	15	350			
Istwert:	560	18	532			

Chargenanalyse / Chemical Composition of Heat / Composition chimique de la coulée						
C %	Si %	Mn %	P %	S %	Al %	Cr %
0,147	0,198	1,147	0,011	0,02	0,023	0
Ni %	N %	Mo %	B %	Ti %	Cu %	Zn %
0	0	0	0	0	0	0
Fe %	Mg %					
0	0					

Probe vom Ring ☒ Probe vom Stab ☐ Probe vom Bolzen ☐
Test on ring of material Test on bar of material Test on stud
Epreuve en bobine Epreuve en bar de fil Epreuve du goujon

Ergebnis der Prüfung: Die gestellten Anforderungen sind erfüllt.
Test result: The results of tests are satisfactory.
Résultats des essais: Les résultats sont satisfaisants.

Köster & Co. GmbH

Werkstatteinverständiger
Inspector of Works
Inspecteur d'Usine
A. P. Völkel

<ul style="list-style-type: none"> Bolzenschweißen Befestigungselemente Bolzenschweißmaschinen Sondermaschinenbau 	<ul style="list-style-type: none"> Betonverbundbau Betonanker Kopfbolzen Verankerungselemente 	<ul style="list-style-type: none"> Fließpresssonderteile Kaltverbrännte Präpansstelle nach Kundenwunsch 	<ul style="list-style-type: none"> Dienstleistungen Schweißtechn. Schulung Schweißtechn. Beratung Lohnschweißarbeiten nach RPD u.ä. Leihgeräteeppool f. d. Bolzenschweißen Engineering v. Anlagen 	<ul style="list-style-type: none"> Software Bauwesen Schweißtechnik
---	---	--	---	--

DIN EN ISO 9001 QS-1898 HH

Köster & Co GmbH
Spreeler Weg 32
D-58256 Ennepetal

Telefon +49 (0)2333 8306-0
Telefax +49 (0)2333 8306-38
E-Mail koeco@bolzenschweisstechnik.de
Internet www.bolzenschweisstechnik.de

Geschäftsführer:
Detlef Köster, Ulrich Kleeschulte
AG Schwelm, HRB 1000
USt-IdNr. DE811181058

Sparkasse Ennepetal
(BLZ 454 510 60) Kto.-Nr. 15 925
Dresdner Bank AG, Hagen
(R17 454 510 60) Kto.-Nr. 15 925